U. S. DEPARTMENT OF THE INTERIOR
U. S. GEOLOGICAL SURVEY

Geophysical Site Characterization of the Midvale Slag Site, Midvale, Utah

by

Karl J. Ellefsen[1] and Regina M. Bochicchio[2]

Open File Report 93-704

---

[1] U. S. Geological Survey, MS 964, Box 25046, Denver, CO 80225
[2] Desert Research Institute, P. O. Box 19040, Las Vegas, NV 89132-0040

1993

ABSTRACT

Using geophysical methods, we have characterized the Midvale Superfund site in Midvale, Utah, a project funded under an Interagency Agreement with Region VIII of the Environmental Protection Agency. On this site are wastes from smelting that occurred between 1871 and 1958. The primary objective of the characterization is to determine the thicknesses of the four slag piles — this information will be used to determine the cost of removing this waste. The secondary objective is to test how well geophysical methods can address some generic problems that exist here and at other sites in the Rocky Mountain states.

We estimated the thicknesses of the slag piles using electromagnetic methods because the slag is much more electrically resistive than the underlying sediments. We made terrain conductivity measurements at stations generally spaced 15.2 m (50 ft) apart along a profile, and we used a least-squares algorithm to estimate the thicknesses. We also made several time-domain electromagnetic measurements, and we estimated the thicknesses using another least-squares algorithm. For the pile of iron slag, the thickness at the southern end is approximately 11 m (35 ft), at the northwestern end 4 m (14 ft), and at the northeastern end 20 m (65 ft). Because the estimates from both types of data are consistent, we are confident in their accuracy. At the northeastern end, the slag might be filling a hole dug for a land fill.

For the pile of copper slag, the thickness in the northeast corner is approximately 6 m (20 ft), and it gradually diminishes to 2 m (7 ft) towards the west, just before the site road. In the southeast corner, which is on the side of a small bluff, the thickness is about 1 m (2 ft), and it gradually increases to approximately 2 m (7 ft) towards the west near the site road. The thickness determined from the one time-domain electromagnetic sounding is virtually identical with the thicknesses determined by the frequency-domain measurements. For the eastern and western piles of the air-quenched slag, the estimated thicknesses are erratic and generally smaller than we expect from our knowledge of the geology. We believe that these mediocre results are due to the heterogeneity of the pile. Nonetheless, after examining the topography and carefully interpreting these estimates, we believe that the eastern pile is approximately 8 m (25 ft) thick and the western pile 6 m (20 ft). For the pile of water-quenched slag, our measurements are very erratic, and again we believe that this phenomenon is due the to heterogeneity of the pile. Here our estimates from the geophysical measurements are not geologically plausible because they are much greater than the height of the pile relative to the flood plain, which is approximately 18 m (60 ft).

We used magnetic field measurements and four types of terrain conductivity measurements to detect the buried foundation of the bag house because such foundations usually contain steel reinforcing rods. The measurements are at closely spaced stations along three profiles that are perpendicular to the long axis of the foundation. The anomalies coincide with the foundation edges and two man-made structures, which we located using old engineering drawings of the site.

To detect the calcine waste, we measured the (electrical) self potential along two profiles. We used this method because sulfur, which is prevalent in this waste, is frequently involved in electrochemical reactions that perturb the electrical field. Large anomalies exist at the edge of the waste. However, large anomalies in the magnetic field and the terrain conductivity also exist at the edge of the pile, and such correlated anomalies are typical of a buried, corroding conductor. Although a portion of the self potential anomaly might be caused by the sulfur, we cannot distinguish it from what might be caused by the conductor. Thus, the results of this test are ambiguous.

The heterogeneities in the slag piles that have irregular, three-dimensional shapes might be the largest impediment to processing the data because our processing algorithms cannot account for this heterogeneity. However, several new algorithms developed at some research universities can account for this heterogeneity, and when they become available for routine processing, then our estimates of the thickness will be more accurate.

At other sites, man-made features that are close to the surface of the ground and contain metal probably can be mapped using magnetic and terrain conductivity methods. Both methods should be used together because the costs of acquiring the data are low and the ambiguity inherent in the interpretation is reduced. The thicknesses of smelting and mining wastes can sometimes be estimated using electromagnetic methods. Success with these methods depends upon large anomalies in the electrical properties of the waste and the degree of heterogeneity.

CONTENTS

LIST OF FIGURES

LIST OF TABLES

1. INTRODUCTION

During August 1992, Michael Strieby, the Remedial Project Manager from Region VIII of the Environmental Protection Agency (EPA), asked the Branch of Geophysics, U. S. Geological Survey to characterize the Midvale Superfund Site using geophysical methods. This site is located in Midvale, which is approximately 10 miles south of Salt Lake City, Utah (Figure 1). On this site are piles of waste that were generated by smelting between 1871 and 1958 (Huntingdon Chen Northern, 1993); since some of the wastes contain toxic substances, the site was placed on the National Priorities List.

The Remedial Project Manager must know the cost of removing those waste piles that are toxic, and a crucial piece of information in this computation is the volume of the piles. Because the lateral extent of the piles can be calculated from aerial photographs and topographic maps, determining the thicknesses is our primary objective in the site characterization. In this report, we describe in detail how we estimated these thicknesses using inexpensive geophysical methods.

Because some problems that exist at this site also exist at other, similar sites in the Rocky Mountain states, our secondary objective was to experiment with several geophysical methods to address two generic problems. (1) When the smelter was operating, the toxic particles in the furnace gases were trapped in the bag house, which is now demolished. Because the rubble and the soil in and around the extant foundation of the bag house probably contain some of the particles, this area might need remediation. We used geophysical methods to find the edges of the foundation. The Midvale site is an ideal location for this geophysical test because the geophysical results can be compared to old engineering drawings of the former buildings and other structures. This test demonstrates how well we can use geophysical methods to detect the buried foundations and other structures at mining and smelting sites. (2) One waste pile contains calcine, which was smelted from arsenopyrite. We tried an electrical geophysical method to detect this waste, a challenging problem because the waste pile and ground around it contain scrap metal and other debris.

This report is divided into six major sections with the first being this introduction. In the second section, we describe the near-surface geology and the significant man-made structures that affect the geophysical measurements. In the third, we summarize a preliminary investigation that established the feasibility of this more-thorough investigation. In the fourth section, we describe how the geophysical data were collected and processed. The interpretation of the data is in the fifth section; also, we show some data strongly affected by heterogeneity, and we discuss the effects that the heterogeneities of the slag have on the interpretation. The final section contains the summary and some suggestions.

For distances and elevations, we use English units because they are used on all engineering drawings and topographic maps. When appropriate, we include the equivalent value in metric units. For the geophysical measurements we use metric units because the

instruments display the data this way and metric units are the world-wide standard in the geophysical industry. This mixture is the best means of presenting the results at this time.

2. GEOLOGY AND MAN-MADE STRUCTURES

The Midvale Superfund Site is located in the Salt Lake Valley, which is bounded by the Wasatch Range on the east and the Oquirrh Mountains on the west. The sediments in the valley, which range in thickness from several hundred to several thousand feet, include lacustrine deposits from ancient Lake Bonneville, mud-rock flows from the mountains, alluvial fans, sand dunes, glacial deposits, and flood plain sediments (Hely et al., 1971, p. 11). The near-surface soil on the site, which is next to the Jordan River (Figure 1), was probably deposited as flood plain sediments.

Some buildings, foundations of demolished buildings, railroad tracks, and other structures that were used in the smelting and refining of ore are still present on the site (Figure 2). Moreover, after the smelting ended, additional structures such as power lines were built on or near the site. In the south central area was a railroad yard; although the tracks are not visible at the surface, they may be buried under slag. Also, a small building was in this yard. In the southeast corner, the railroad tracks are visible at the surface. East of these tracks, just beyond the edge of the site, is an electrical power line that trends north-south. Across the middle of the site is another electrical power line that trends east-west. In the center of the site is a lead refinery, which is still standing. Just to the east is an open area in which many buildings related to the smelting were located. The buildings were demolished, and their foundations are now filled with rubble and tailings from the Sharon Steel Site just south of 7800 South Street. Through this open area passes a power line to the refinery. North of the refinery is a railroad track, which is still being used. The track trends east-west through most of the site; near the western side it turns towards the south, passes outside the boundary of the site and then parallels the site along its western edge. Also along the western edge is an electrical power line that trends north-south. The northern end of the site is covered with excess rock and soil from the construction of Interstate Highway 15 (Figure 1). In the northeast corner is a garbage dump (M. Strieby, 1993, person. commun.) that is probably covered by this rock and soil. Scattered throughout the site are abandoned trucks, bulldozers, and other machinery. The entire site is surrounded by a metal fence.

Five large piles that contain wastes from smelting are on the site (Figure 2). (1) In the southeast corner is calcine, which is rich in sulfur and probably arsenic. This waste is reddish-brown, contains large flecks of yellow, and is very fine-grained. (2) In the south central area is the copper slag. It appears black and glassy; it has the consistency of an unconsolidated, coarse sand. The elevation of the upper surface of the pile is greatest along the eastern edge, which is formed by a terrace, and the elevation decreases to the west. Near the site road is the western edge of pile; from here to the Jordan River are sediments. (3) In the west central area are two piles of air-quenched slag. The slag on the tops and most sides is gray and unconsolidated; its consistency is like a very coarse gravel. Along the steep southern side of the easternmost pile, the slag is semi-consolidated. The

dips of the sides, except the side that we just noted, vary approximately from 30 to 40 degrees. (4) In the northwest corner is water-quenched slag. At the top and along most of the sides, this black, glassy slag has the consistency of an unconsolidated, coarse sand. Along the southern side near the bottom, the slag is semi-consolidated. The dips of the sides of this enormous pile vary approximately from 30 to 40 degrees. (5) In the northeast corner is the iron slag. At the top, this slag has the consistency of a unconsolidated, very coarse gravel, but the slag exposed along the sides is partially consolidated. The dips of the sides vary approximately from 40 to 70 degrees. The southern edge of the pile is bounded by a cement platform that extends to the railroad track. The ground near these five piles is covered by a thin layer of slag.

3. PRELIMINARY INVESTIGATION

To determine whether we could estimate the thicknesses of the waste piles using electrical methods, a preliminary investigation was performed using surface and borehole geophysical methods. On September 9, 1992 R. Horton (1992, written commun.) measured electrical properties using a terrain conductivity meter (Geonics EM-31) and a very low frequency resistivity meter (Geonics VLF-16R) that are primarily surface profiling instruments. From these measurements we learned that (1) the resistivity of the slag is greater than that of the underlying material, (2) the apparent resistivity measured at the top of the slag piles is approximately 100 Ω-m, (3) the apparent resistivity at one exposure of natural sediments is approximately 15 Ω-m, and (4) the apparent resistivity of the calcine waste is approximately 15 Ω-m. On October 22 and 23,1992 thirteen monitoring wells, (Figure 3), which were installed during a previous site investigation, were logged with an induction tool (Appendix A). From these logs, we learned that the resistivities of these soils around the wells range from 10 to 30 Ω-m. If we assume that the sediments under the waste piles are also in this range, then the significant contrast in the resistivity of the slag and sediment might be exploited to estimate the thicknesses of the slag piles but not the calcine waste.

Horton (1992, written commun.) also measured the magnetic susceptibilities of several samples of waste using a portable magnetic susceptibility meter (Geoinstruments JH-8); the values vary enormously within some slag piles indicating that these piles are very heterogeneous in their magnetic properties. The monitoring wells were also logged with neutron and gamma tools, and the results are in Appendix A.

4. DATA COLLECTION AND PROCESSING

We collected six types of surface geophysical data at the Midvale Superfund Site between February 16 and 23,1993 and between June 2 and 6, 1993. Since the type of data, the acquisition geometry, and the processing depended upon the geophysical objective, we organize the discussion of these topics by the objective. In the last part of this section, we discuss how we surveyed our locations.

4.1 Thicknesses of Slag Piles

The important result of the preliminary investigation is that we might be able to estimate the thicknesses of the slag piles using either electrical resistivity or electromagnetic geophysical methods. We chose to use electromagnetic methods for two reasons. (1) With the resistivity method, a high contact resistance between the electrodes and the slag might exist, reducing the amount of current that can be injected. With little current, the accuracy of the measurements is lower. With electromagnetic methods, direct electrical contact with the slag does not occur. (2) Usually, fewer people are needed to collect electromagnetic data than are needed to collect resistivity data.

We collected the electromagnetic data using two types of terrain conductivity meters and using time-domain electromagnetic soundings. Both terrain conductivity meters operate similarly: a receiving coil measures the oscillating magnetic fields generated by a transmitting coil and by eddy currents in the ground (Frischknecht et al., 1991, p. 106-110; Telford et al., 1976, p. 500-631). For one instrument, the Geonics EM-31, the coil separation is fixed at 3.7 m (Geonics Ltd., 1984); for the other, the Geonics EM-34, the separations are 10, 20, and 40 m (Geonics Ltd., 1987). To obtain information from different depths, the measurements for both instruments were made with the coils either horizontal coplanar (HCP) or vertical coplanar (VCP). Altogether, we made eight terrain conductivity measurements at each station.

The terrain conductivity data were collected along lines called profiles consisting of approximately 10 to 15 stations (Figure 3). The profiles on the tops of piles were for estimating their thicknesses; the profiles near the bases of the piles were for estimating the resistivities of the soils and sediments. The spacing between the stations is usually 15.2 m (50 ft); we chose this distance because it is small enough to detect significant changes in the thicknesses of the slag piles but large enough to minimize the number of measurements. Sometimes we made extra EM-31 measurements between stations to carefully monitor the changes in the near-surface electrical properties, and sometimes we reduced the station spacing on short profiles because we wanted at least 8 stations on each profile. The EM-31 data and the EM-34 data for every profile are tabulated in Appendices B and C, respectively.

Our processing algorithm, which is described in the next paragraph, cannot account for topography. Therefore, we tried to collect data that should be unaffected by topography: we kept the distance between the profiles and the sides of the piles greater than the largest coil spacing, 40m. We could not meet this criterion for profiles A1, A2, and A3 and for the ends of profile W3 (Figure 3). Electrical conductors such as buried metal, fences, and steel-reinforced concrete perturb the terrain conductivity measurements. Insofar as possible we kept away from these conductors, although sometimes the ends of profiles are near them causing anomalies in the data. All terrain conductivity measurements, except those on profiles P1 and P2, were made in February; at this time the ground was nearly saturated from melting snow and rain. Because water in the pores of sediments can raise

electrical conductivity, our measurements might higher than identical measurements made during a dry season.

We processed the terrain conductivity data using a nonlinear least-squares inversion developed by Anderson (1992). The most important assumption about the mathematical model used in this inversion is that the ground consists of flat, horizontal layers that extend laterally to infinity. The implication of this assumption is that, when the geology changes rapidly in a horizontal direction, the estimates of the thickness and the resistivities may not be accurate. Other assumptions are in Anderson (1992) and Ward and Hohman (1987, p. 133). For the slag piles, we found that a two layer model is satisfactory: the upper layer represents the slag and the lower layer, which is a half space, represents the underlying soil and sediment. The inversion estimates the thickness of the first layer and the resistivities of both layers.

For the time-domain electromagnetic method, a steady-state magnetic field is generated by a current passing through a coil on the ground. The current is shut-off, inducing eddy currents in the ground, and the decay of the magnetic field is measured (Kaufman and Keller, 1983, p. 315-338). We used a Geonics EM-47 transmitter (Geonics, 1989) to generate the original magnetic field and a Geonics EM-37 receiver (Geonics, 1985) to measure the decaying field. The transmitting coil was square, and each side was 38.1 m (125 ft) long. The receiving coil was at the geometric center of the transmitting coil. Measurements were made at 30 Hz and 315 Hz. For each frequency, 256 measurements were usually stacked to make one data set, and then five data sets were averaged. Extensive details about the field procedures are in Fitterman (1993, written commun.).

We used the soundings on the slag piles to estimate their thicknesses, and the soundings on the ground near the piles to estimate the resistivities of the soils and sediments. For the soundings on the piles, we placed the transmitting coil close to the center to minimize the three-dimensional effects that the steep sides might have on the data. Since the upper surfaces of the two piles of air-quenched slag are rugged and the areas of these surfaces are small compared to that of the transmitting coil, we did not make any measurements here. Soundings S2 and S3, which are on the water-quenched slag, might contain some spurious noise because the data were collected during an electrical storm that was about 15 miles west of the site. The data for every sounding are tabulated in Appendix D.

To process the time-domain electromagnetic data, we used a commercial software package called Temix (Interpex, 1989). The most important assumption about the mathematical model for this program is that the ground consists of flat, horizontal layers that extend laterally to infinity. Other assumptions are in Ward and Hohman (1987, p. 133). Forward modeling is used to find approximate thicknesses and resistivities for each layer that are geologically reasonable, and then a least-squares inversion is used to find the optimum values.

4.2 Bag House Foundation

We observed large metal rods near the bag house foundation, and so we suspect that it might be made with steel reinforced concrete. When metal is close to the surface, it usually can be detected with electrical or magnetic methods, and for this reason we decided to measure the near-surface electrical properties and the magnetic field.

The electrical properties were measured with the terrain conductivity meter (EM-31) in the horizontal coplanar configuration, which is described in section 4.1. We measured the in-phase and out-of-phase (quadrature) components of the magnetic field. The former is valuable because it is especially sensitive to large metallic objects (Geonics, 1987); the latter is the standard terrain conductivity measurement. Furthermore, we made these two measurements with the axis between the coils parallel and perpendicular to the profile, which we call the in-line and the cross-line directions, respectively. A difference between the in-line and cross-line measurements indicates that the ground is laterally inhomogeneous (Geonics, 1987) — we expect this property near the foundation. The data are tabulated in Appendix B.

The magnetic field was measured with a nuclear precession magnetometer, EG&G Geometrics G856, which is described in EG&G Geometrics (1984). Details about the physical principles of this instrument are in Telford et al. (1976, p. 145-146). To determine if the temporal variations in the field and the changes in the instrument response were significant, we measured the magnetic field at the first station in a profile when we began the profile and then again when we finished it. The data are tabulated in Appendix E.

To determine the exact location and orientation of the bag house, we collected data along three parallel profiles that are perpendicular to the long, east-west axis of the bag house foundation (Figure 3). We chose three profiles because we would be able to correlate the data from one profile with the data from another, increasing our confidence in our interpretation. Since we did not know how wide the anomalies would be, we chose a station spacing of 1.5 m (5 ft); this distance is small enough to detect small but significant anomalies and large enough to minimize the amount of data to be collected.

Corrections to the magnetic field data for the temporal variations in the magnetic field and for changes in the instrument response are unnecessary because they are insignificant compared to the anomalies: typical small anomalies are approximately 150 nT whereas the sum of the variations and changes are approximately 10 nT. Only one processing step was applied to the electromagnetic and magnetic data: the mean value of the data along each profile was subtracted from the data. The resulting data shows the anomalies, what we are trying to detect.

4.3 Calcine Waste

Frequently, bodies of sulfide minerals create an electric field from the electrochemical reactions occurring within them (Telford et al., 1976, p. 458-460). This field can be detected by measuring the electric potential around the body, called the self potential (Corwin, 1990). The calcine waste contains large, visible flecks of sulfur. Therefore, we took self potential measurements to see if the calcine waste could be mapped from anomalies assoicated with the sulfur.

To collect the self potential data, we used non polarizing electrodes consisting of plaster of Paris with a small amount of lead chloride. We placed one electrode in the soil at the western end of profile P1 (Figure 3); this electrode remained here for all measurements along profiles P1 and P2. At each station, we placed the other electrode at the bottom of a hole about 8 cm (3 in) deep where moisture in the slag reduced the contact resistance. The potential and resistance were measured with a standard digital multimeter with a high input impedance, and these data are tabulated in Appendix F. At a few stations we checked the accuracy of the potential and resistance measurements by comparing them with measurements obtained with another multimeter; in all cases the two sets of measurements are virtually identical. The resistances generally range between 10 and 50 kΩ indicating that the potential measurements are reliable; only 9% of the 77 measurements exceed 50 kΩ. We did not make any additional measurements near the base electrode to account for drift; this omission is not a significant problem because we only want to detect anomalies.

Because we are concerned that the self potential anomalies could be caused by buried metal, which is ubiquitous at this site, we also collected terrain conductivity data (EM-31) and magnetic field data along profiles P1 and P2. We collected the conductivity data in the inline, horizontal coplanar configuration, which is described in section 4.1 and 4.2; the data are tabulated in Appendix B. We collected the magnetic field data using the procedures described in section 4.2; the data are tabulated in Appendix E.

Since we only wanted to detect anomalies in the self potential, the magnetic field, and the terrain conductivity data, the data do not need to be processed. Also, corrections to the magnetic field data are unnecessary because they are sufficiently small.

4.4 Other Data

At the start of the project, we thought that we could correlate changes in the mineralogy of the slag with changes in its magnetic properties. For this reason, we measured the magnetic field and the magnetic susceptibility along several profiles. The procedures for the magnetic field measurements are described in section 4.2, and the data are tabulated in Appendix E. We measured the susceptibility with a Geoinstruments Susceptibility Meter JH-8, and the data are listed in Appendix G. Because we lacked time and money to determine the mineralogical properties of the slag, we did not analyze the magnetic data.

W. Frangos collected and interpreted resistivity data near the calcine waste, and his work is described in Appendix H.

4.6 Surveying

To determine the locations of the profiles and soundings, we used the topographic maps prepared by Intermountain Aerial Surveys for the EPA, for which the grid is the state plane coordinates. These maps are well suited for this purpose because they are detailed: the scale is 1:1200, and the contour interval is 2 ft. We used compass bearings to prominent man-made structures such as electrical utility poles and corners of buildings to determine the location of a point. Then we checked the location by comparing the topography around the point to that indicated by the contours on the map. We believe that the locations are usually accurate to within 20 ft.

5. RESULTS AND DISCUSSION

5.1 Thicknesses of Slag Piles

In this section, we present cross sections of the slag piles showing their thicknesses. To develop these sections, we used the estimated thicknesses that we calculated using the methods described in section 4.1. To get the elevations of the slag-sediment interface, the thicknesses were subtracted from the station elevations, which we picked from the topographic maps prepared by Intermountain Aerial Surveys. These predicted elevations are erratic, and so on the cross sections we drew smooth lines to represent the interface. The sections are longer than the profiles because we want show the topography near the pile. Since knowing how much confidence to place in these cross sections is important, we also show how well the predicted data, which is calculated by the processing algorithm, fit the field data.

For the pile of water-quenched slag, we could not calculate any thicknesses that are geologically reasonable. We believe that our problems are due to the heterogeneity of this pile, and we discuss our measurements in detail in section 5.4.

5.1.1 Air-Quenched Slag Piles

On the easternmost pile along profile A1, we estimated thicknesses at stations 3, 5, 6, 7, 8, and 10. We did not process the data from the ends of this profile because at both locations either the transmitting or receiving coil for the EM-34 was on the steep side of the pile. Also we did not include the EM-34 data at the 40 m spacing in the processing because these data are erratic. The predicted data and the field data match moderately well (Figures 4 and 5). The ranges in resistivities for the slag and the underlying sediment are consistent with what we measured in other parts of the site. The estimated thicknesses of the slag at six stations range from 5 to 10 m (17 to 32 ft) (Figure 6). Judging from the topography of the pile and the surrounding ground, the larger estimates seem more plausible.

Regarding these results, we asked ourselves two questions: "Why is the range in thickness so large?" and "Why do most of the estimated thicknesses appear to be too small?" The slag on the southern side of the pile is semi-consolidated, whereas the slag on the top and the other sides is loose. This difference indicates to us that the pile is laterally heterogeneous. Also, the steep sides of the pile are within 15 m (50 ft) of the profile, which is close enough to affect the conductivity measurements, particularly for the larger inter-coil spacings. Since the mathematical model on which the inversion is based does not account for lateral heterogeneity and topography, we are not confident in the estimated thicknesses, even though the residuals are small.

On the westernmost pile along profiles A2 and A3, we estimated the thickness at all stations except station 1 on A2 because it is too close to the edge. We omitted all horizontal coplanar data and the vertical coplanar data at the 40 m spacing because they are too erratic. Even though we only had three measurements at each station, we wanted the least-squares solution to be over determined because in this case the effect of random noise on the estimates of the model parameters will be reduced. To this end, we fixed the resistivities of the slag and sediment at 100 Ω-m and 30 Ω-m, respectively, which are typical values that we measured at the site. Thus, we only estimated the thickness of the slag. For profile A2, the fit between the predicted and field data is fair (Figure 7); the estimated thicknesses range from 2 to 5 m (8 to 17 ft) (Figure 8). For profile A3, the fit is also fair (Figures 9), and the estimated thicknesses range from 2 to 9 m (7 to 28 ft) (Figure 10). From examining the topography, we believe that the actual thickness is close to 6 m (20 ft). The wide range in the estimates may be due to heterogeneity of the pile, the same problem that we encountered with the easternmost pile. The erratic character of the horizontal coplanar data supports this hypothesis because these data are usually more affected by electrical heterogeneities at depth than vertical coplanar data.

5.1.2 Iron Slag Pile

Along profile I1, we estimated the thicknesses and resistivities at all but the last three stations; at these three, which are on a cement foundation, the measured conductivities are high. The predicted data match the field data reasonably well (Figures 11 and 12). The estimated resistivities for the slag and sediment are consistent with the other estimates throughout the site. At the northern end of the profile the estimated thickness of the slag is approximately 4 m (14 ft); at the southern end approximately 11 m (37 ft). Accounting for the change in elevation along the profile, the predicted elevations of the slag-sediment interface at all stations except two, which cluster about 4275 ft (Figure 13). Judging from the topography near the pile, this prediction is plausible.

From the terrain conductivity data collected along profile I2, we estimated thicknesses and resistivities at all stations. The match between the field and predicted data for the horizontal coplanar configuration is satisfactory (Figure 14). The match for the vertical coplanar configuration is poor (Figure 15): the predicted data are usually too high for the 10 and 20 m spacings and too low for the 40 m spacing. We were unable to improve the

fit using a model with three layers; the misfit might be due to lateral heterogeneity. At all stations the estimated resistivities for the slag and the sediment are consistent with what we measured throughout the site (Figure 16). For the six stations at the southern end of the profile, the estimated thicknesses of the slag range from 10 to 13 m (32 to 42 ft), which are consistent with the estimates from the time-domain electromagnetic data and with the estimates along profile I1 (Figure 13). At the northern end of the profile, the estimated thicknesses at all stations except one are much larger, ranging up to 20 m (65 ft). Because the ground near the pile is flat, we did not expect this increase in thickness. Nonetheless, the general trend of the estimates might be correct: the slag might be filling a portion of the buried dump that is near the pile (Figure 2).

From the time-domain electromagnetic data, soundings S4 and S5, which are close to profile I2, we estimated how the electrical conductivity changes with depth. For soundings S4, the match between the field and predicted data is good (Figure 17). In the model developed for sounding S4 (Figure 18), the first layer has a low resistivity and is approximately 1 m (3 ft) thick. We needed this layer in the processing to obtain a reasonable fit to the field data, although it was unnecessary when we processed the terrain conductivity data. The middle and bottom layers represent the slag and the underlying sediments, respectively; their resistivities are similar to the resistivities estimated along profiles I1 and I2. The thickness of the slag is approximately 10 m (33 ft). From the data that we collected at sounding S5 (Figure 19), we obtained a model very similar to that for S4 (Figure 20), and we interpreted the layers similarly. The only notable difference in this model is that it has a fourth layer beginning at approximately 18 m (59 ft); again, we needed this layer to get a reasonable match between the field and predicted data.

5.1.3 Copper Slag Pile

For the first four stations along profile M1, we used all the data except those for the horizontal coplanar configuration at the 40 m spacing because they are too erratic. For the next five stations, we only used the vertical coplanar data at the 3.7, 10, and 20 m spacings because all the other data are too erratic. To keep the least-squares inversion over determined for these five stations, we set the resistivities of the slag and sediment to 210 and 35 Ω-m, respectively, which are suitable averages for this pile. We did not process the data from the last four stations, which are west of the site road, because they are too erratic. The data predicted by the inversion fit the field data moderately poorly (Figures 21 and 22). At the first four stations, the estimated resistivities for the sediment are consistent with other estimates at the site. The estimated resistivities for the slag are higher than the estimates for the other slag piles but are consistent with the estimates along the other three profiles over this pile. The estimated thicknesses are between 1 and 7 m (2 and 23 ft), a broader range than we expect. These modest results are probably due to the heterogeneity of this pile: it may contain scrap metal since it is above an old railroad yard (Figure 2). After accounting for the topography, the estimates of the elevation of the slag-sediment interface cluster about 4290 ft (Figure 23), which is consistent with the predictions from the terrain conductivity data along other profiles and from the time-domain electromagnetic data. The straight line that we drew to represent the slag-

sediment interface ties with the lines on profiles M3 and M4. The line dips slightly westward towards the Jordan River, an attitude that we expect in a flood plain. Going from east to west along this profile, the thickness of the pile diminishes.

At stations 1 through 8 along profile M2, we only used the data for the vertical coplanar configuration at the 3.7, 10, and 20 m spacings. The other data at these stations as well as all data from stations 9 and 10 are too erratic to be processed. To keep the inversion over determined, we set the resistivity of the slag to 210 Ω-m. We tried different values for the resistivity of the sediment until the fit to the field data was good (Figure 24), although we never let this parameter vary during an inversion. The values giving the best fit varied between 25 and 40 Ω-m, a range that is consistent with other measurements at this site. The estimated thicknesses range from 1 and 3 m (2 to 10 ft) and increase from east to west. They are consistent with the estimates along profiles M3 and M4 near this profile. After accounting for the topography, the estimated elevation of the slag-sediment interface is approximately 4300 ft at the eastern end of the profile and drops uniformly to approximately 4290 ft at the western end (Figure 25). At this location in the flood plain, we expect such a westward dip.

At stations 3 through 16 along profile M3, we processed only the data for the vertical coplanar configuration at the 3.7, 10, and 20 m spacings. The other data and the data from the other stations were not processed because they are too erratic. To keep the inversion over determined, we used the same procedure that we used along profile M2. The fit between the predicted and field data is moderately good (Figure 26). The values for the resistivity of the sediment vary between 20 and 37 Ω-m, and this range is consistent with other measurements at the site. The estimated thicknesses range from 0.3 to 4 m (1 to 12 ft) and are consistent with the nearby estimates from profiles M1 and M2. Our estimate of the slag-sediment interface is at approximately 4290 ft (Figure 27) and its apparent dip is small, a result that we expect along a line that parallels the river in a flood plain.

Along profile M4, we processed the data at stations 1 through 10 and 14 through 16. The data from stations 11 through 13 are too erratic, and station 17 is too close to a metal fence. Also, at stations 6 through 10 we excluded from the processing the horizontal coplanar data for the 40 m spacing because they are too erratic. Similarly, at stations 14 through 16 we excluded all horizontal coplanar data and the vertical coplanar data at the 40 m spacing. For the last three stations, we kept the inversion over determined using the same procedure that we used for profiles M2 and M3. The fit between the predicted and the field data is satisfactory at most stations except 6 through 10 where it is poor (Figures 28 and 29). The estimated resistivities for the slag and sediment are consistent with those along other profiles. The range in the estimated thicknesses for the first two groups of stations is small — from 5 to 7 m (16 to 22 ft). These estimates are consistent with those at nearby stations on profile M1 and with that from the time-domain electromagnetic data. At the last group of stations near the southern end, the estimates range from 0.3 to 1 m (1 to 3 ft) and are consistent with those on profile M2. The slag-sediment interface is at

approximately 4290 ft at the northern end of the profile and at 4300 ft at the southern end (Figure 30). At both locations, it has little dip as we expect.

Near the intersection of profiles M1 and M4, we collected the time-domain electromagnetic data, sounding S7. The match between the predicted and field data is good (Figure 31). The first layer in the model, which represents the slag, is 5.1 m (17 ft) thick, and its resistivity is 150 Ω-m (Figure 32). Both estimates are similar to what we determined from the terrain conductivity data. The resistivities of the deeper layers vary between 15 and 60 Ω-m. Although this model has more layers at depth than that used for the terrain conductivity data, their resistivities are similar.

5.2 Bag House Foundation

We made a map of the bag house foundation and other man-made structures near it from the old engineering drawings of the site. Using the foundation of an old smelter chimney, which is on the drawings and is still extant, as an approximate reference, we plotted on the map the anomalies from the three profiles. We observed that the anomalies are associated with the man-made structures. We then shifted the location of the profiles about 15 ft to get an optimal fit between the anomalies and the structures (Figures 33, 34, 35, 36, and 37).

Anomalies in all five types of data — magnetic field, conductivity in the inline direction, conductivity in the crossline direction, in-phase component in the inline direction, and in-phase component in the crossline direction — exist above all man-made structures — the walls of the foundation, a wall or metal duct north of the foundation, and a railroad track south of the foundation. In addition, the anomalies on different profiles correlate well. The relative sizes of the anomalies among the different data sets vary, and consequently if we use all five types together we have the best chance of finding a buried structure.

5.3 Calcine Waste

At the edge of the calcine waste along profile P1 are large anomalies in the self potential data (Figure 38), the terrain conductivity data (Figure 39) and the magnetic data (Figure 40). Similar, correlated anomalies exist along profile P2 (Figures 41, 42, and 43). Anomalies like these can be caused by a buried, corroding conductor; the presence of such a conductor is plausible because throughout this area are abandoned railroad tracks, a barbed wire fence, and metallic junk. Nonetheless, the calcine waste might be generating a potential anomaly, but the anomaly supposedly due to the conductor is masking it. For this reason, the results of this test are ambiguous.

Our profiles end near the western edge of the waste pile; to the east is private property. For an ideal survey, we would have either extended the two profiles across and beyond the waste pile or, even better, collected the data along many parallel profiles over the pile.

At approximately 400 ft on profile P1, anomalies appear on self potential data, terrain conductivity data, and magnetic field data. Similar, correlated anomalies appear on profile P2 also at 400 ft. These anomalies might be caused by another buried, corroding conductor.

5.4 Heterogeneity of the Piles

Our problems with the processing and interpretation of the terrain conductivity data and the time-domain electromagnetic data are probably due to the heterogeneity of the slag piles. This heterogeneity is manifested in the geophysical measurements as large changes between adjacent stations. We observed that the horizontal coplanar data are always more erratic than the vertical coplanar data are; this phenomenon occurs in other investigations too (Fitterman, 1993, person. commun.). We also observed that the data collected with the large inter-coil spacings are usually more erratic than the data collected with the small inter-coil spacings. The data collected at the large inter-coil spacings are more affected by lateral variations in the ground than data at the small spacings.

The data collected on the water-quenched slag are good examples of erratic measurements. If the pile were homogeneous, then all measurements of the same type would be equal. However, the terrain conductivity data and magnetic data change dramatically along profile W1 (Figures 44, 45 and 46), and the time-domain electromagnetic data from adjacent soundings, S2 and S3, are very different (Figures 47 and 48). Because of these erratic measurements, our estimates of the thickness of the pile, which we did not include in this report, are implausible. This failure was surprising to us because, from our observations of the surface of the pile, we thought it was mostly homogeneous. Also, the data collected for the background lines are very erratic, and for this reason we did not interpret them.

On the other piles, the heterogeneity diminished the quality of our estimates. This problem is particularly severe on the air-quenched slag: most estimates of the thickness of the slag are not plausible. On the piles of iron slag and of copper slag, the problem is less severe and is manifested in the scatter of the estimates. Although we often obtained reasonable estimates by eliminating erratic data, this technique has a significant disadvantage: because of the paucity of data the estimates are poorly constrained and are strongly affected by noise. Consequently, the estimates obtained with this technique must be carefully evaluated.

6. SUMMARY AND SUGGESTIONS

We estimated the thicknesses of the iron slag pile along two profiles using terrain conductivity data and at two soundings using time-domain electromagnetic data. Because the estimates are independent, virtually identical, and geologically plausible, we are confident in their accuracy. Our success with the four profiles and one sounding on the copper slag is similar. For the eastern and western piles of air-quenched slag, our estimated thicknesses from the terrain conductivity data are somewhat erratic and smaller

than what we expect from our knowledge of the geology. We attribute our mediocre results to the heterogeneity of these two piles. For the pile of water-quenched slag, we were unable to obtain geologically reasonable estimates of its thickness from both types of data. Again, we attribute these poor results to the strong heterogeneity of the pile.

Using a terrain conductivity meter (EM-31) and a magnetometer, we successfully located the bag house foundation and other man-made structures near it. The four types of data from the EM-31 — apparent conductivity in the inline direction, apparent conductivity in the crossline direction, in-phase component in the inline direction, and in-phase component in the crossline direction — plus the magnetic field data are complementary. Interpreting one type of data was difficult because the sizes of some anomalies are small. However, when all five types were combined, the interpretation was straightforward.

Large anomalies in the self potential, terrain conductivity, and magnetic field exist at the boundary of the calcine waste pile. Although the calcine waste might have an anomalous potential due to electrochemical reactions with the sulfur in the waste, the anomalies are more characteristic of a buried, corroding conductor. For this reason, our self potential measurements have not conclusively demonstrated that sulfide-rich waste can be mapped with the self potential method. Because self potential anomalies are caused by substances that are important in environmental investigations and because the data collection is fast and inexpensive, this method could be valuable at other sites.

Our data indicate that the slag piles are heterogeneous in the electrical and magnetic properties. As a result, our processing algorithm, which currently is the only method that is practical, is inadequate for about half the data. With other types of electromagnetic data and with more sophisticated algorithms, we could improve our estimates of the thicknesses of the slag piles.

We would like to make several specific suggestions that might help Remedial Project Managers characterizing other smelting and mining sites. First, man-made features that are close to the surface of the ground and contain metal probably can be mapped using magnetic and terrain conductivity methods. Both methods should be used together because the costs of acquiring the data are low and the ambiguity inherent in the interpretation is reduced. Regarding the last point, the interpretation of geophysical data always involves some uncertainty, but when data from two or more methods are interpreted together the uncertainty is usually reduced. Second, the thicknesses of smelting and mining wastes can sometimes be estimated using electromagnetic methods. Success with these methods depends upon large anomalies in the electrical properties of the waste and the degree of heterogeneity. Sometimes other geophysical methods such as ground penetrating radar or seismic refraction could be more successful, and so Remedial Project Managers might want to consider them.

We would also like to make several general suggestions that might help Remedial Project Managers characterizing any site. First, a geophysicist needs information about the contamination problems, the geology, and the hydrology to properly characterize the site.

Even if this information is not available at the start, it is still valuable later. Second, a small-scale preliminary investigation is invaluable. From this investigation, the geophysicist will learn what physical properties associated with the characterization problem are anomalous. Then, the geophysicist will either pick the most suitable geophysical method or stop work if nothing is suitable. Much taxpayer money can be saved, and the geophysicist as well as the Remedial Project Manager can avoid considerable embarrassment. Third, Managers probably should not rely entirely upon geophysical characterization because it is sometimes unsuccessful. At first, Managers might try geophysical methods because they are inexpensive and nonintrusive. Then, Managers might try other methods either to confirm the geophysical results or to obtain the needed information when the geophysical methods fail.

7. ACKNOWLEDGEMENTS

J. Williams helped us with the field work during February; her diligence and thoughtful suggestions helped the work proceed smoothly. D. Fitterman taught us how to collect, process, and interpret time-domain electromagnetic data. R. Horton helped us prepare the equipment for the field work and gave us many helpful suggestions and ideas. R. Hodges and J. Hutchens collected the well logging data. D. Hoover lent us his electrodes for self potential measurements and helped us interpret the data. W. Frangos helped us collect the self potential data. J. Kibler made some figures and plotted the logging data.

This work was supported by Region VIII of the Environmental Protection Agency under Interagency Agreement DW14953595-01-0.

8. REFERENCES

Anderson, W. L., 1992, Interactive inversion of dipole loop-loop electromagnetic data for layered earth models using numerical integration and complex image theory (version 1.0): U. S. Geological Survey Open File Report 92-553-A and Open File Diskettes 92-553-B.

Corwin, R. F., 1990, The self-potential method for environmental and engineering applications, *in* Ward, S. H., ed., Geotechnical and environmental geophysics, vol I: review and tutorial: Tulsa, Oklahoma, Society of Exploration Geophysicists, 389 p.

EG&G Geometrics, 1984, Model G-856, Proton Precession Magnetometer, Operators Manual: available from EG&G Geometrics, 395 Java Drive, Sunnyvale, CA, 94089.

Geoinstruments, Susceptibility Meter, JH-8, Operation Manual: available from Geoinstruments ky, Punapaadentie 6, SF 00930, Helsinki 93, Finland.

Frischknecht, F. C., Labson, V. F., Spies, B. R., and Anderson, W. L., 1991, Profiling methods using small sources, *in* Nabighian, M. N., ed., Electromagnetic methods in

applied geophysics — Applications, Part A: Tulsa, Oklahoma, Society of Exploration Geophysicists, 520 p.

Geonics Limited, 1984, Operating manual for EM31-D non-contacting terrain conductivity meter: available from Geonics Limited, 1745 Meyerside Dr. Unit 8, Mississauga, Ontario, Canada, L5T 1C5.

Geonics Limited, 1985, EM37 operating instructions: available from Geonics Limited, 1745 Meyerside Dr. Unit 8, Mississauga, Ontario, Canada, L5T 1C5.

Geonics Limited, 1987, EM31-3 operating manual: available from Geonics Limited, 1745 Meyerside Dr. Unit 8, Mississauga, Ontario, Canada, L5T 1C5.

Geonics Limited, 1989, Geonics protem EM system, Protem operating instructions: available from Geonics Limited, 1745 Meyerside Dr. Unit 8, Mississauga, Ontario, Canada, L5T 1C5.

Hely, A. G., Mower, R. W., and Harr, C. A., 1971, Water resources of Salt Lake County, Utah: State of Utah, Department of Natural Resources, Technical Publication 31.

Huntingdon Chen Northern, 1993, History of the Midvale slag superfund site, Midvale, Utah: available from Huntingdon Chen Northern, 1127 West 2320 South, Suite B, Salt Lake City, Utah, 84119.

Interpex, 1989, Temix: available from Interpex Limited, P. O. Box 839, Golden, CO.

Kaufman, A. A., and Keller, G. V., 1983, Frequency and transient soundings: Elsevier Science Publishers B. V., 685 p.

Keys, W. S., 1990, Borehole geophysics applied to groundwater investigations: Techniques of water resources investigations of the U. S. Geological Survey, Book 2, Chapter E2, 150 p.

McNeil, J. D., 1990, Use of electromagnetic methods for groundwater studies, *in* Ward, S. H., Geotechnical and environmental geophysics, vol. I: Review and tutorial: Tulsa, OK, Society of Exploration Geophysicists, 389 p.

Telford W. M., Geldart, L. P., Sheriff, R. E., and Keys, D. A., 1976, Applied Geophysics: Cambridge University Press, 860 p.

Ward, S. H., and Hohman, G. W., 1977, Electromagnetic theory for geophysical applications, *in* Nabighian, M. N., ed., Electromagnetic methods in applied geophysics — Theory, Volume I: Tulsa, Oklahoma, Society of Exploration Geophysicists, 513 p.

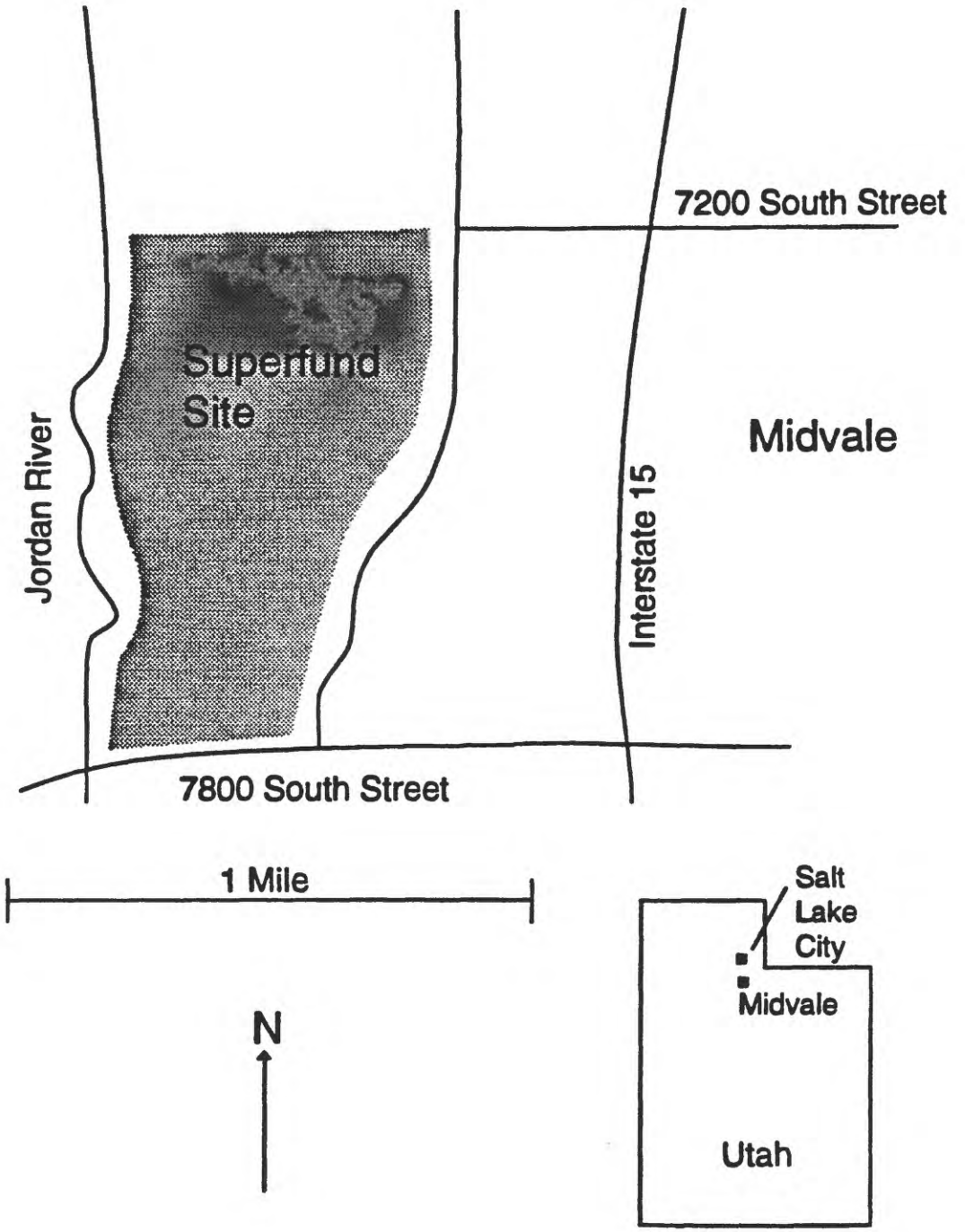

Figure 1. Location of the Midvale Superfund Site.

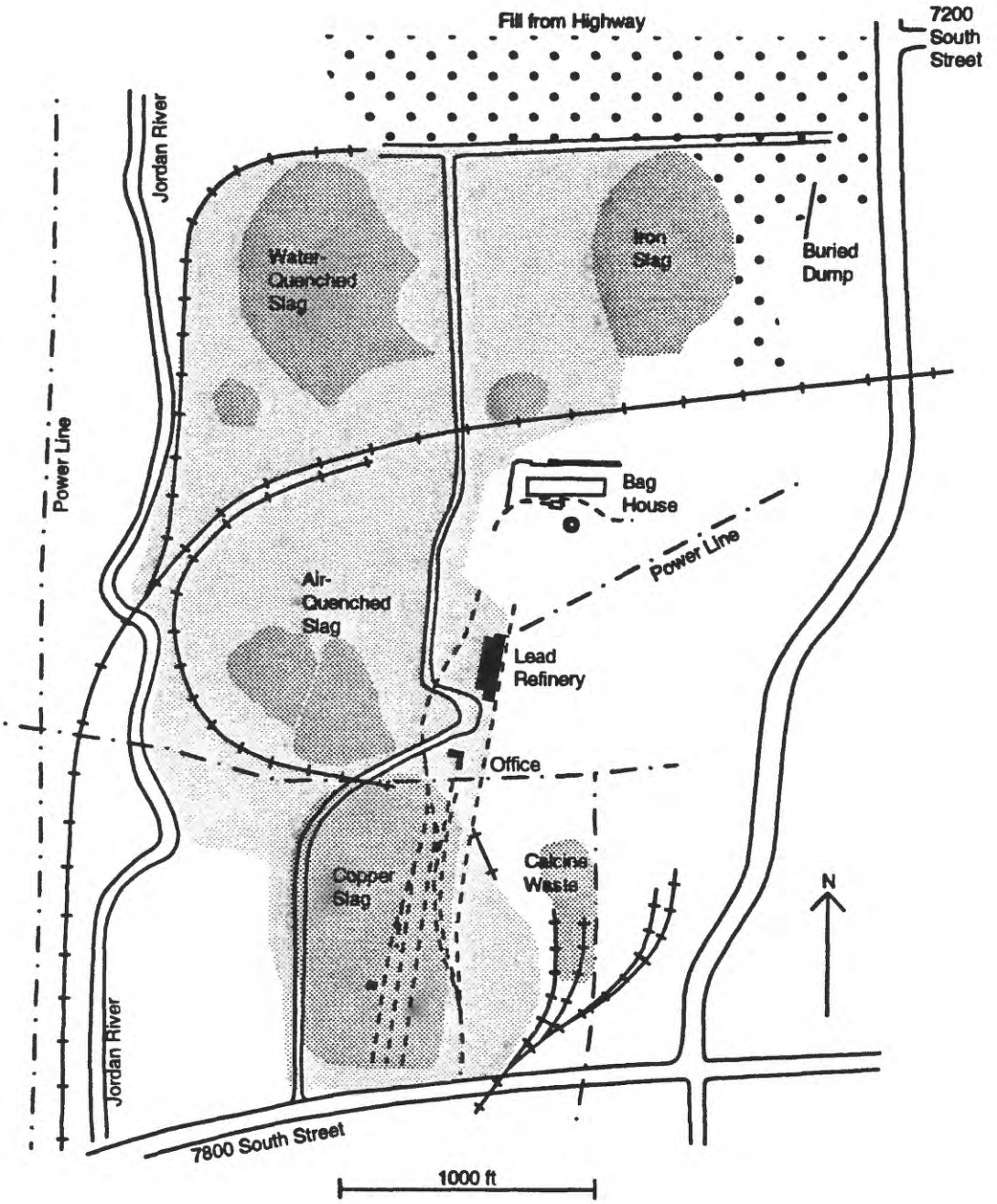

Figure 2. Man-made structures and waste piles on the superfund site. The dark grey areas represent the waste piles; the light grey areas the thin layer of slag at the surface. The solid polygons represent existing buildings; the open polygons buildings that were recorded on engineering drawings but are now demolished. The dotted lines represent railroad tracks recorded on engineering drawings but now are not visible at the surface. Only those man-made structures that might affect our interpretation of the geophysical data are on this map; many others exist.

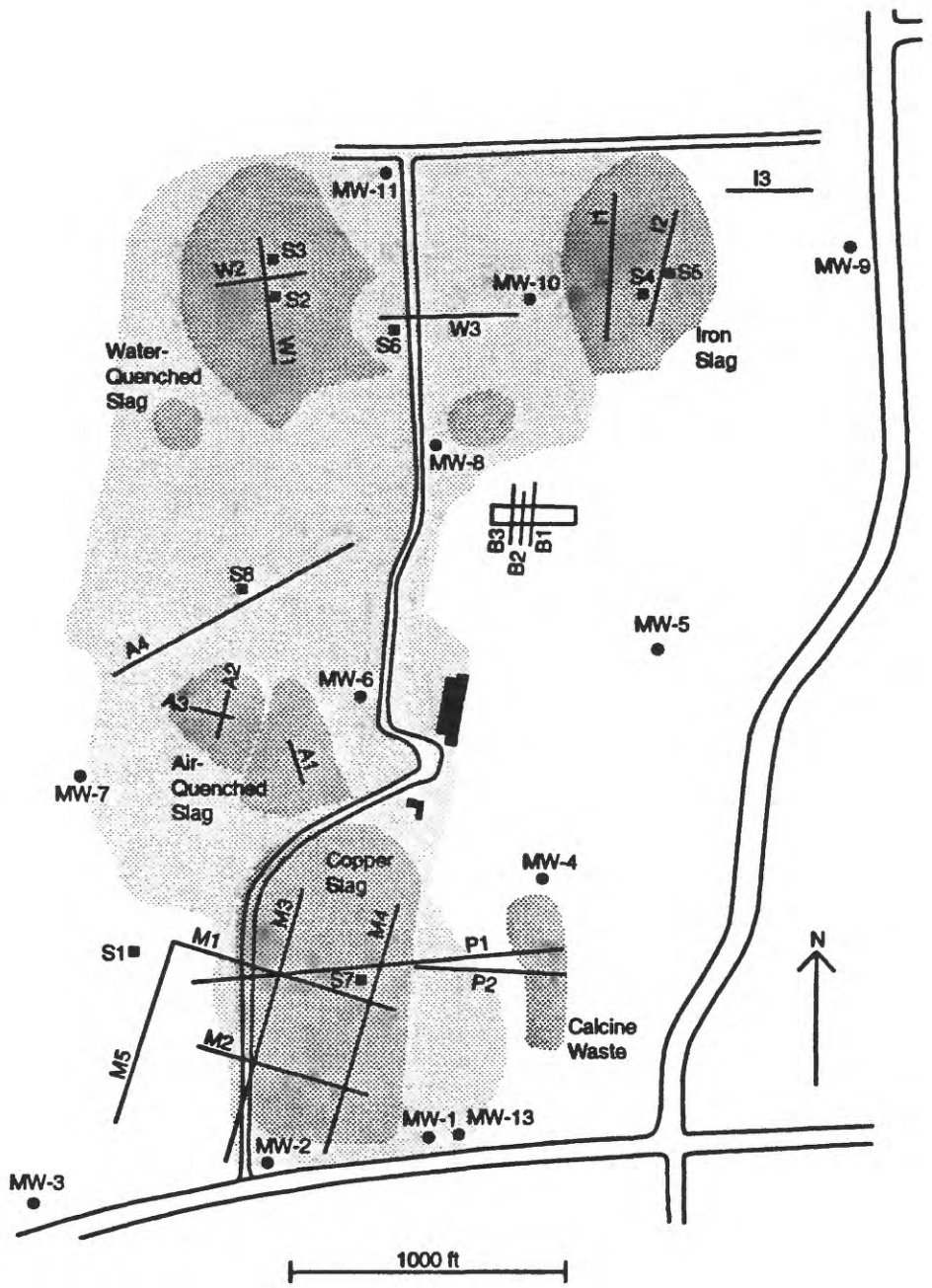

Figure 3. Locations of profiles, soundings, and monitoring wells at the superfund site. The profiles are symbolized by the labeled black lines. The soundings are symbolized by the black squares, and their labels begin with "S". The monitoring wells are symbolized by the black circles, and their labels begin with "MW". Monitoring well MW-12 is not shown because it is approximately 1 mile north of the water quenched slag.

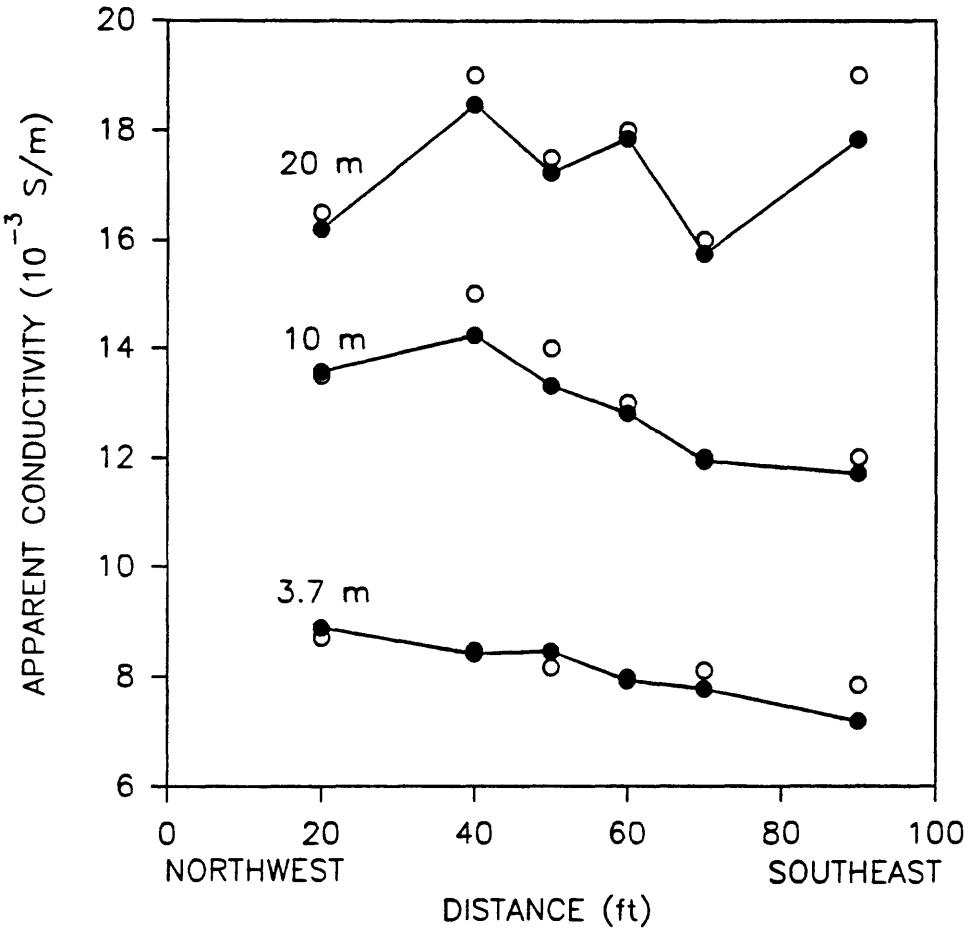

Figure 4. Terrain conductivity data in the HCP configuration for profile A1. The open circles are the field data, the solid circles are the data predicted by the inversion, and the three distances refer to the inter-coil spacing.

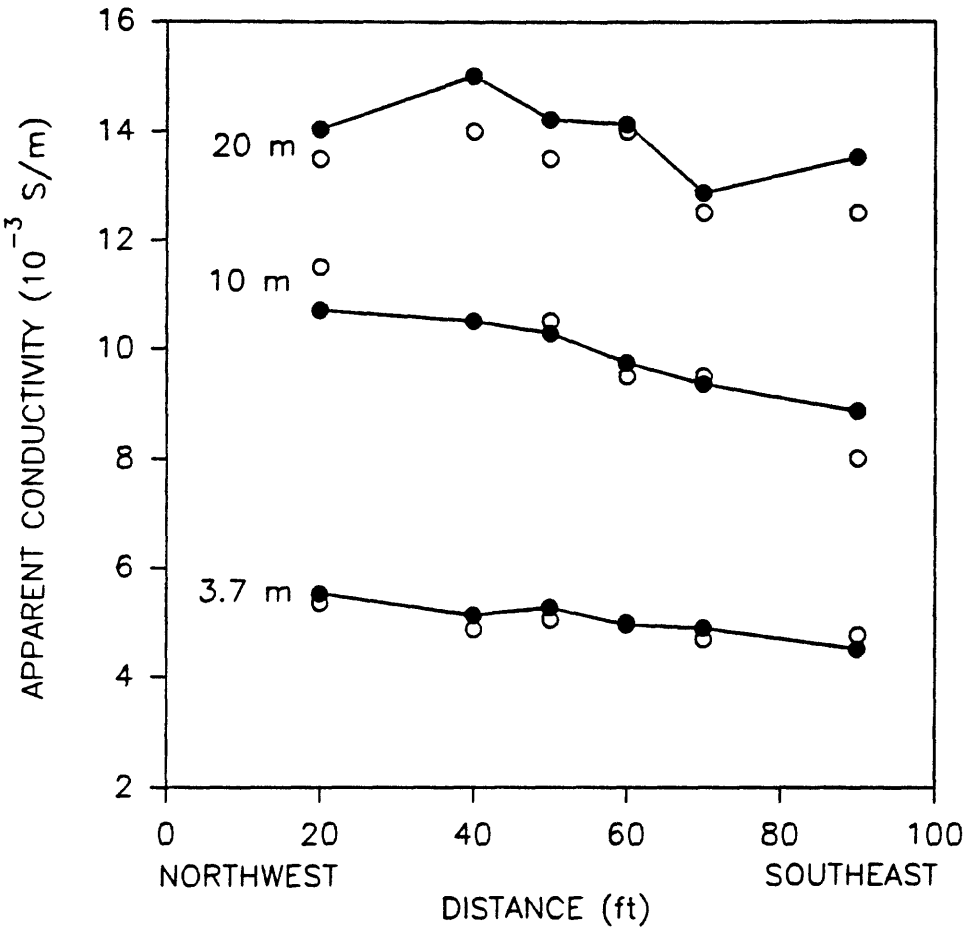

Figure 5. Terrain conductivity data in the VCP configuration for profile A1. The open circles are the field data, the solid circles are the data predicted by the inversion, and the three distances refer to the inter-coil spacing.

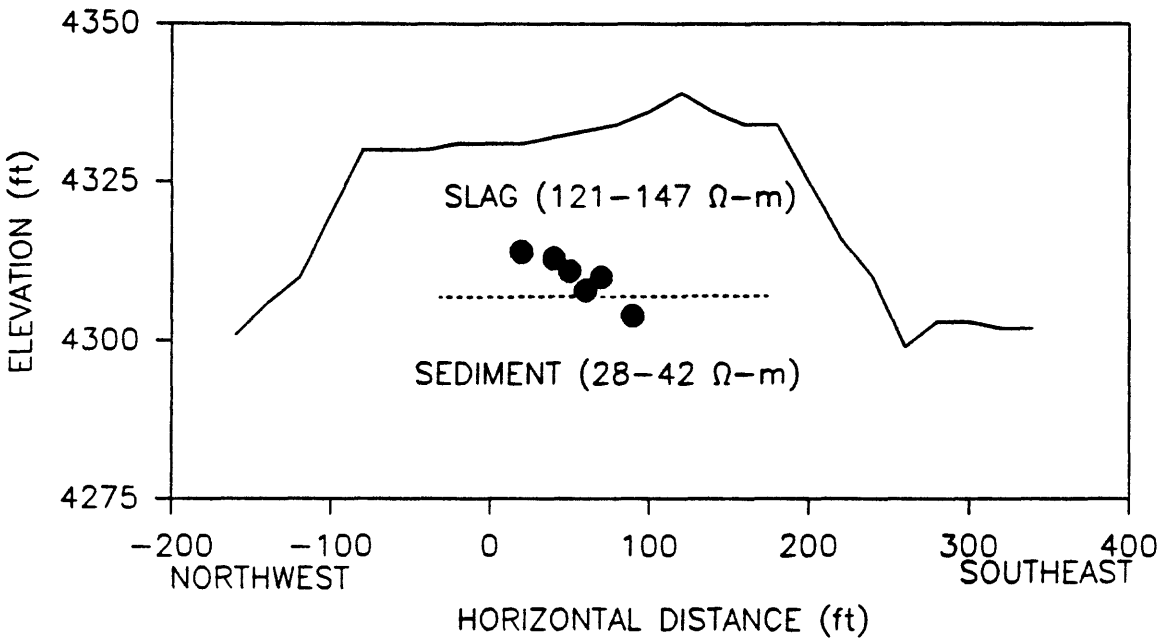

Figure 6. Cross section through the eastern, air-quenched, slag pile along profile A1. The solid line represents the upper surface of the pile, the solid circles the slag-sediment interface estimated from the data, the dotted line our estimate of the location of the interface. Distances are measured with respect the northernmost station; the vertical exageration is 4.

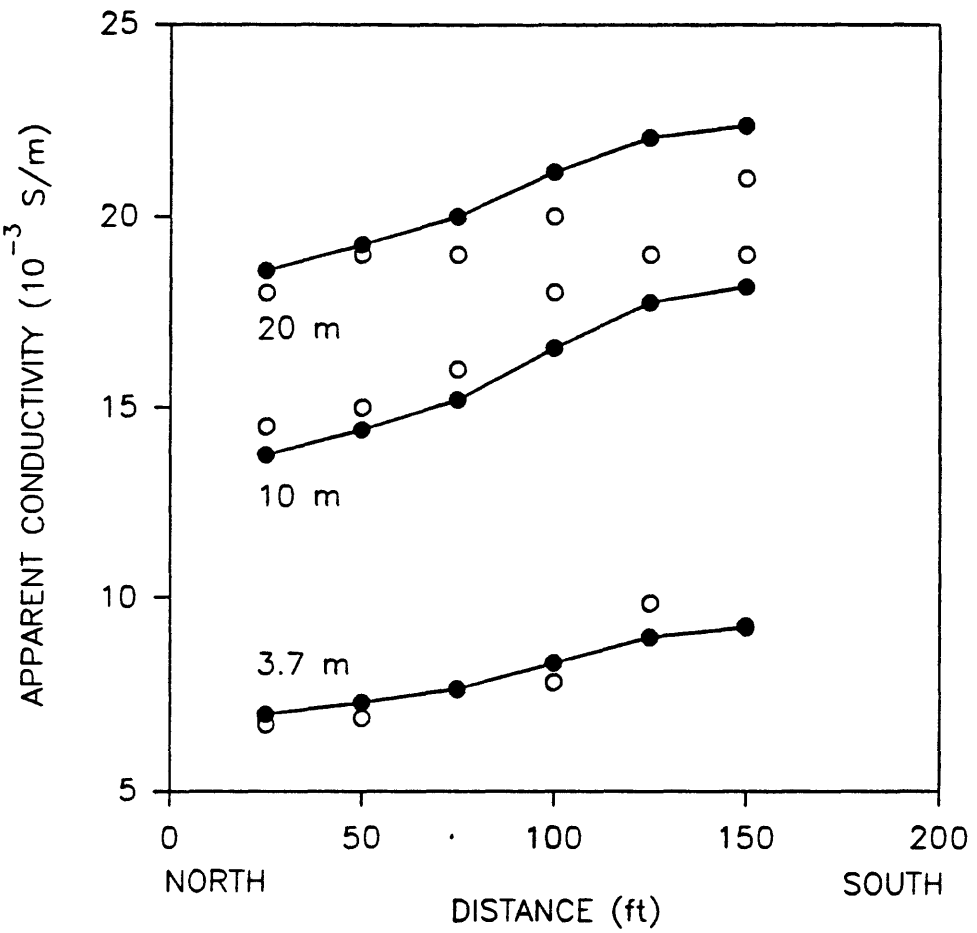

Figure 7. Terrain conductivity data in the VCP configuration for profile A2. The open circles are the field data, the solid circles are the data predicted by the inversion, and the three distances refer to the inter-coil spacing.

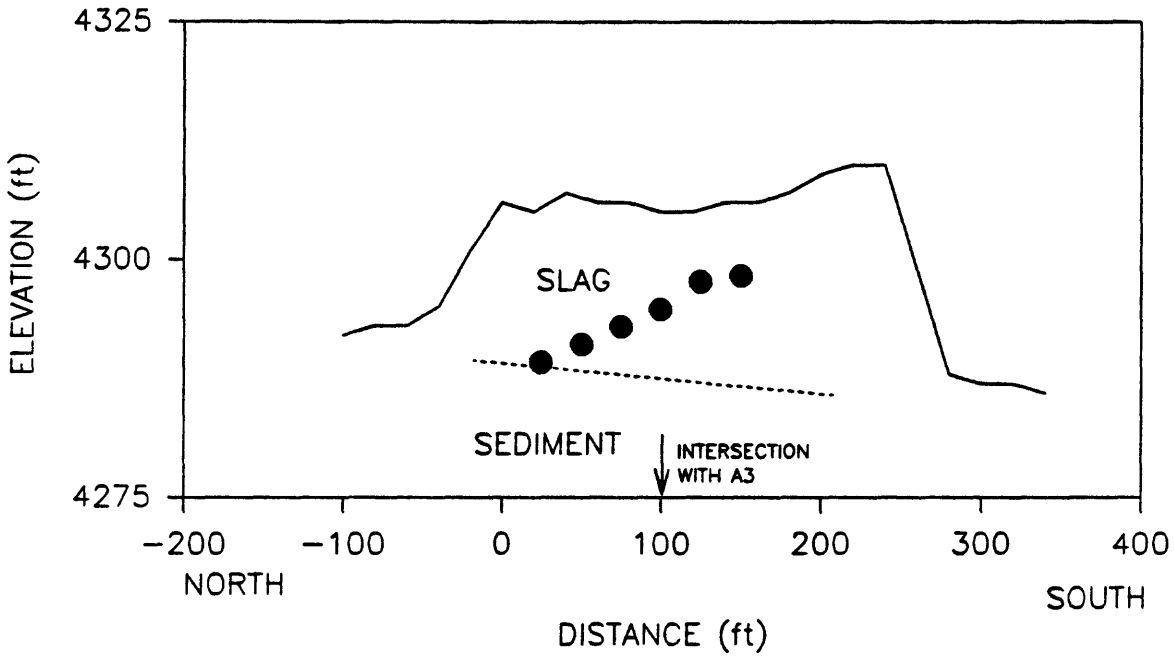

Figure 8. Cross section through the western, air-quenched, slag pile along profile A2. The solid line represents the upper surface of the pile, the solid circles the slag-sediment interface estimated from the data, the dotted line our estimate of the location of the interface. The ranges in resistivities are the minimum and maximum values estimated from all stations along the profile. Distances are measured with respect the northernmost station; the vertical exageration is 6.

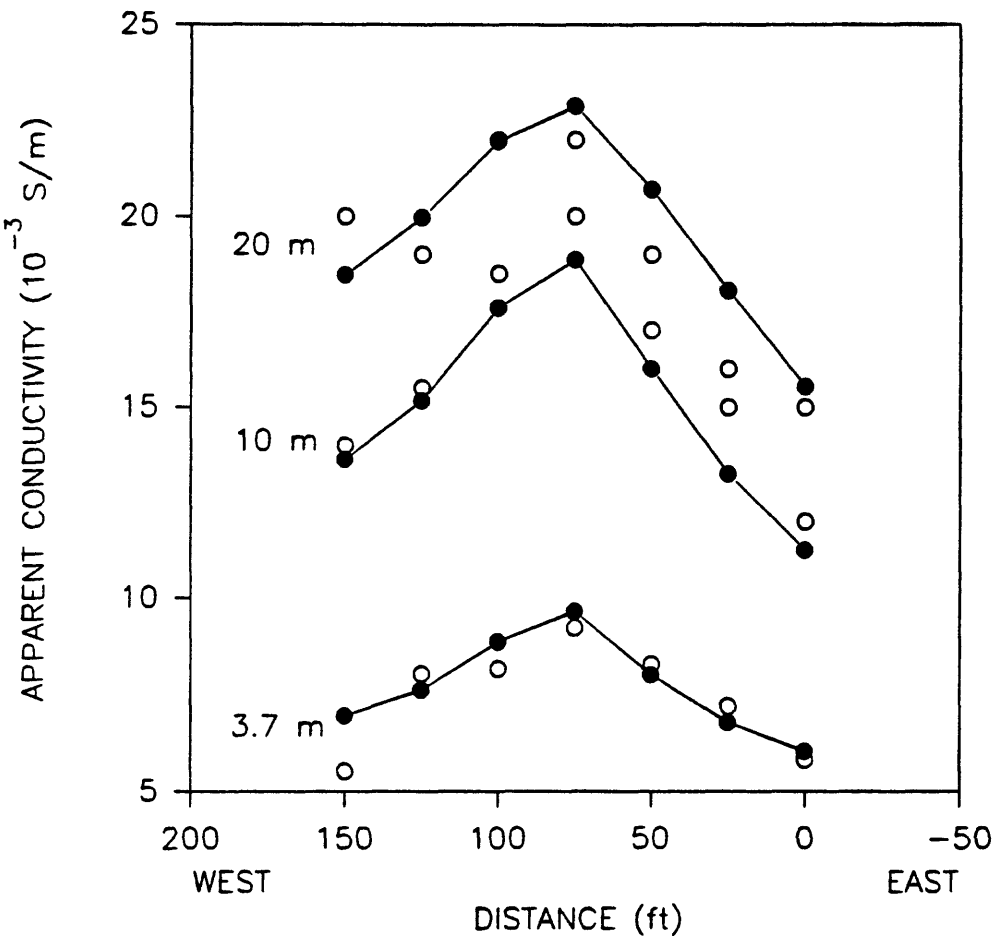

Figure 9. Terrain conductivity data in the VCP configuration for profile A3. The open circles are the field data, the solid circles are the data predicted by the inversion, and the three distances refer to the inter-coil spacing.

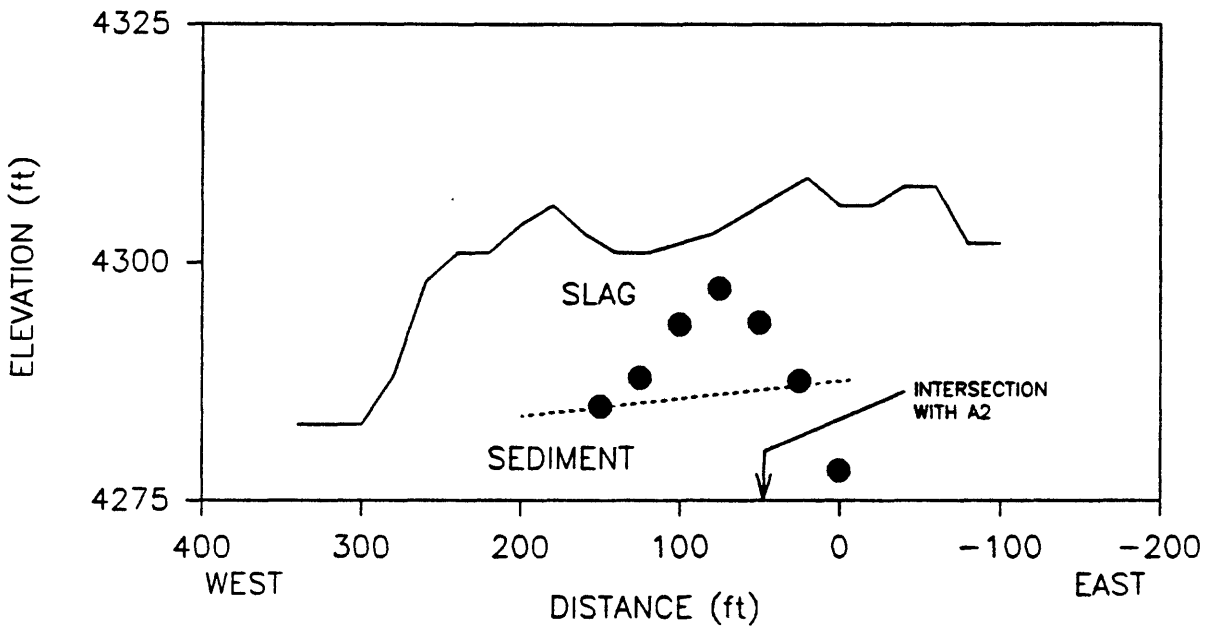

Figure 10. Cross section through the western, air-quenched, slag pile along profile A3. The solid line represents the upper surface of the pile, the solid circles the slag-sediment interface estimated from the data, the dotted line our estimate of the location of the interface. Distances are measured with respect the easternmost station; the vertical exageration is 6.

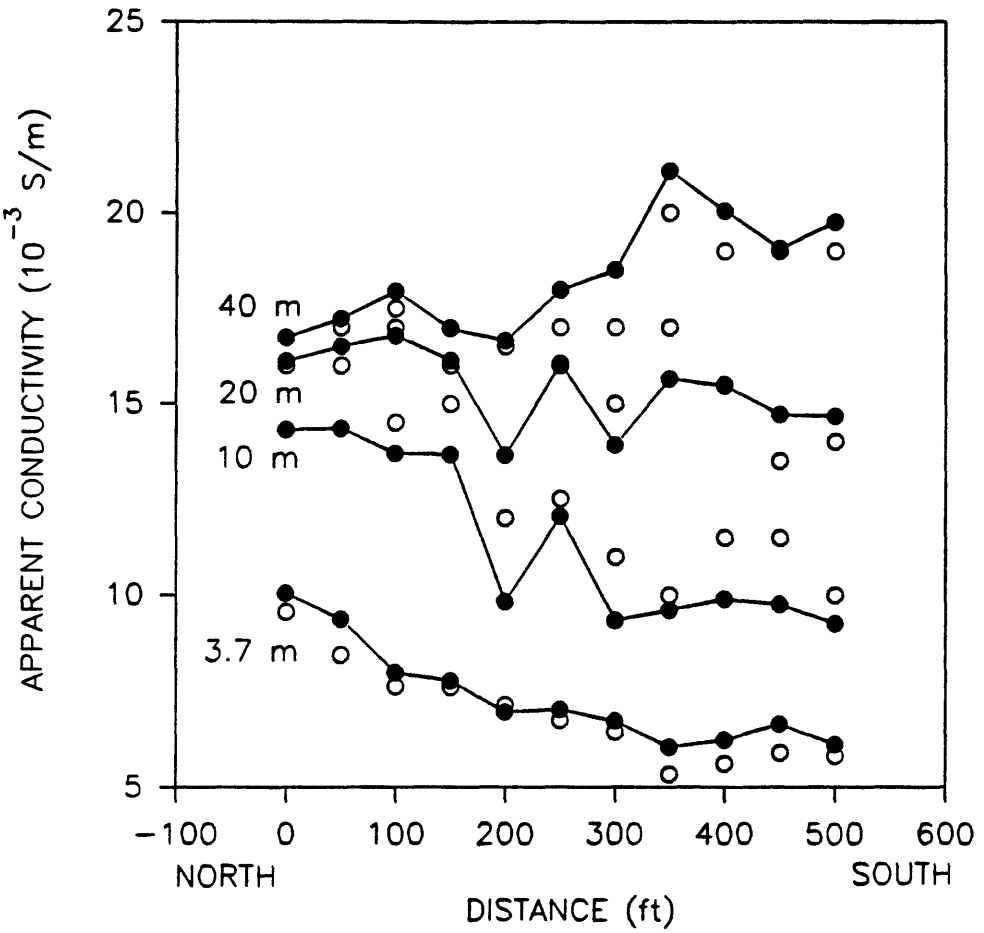

Figure 11. Terrain conductivity data in the HCP configuration for profile I1. The open circles are the field data, the solid circles are the data predicted by the inversion, and the four distances refer to the inter-coil spacing.

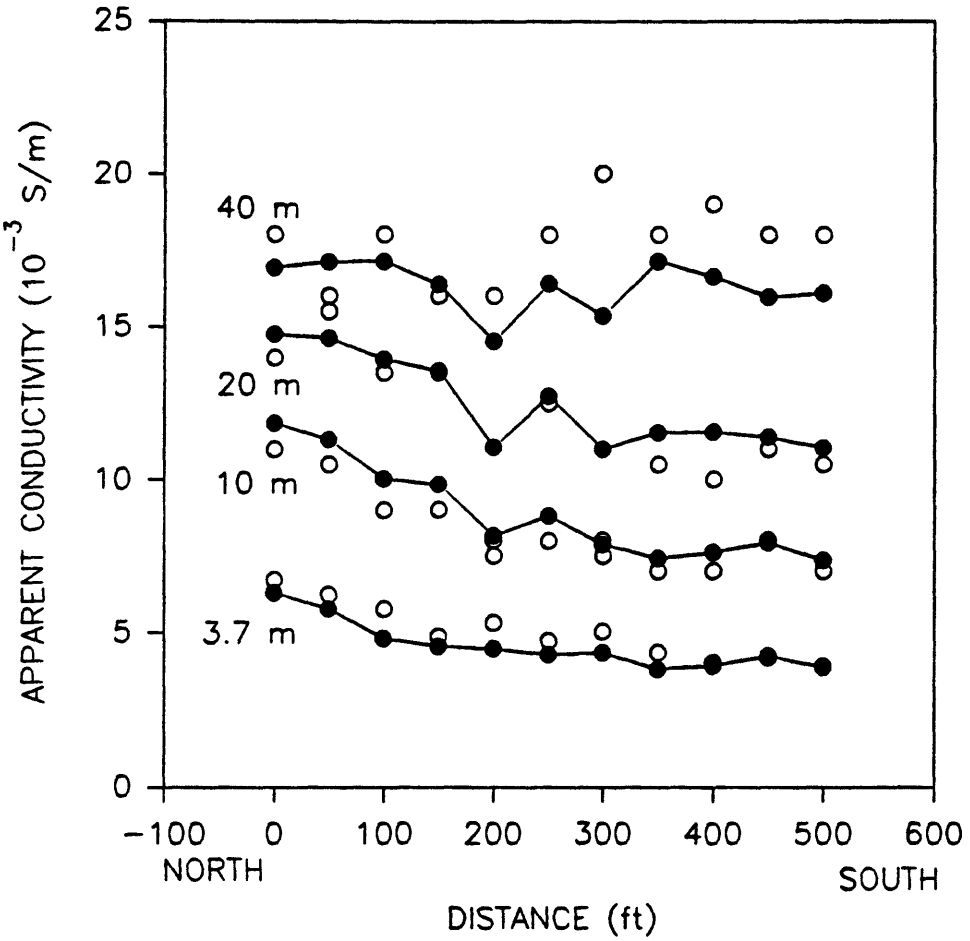

Figure 12. Terrain conductivity data in the VCP configuration for profile I1. The open circles are the field data, the solid circles are the data predicted by the inversion, and the four distances refer to the inter-coil spacing.

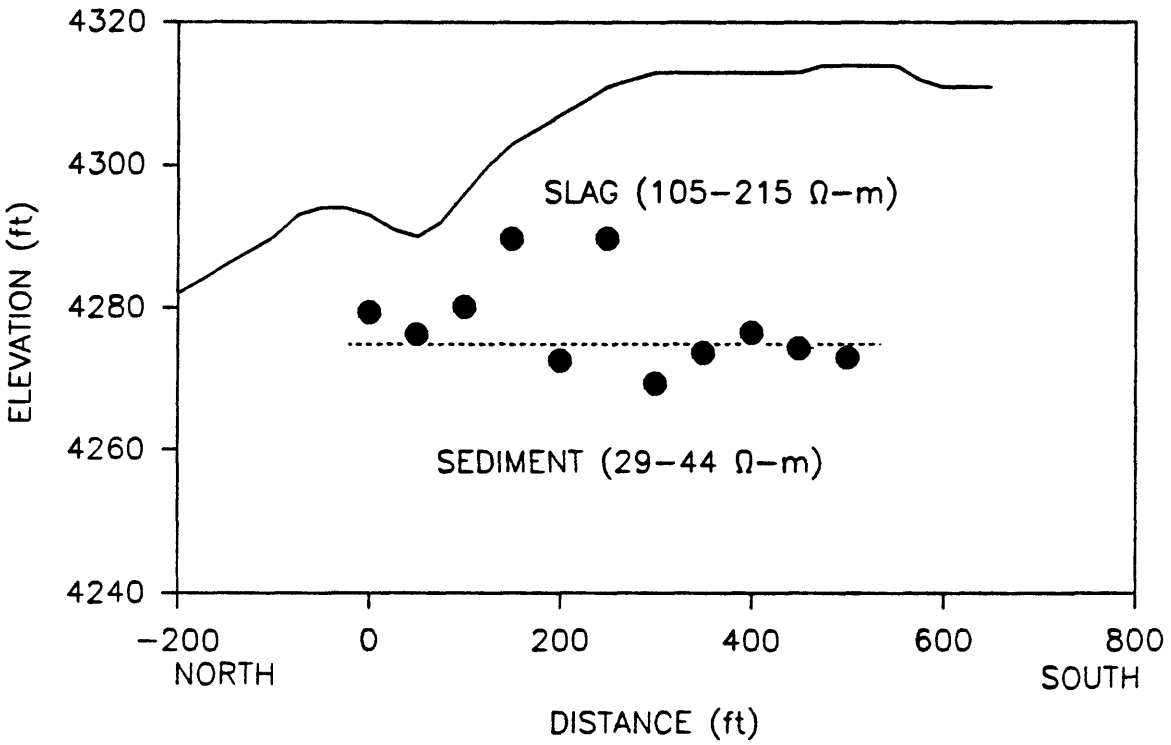

Figure 13. Cross section through the iron slag pile along profile I1. The solid line represents the upper surface of the pile, the solid circles the slag-sediment interface estimated from the data, the dotted line our estimate of the location of the interface. The ranges in resistivities are the minimum and maximum values estimated from all stations along the profile. Distances are measured with respect the northernmost station; the vertical exageration is 7.5.

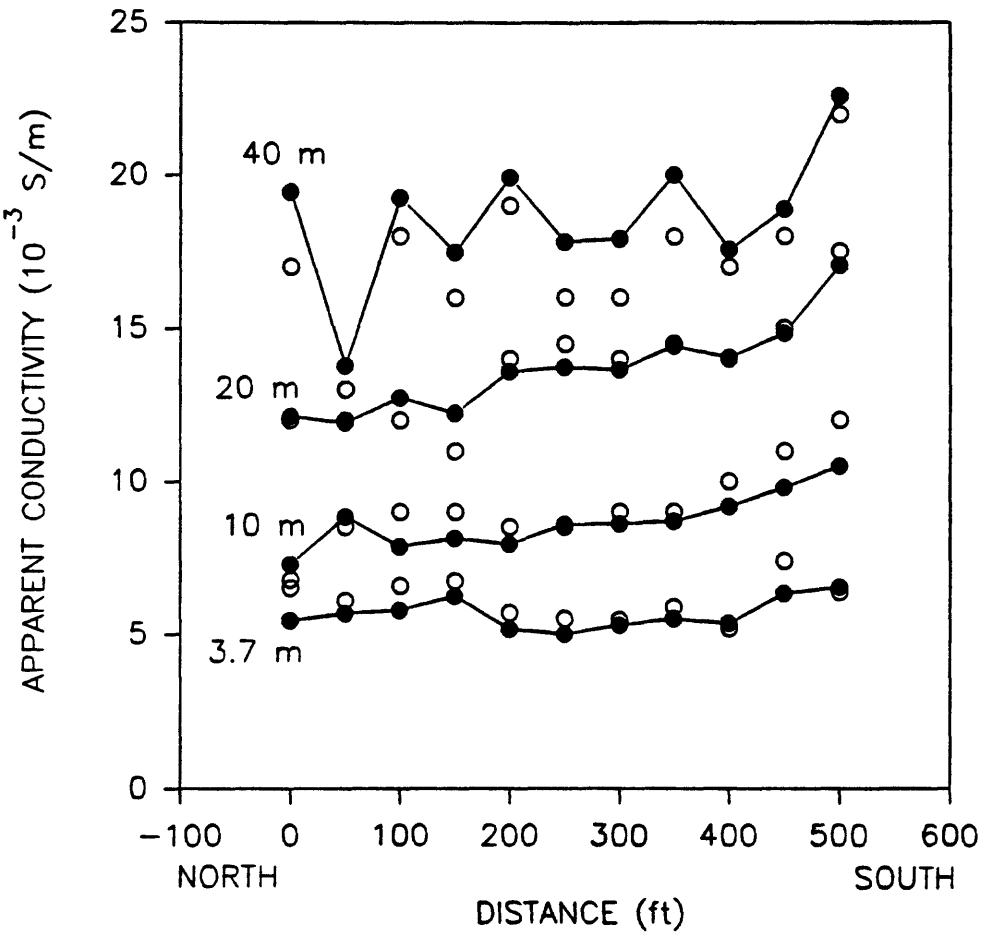

Figure 14. Terrain conductivity data in the HCP configuration for profile I2. The open circles are the field data, the solid circles are the data predicted by the inversion, and the four distances refer to the inter-coil spacing.

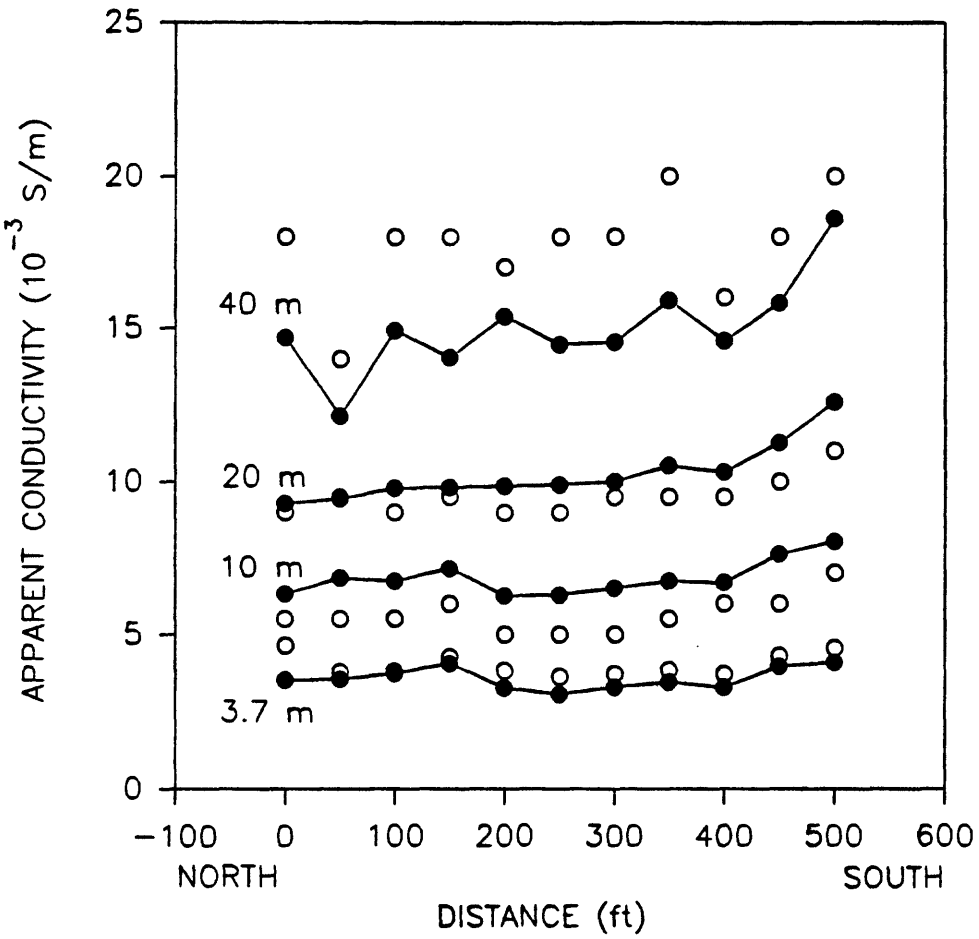

Figure 15. Terrain conductivity data in the VCP configuration for profile I2. The open circles are the field data, the solid circles are the data predicted by the inversion, and the four distances refer to the inter-coil spacing.

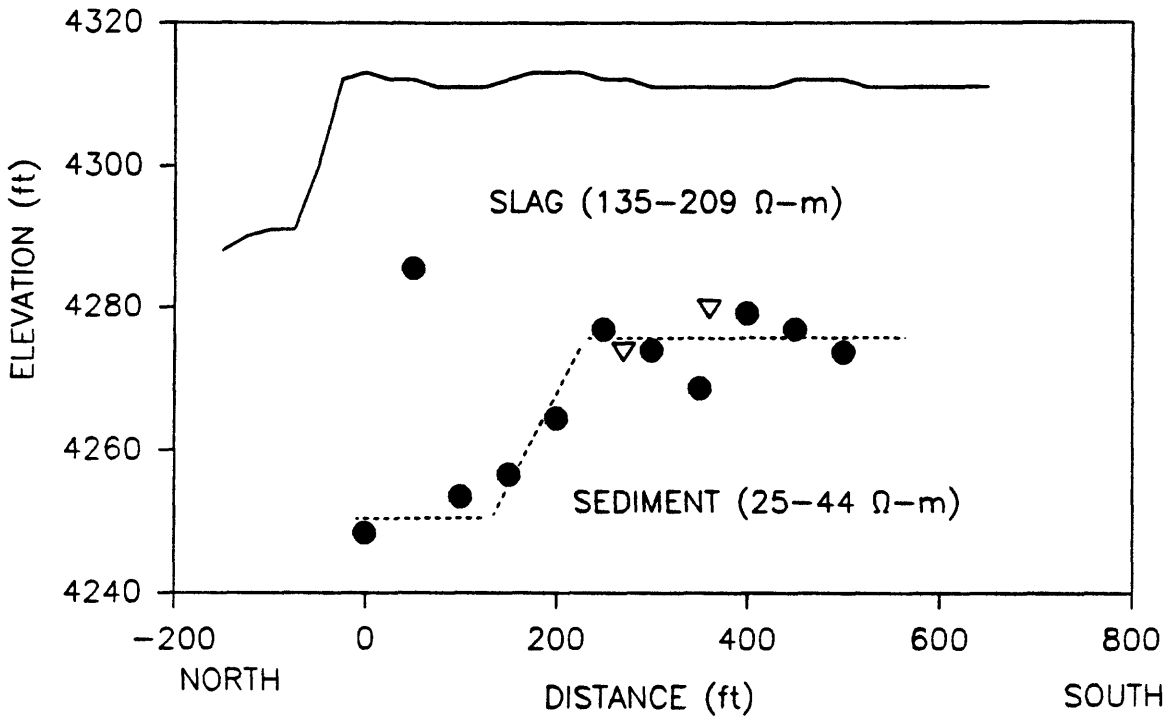

Figure 16. Cross section through the iron slag pile along profile I2. The solid line represents the upper surface of the pile, the solid circles the slag-sediment interface estimated from the terrain conductivity data, the open triangles the interface estimated from the time-domain electromagnetic data, the dotted line our estimate of the location of the interface. The ranges in resistivities are the minimum and maximum values estimated from all stations along the profile. Distances are measured with respect the northernmost station; the vertical exageration is 7.5.

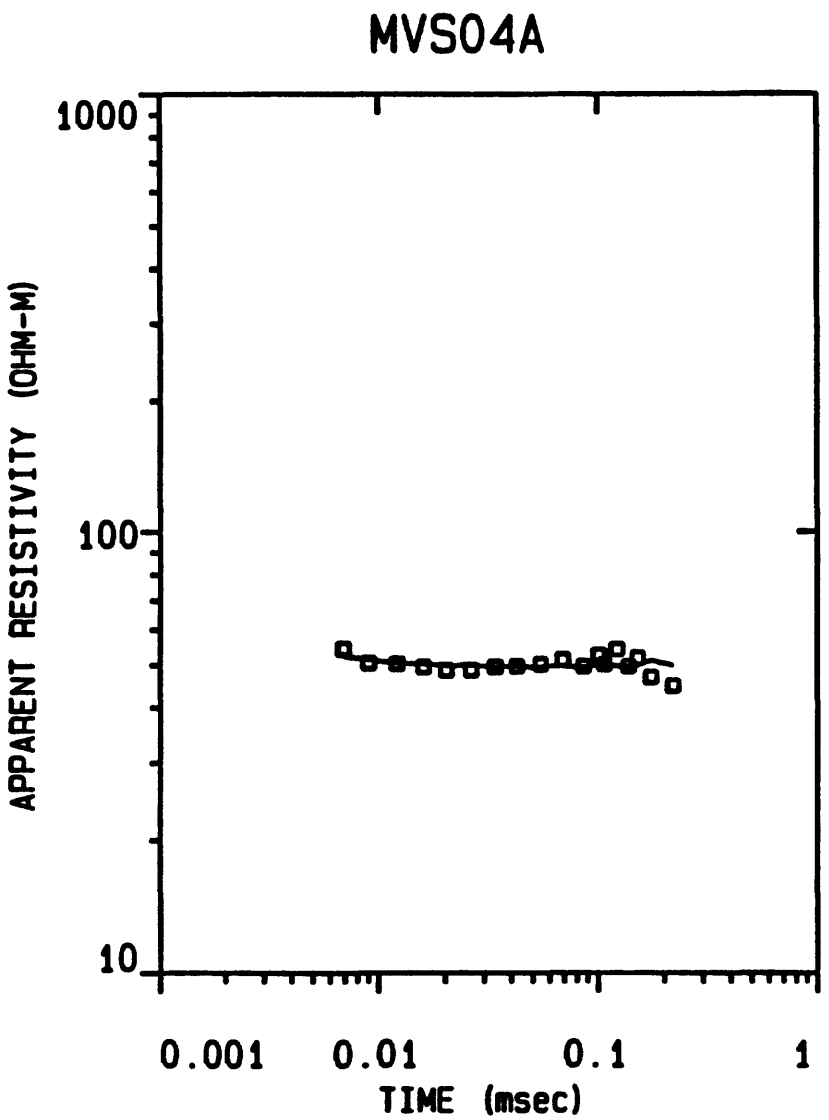

Figure 17. Time-domain electromagnetic data collected at sounding S4, which is near profile I2. The open squares are the field data, the solid line the data predicted by the inversion.

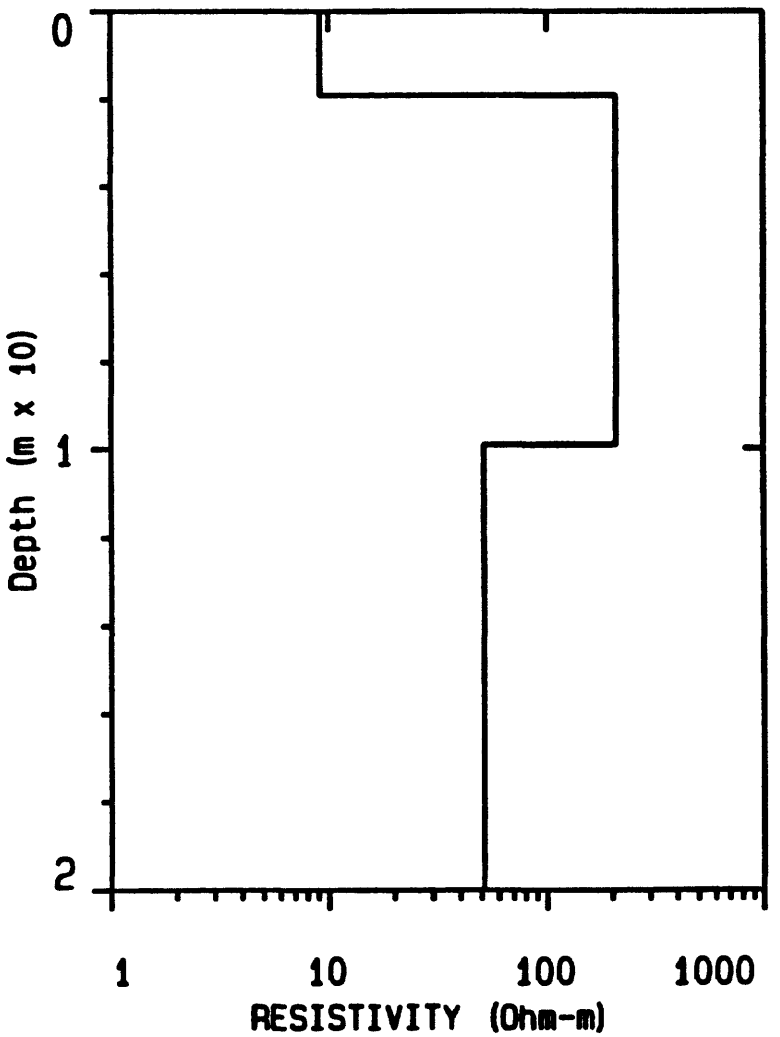

Figure 18. Electrical model of the near-surface determined by the inversion of the time-domain electromagnetic data from sounding S4.

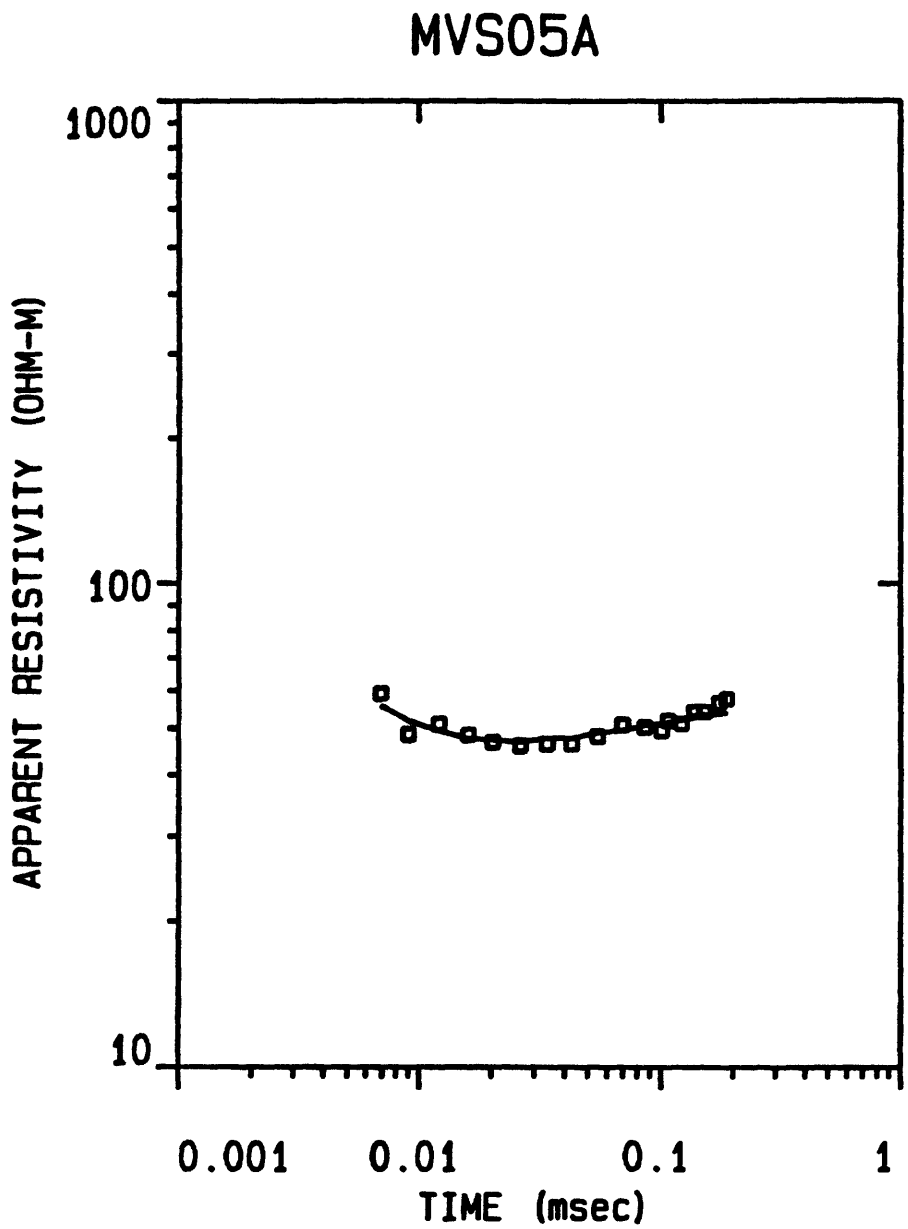

Figure 19. Time-domain electromagnetic data collected at sounding S5, which is near profile I2. The open squares are the field data, the solid line the data predicted by the inversion.

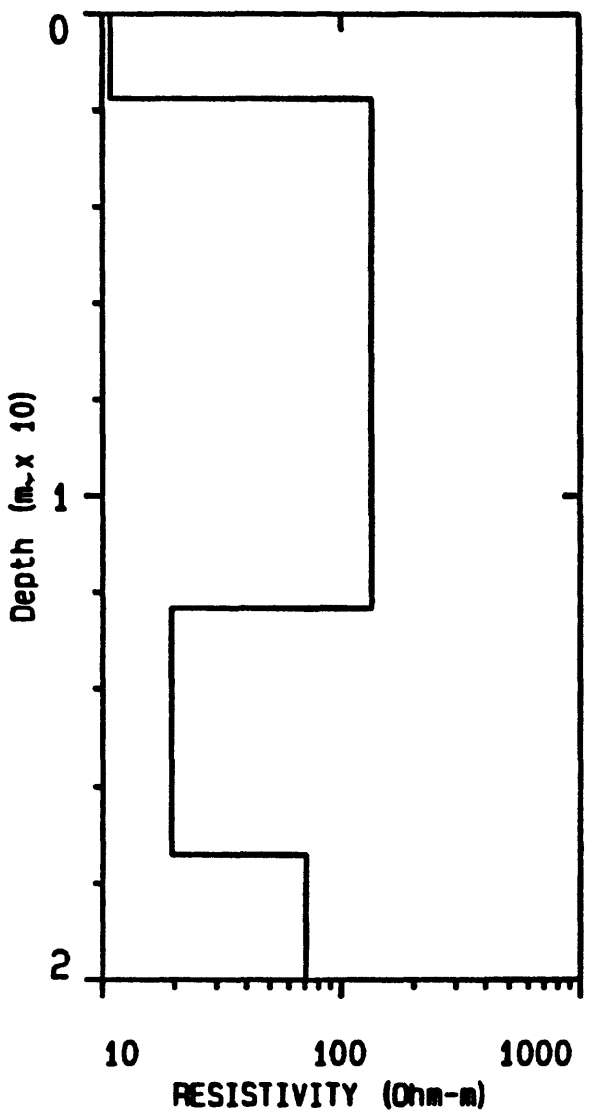

Figure 20. Electrical model of the near-surface determined by the inversion of the time-domain electromagnetic data from sounding S5.

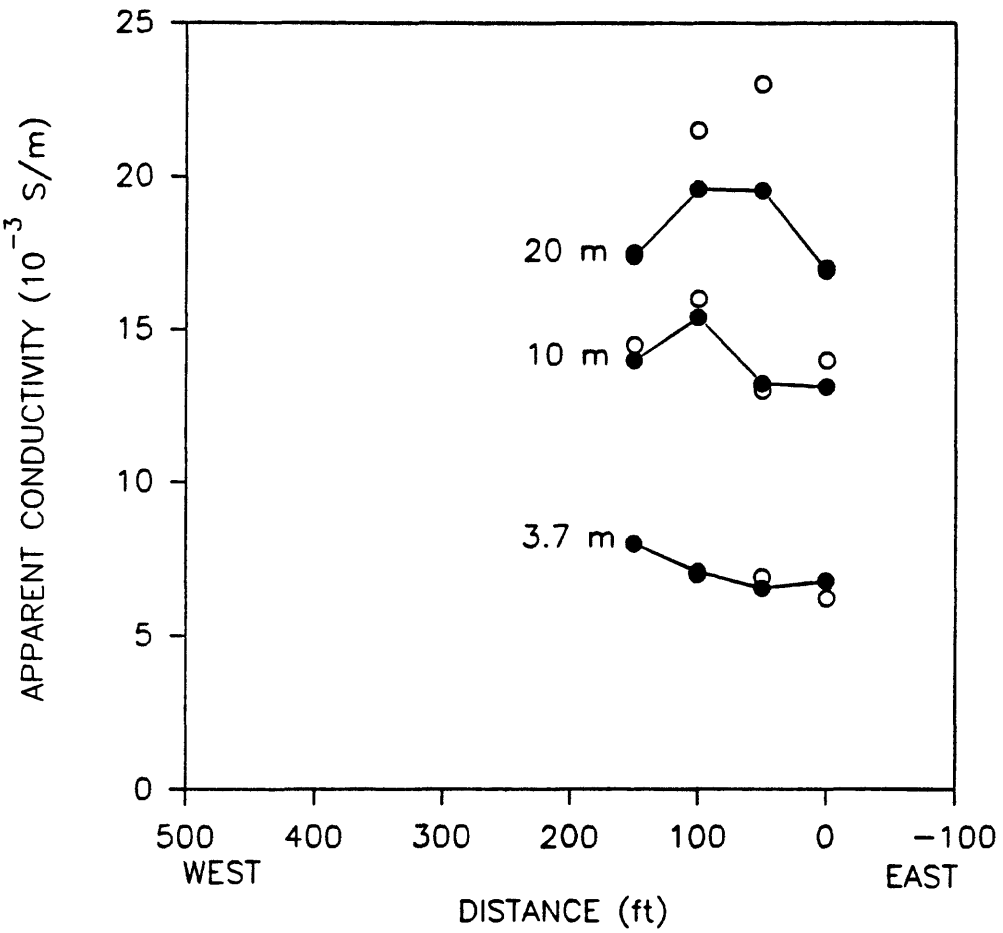

Figure 21. Terrain conductivity data in the HCP configuration for first four stations along profile M1. The open circles are the field data, the solid circles are the data predicted by the inversion, and the three distances refer to the inter-coil spacing.

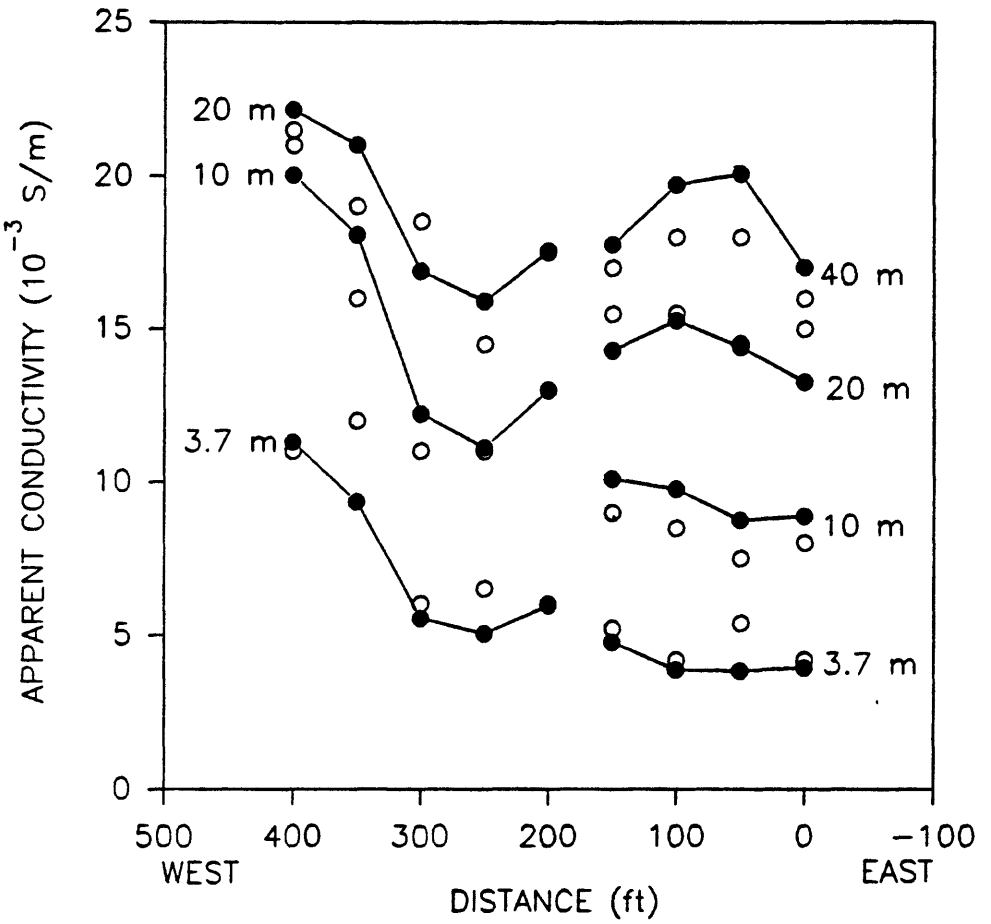

Figure 22. Terrain conductivity data in the VCP configuration for profile M1. The open circles are the field data, the solid circles are the data predicted by the inversion, and the four distances refer to the inter-coil spacing.

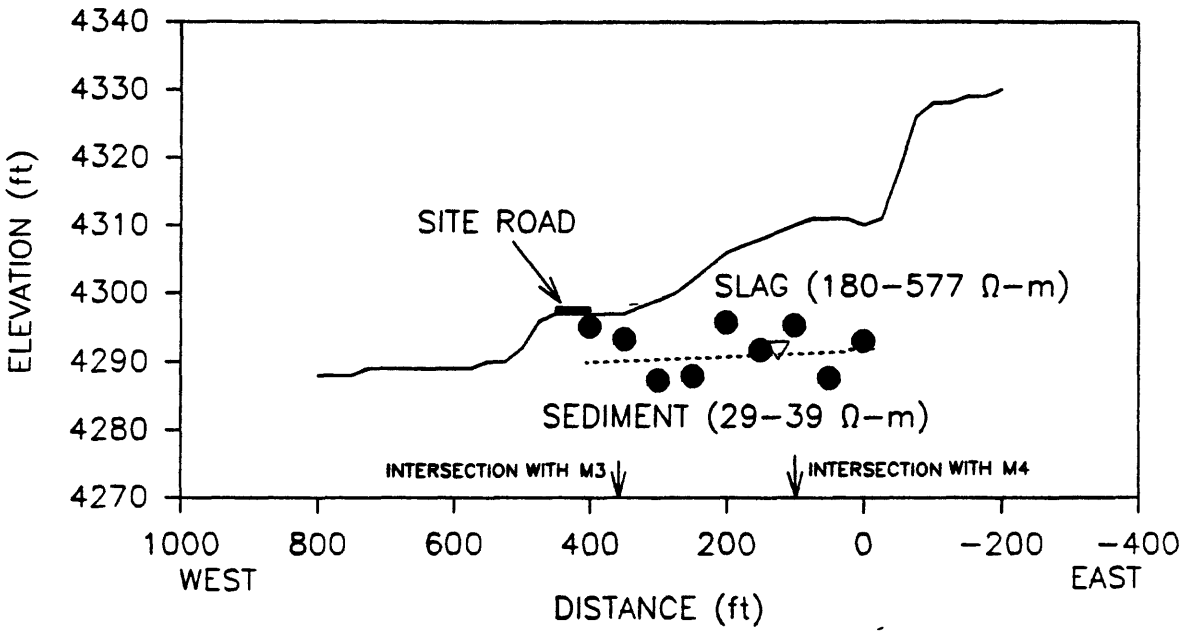

Figure 23. Cross section through the mixed slag pile along profile M1. The solid line represents the upper surface of the pile, the solid circles the slag-sediment interface estimated from the terrain conductivity data, the open triangle the slag-sediment interface estimated from the time-domain electromagnetic data, the dotted line our estimate of the location of the interface. The ranges in resistivities are the minimum and maximum values estimated from the first four stations. Distances are measured with respect the easternmost station; the vertical exageration is 10.

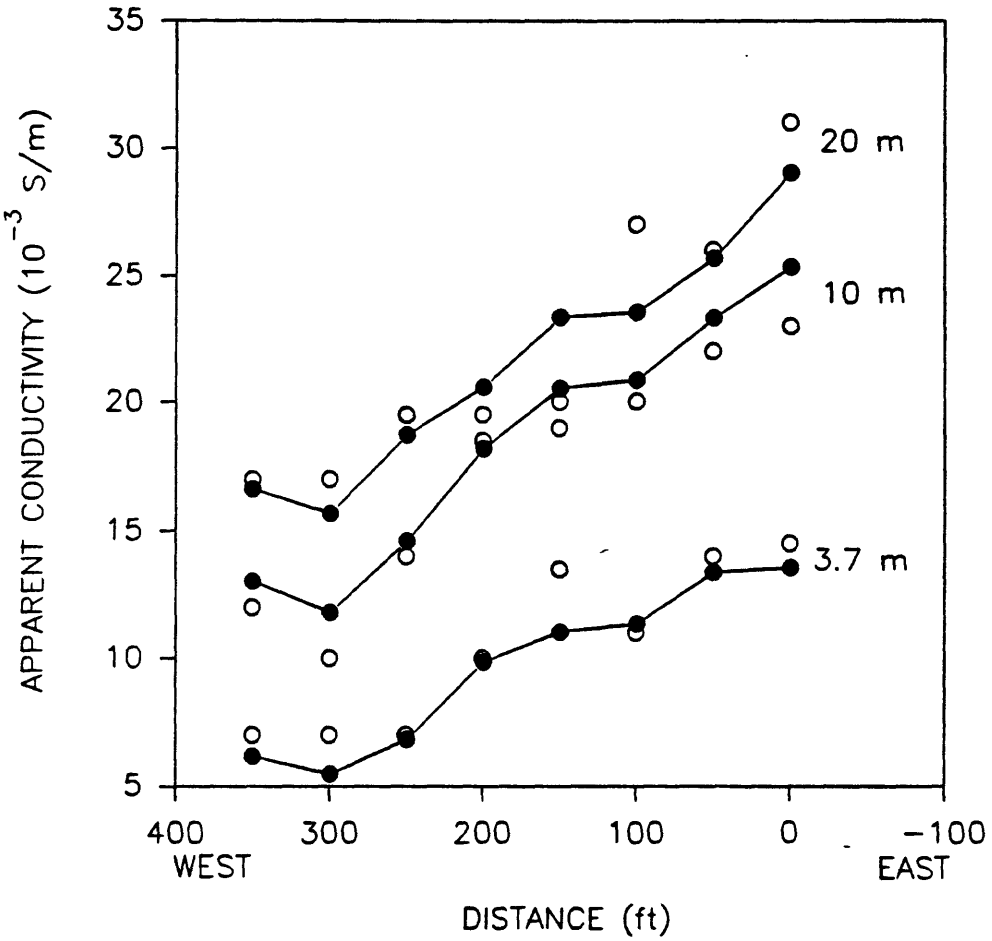

Figure 24. Terrain conductivity data in the VCP configuration for profile M2. The open circles are the field data, the solid circles are the data predicted by the inversion, and the three distances refer to the inter-coil spacing.

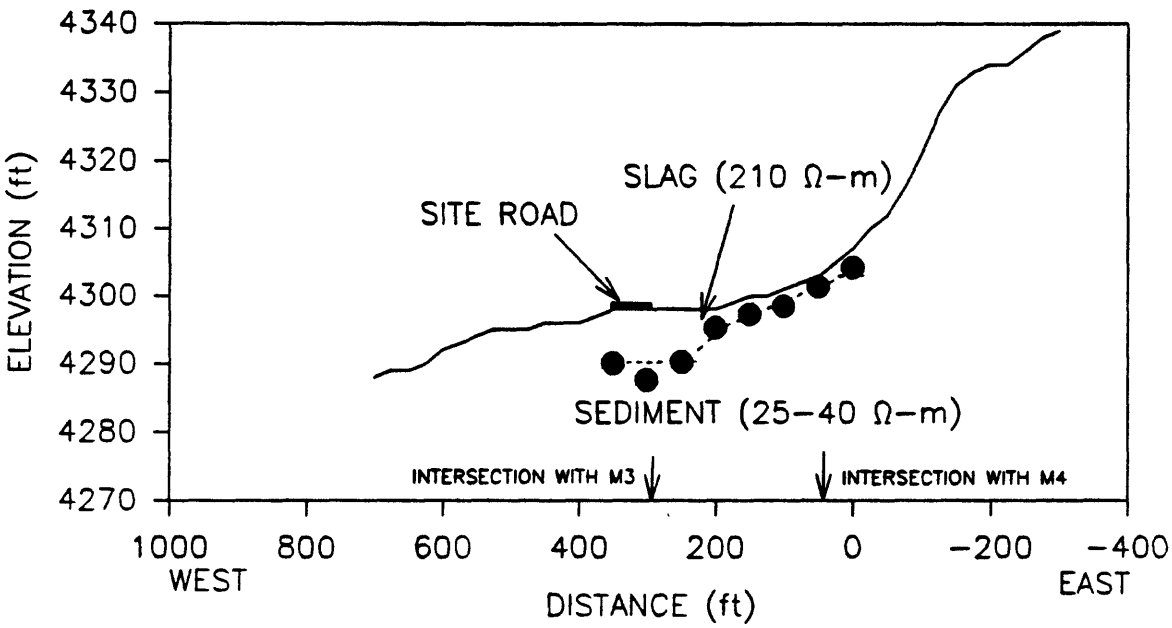

Figure 25. Cross section through the mixed slag pile along profile M2. The solid line represents the upper surface of the pile, the solid circles the slag-sediment interface estimated from the data, the dotted line our estimate of the location of the interface. Distances are measured with respect the easternmost station; the vertical exageration is 10.

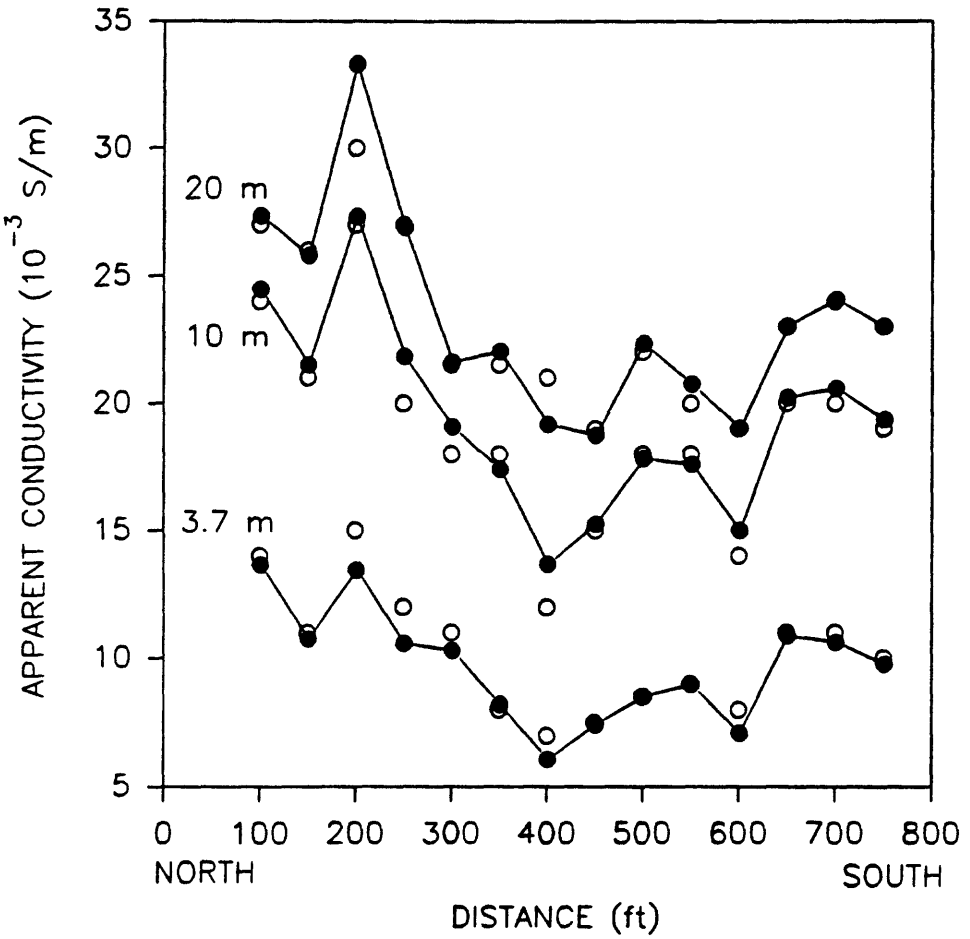

Figure 26. Terrain conductivity data in the VCP configuration for profile M3. The open circles are the field data, the solid circles are the data predicted by the inversion, and the three distances refer to the inter-coil spacing.

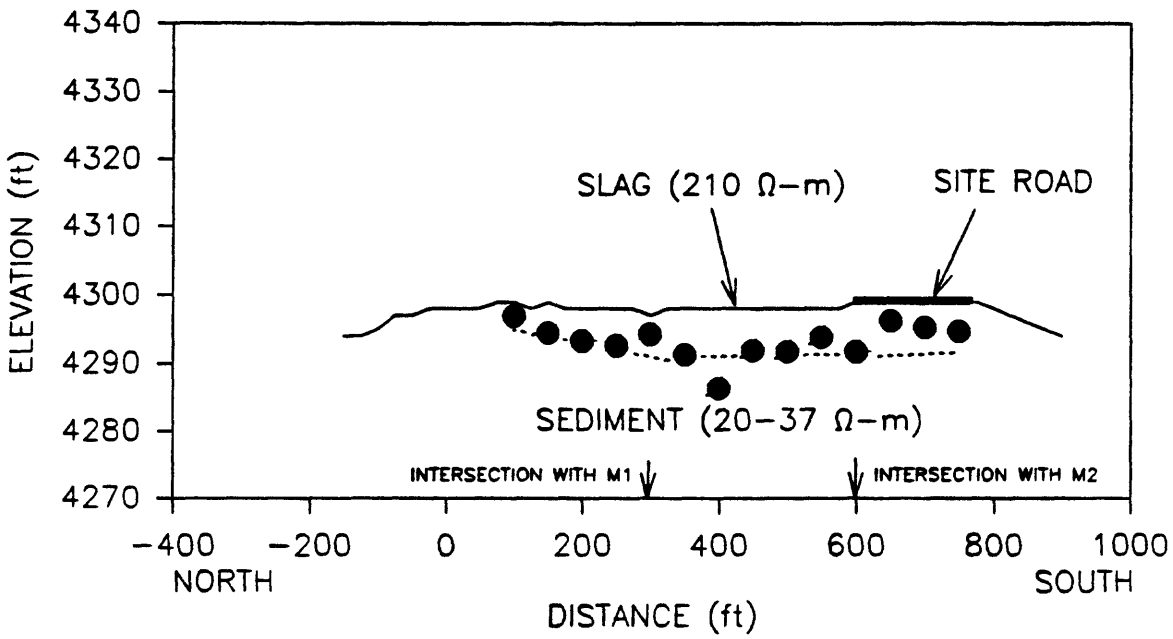

Figure 27. Cross section through the mixed slag pile along profile M3. The solid line represents the upper surface of the pile, the solid circles the slag-sediment interface estimated from the data, the dotted line our estimate of the location of the interface. Distances are measured with respect the northernmost station; the vertical exageration is 10.

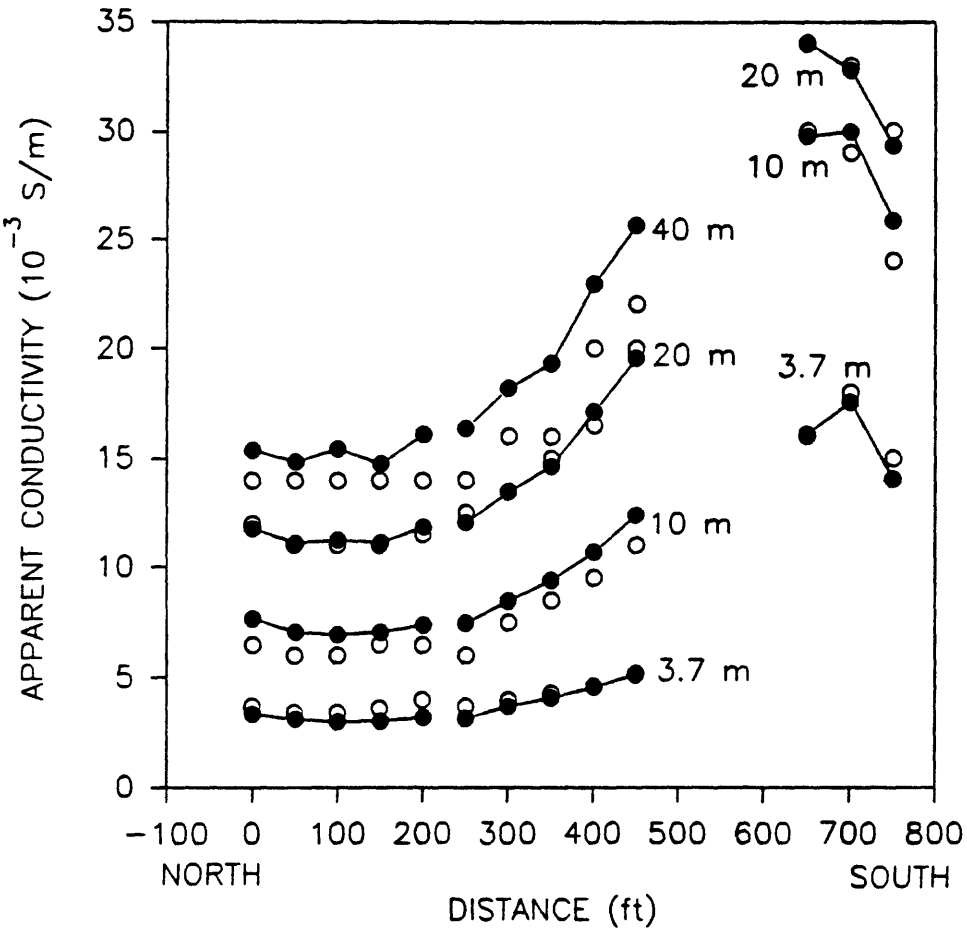

Figure 28. Terrain conductivity data in the HCP configuration for profile M4. The open circles are the field data, the solid circles are the data predicted by the inversion, and the four distances refer to the inter-coil spacing.

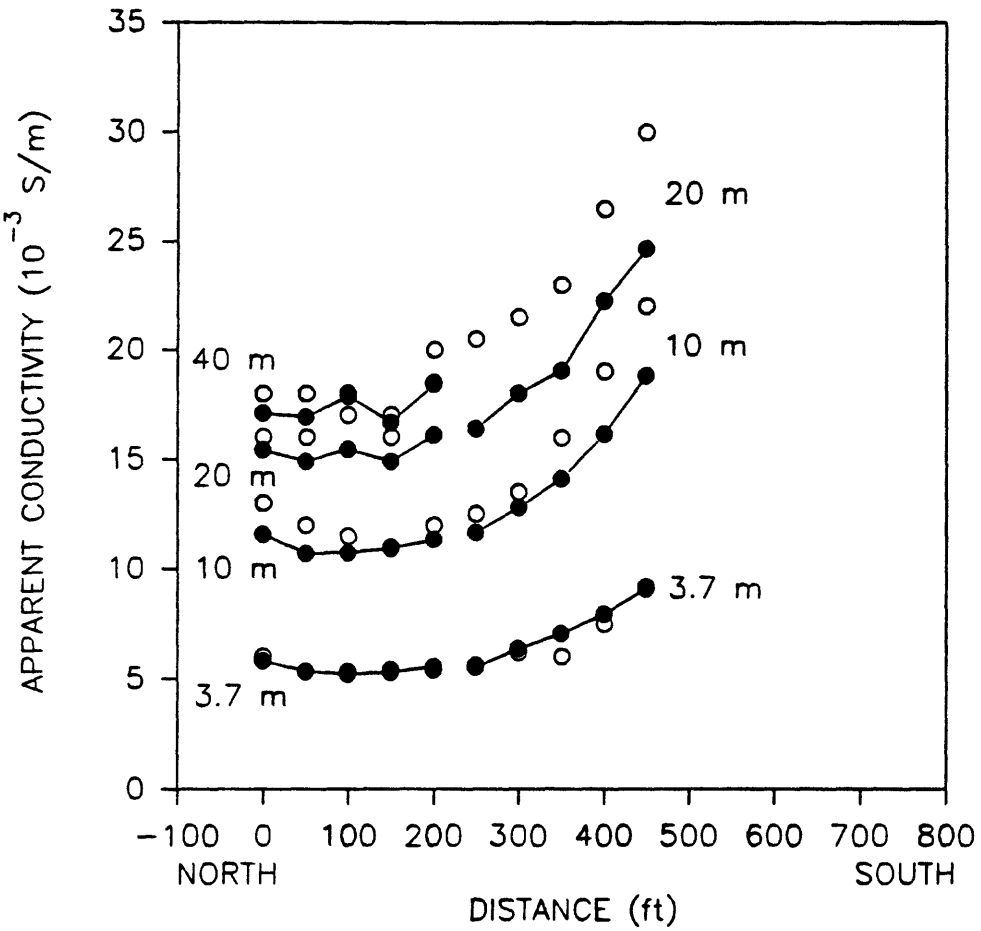

Figure 29. Terrain conductivity data in the VCP configuration for profile M4. The open circles are the field data, the solid circles are the data predicted by the inversion, and the four distances refer to the inter-coil spacing.

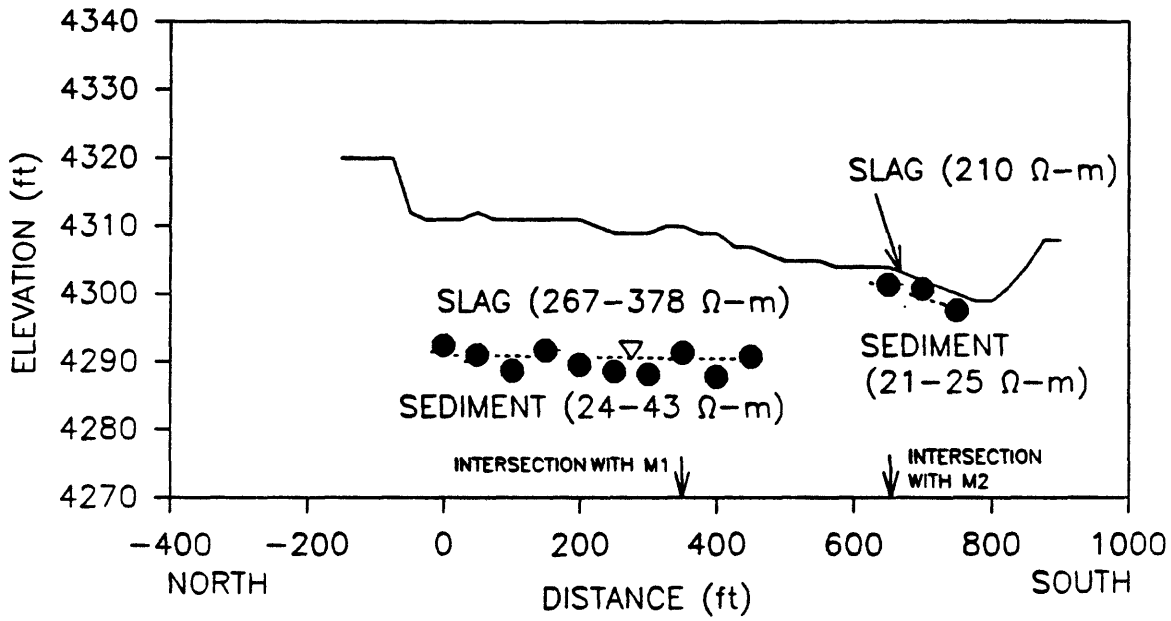

Figure 30. Cross section through the mixed slag pile along profile M4. The solid line represents the upper surface of the pile, the open triangle the slag-sediment interface estimated from the time-domain electromagnetic data, the solid circles the slag-sediment interface estimated from the data, the dotted line our estimate of the location of the interface. Distances are measured with respect the northernmost station; the vertical exageration is 10.

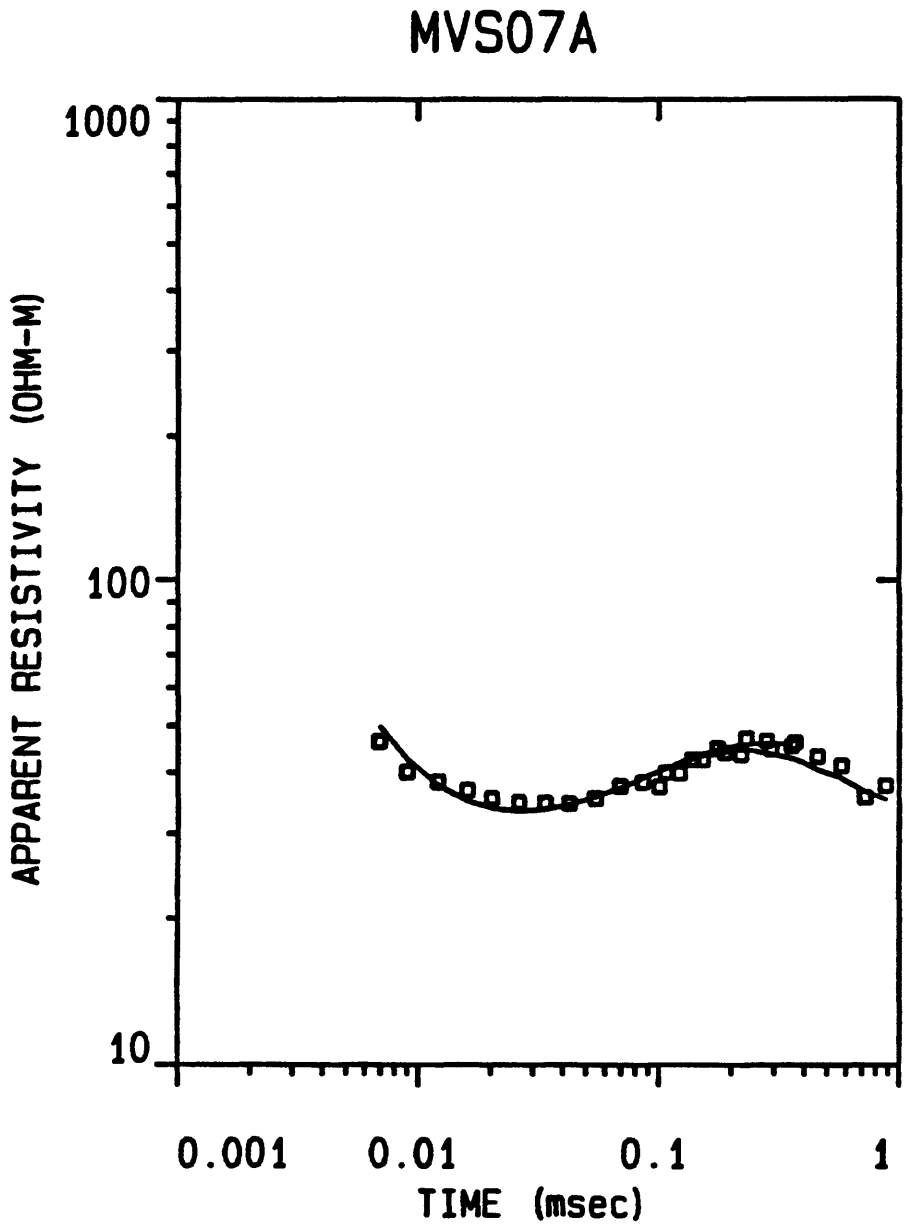

Figure 31. Time-domain electromagnetic data collected at sounding S7, which is near profiles M1 and M4. The open squares are the field data, the solid line the data predicted by the inversion.

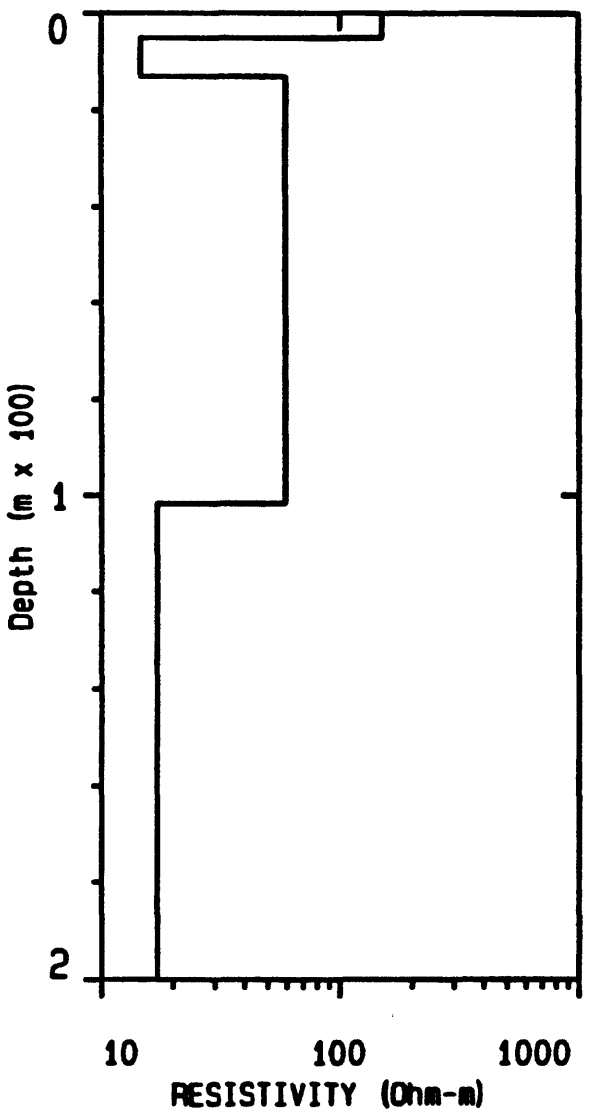

Figure 32. Electrical model of the near-surface determined by the inversion of the time-domain electromagnetic data from sounding S7.

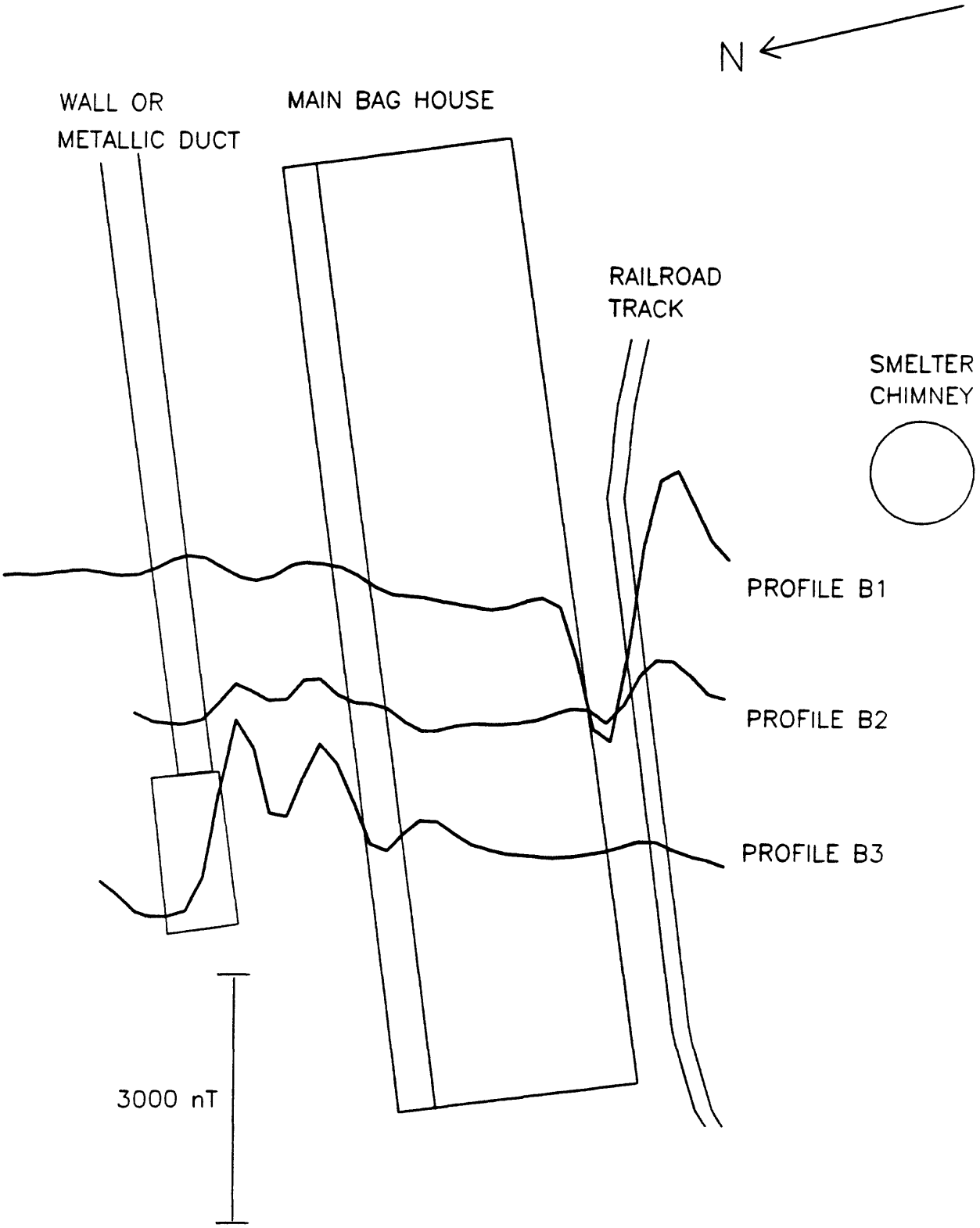

Figure 33. Magnitude of the magnetic induction field along the three profiles over the bag house.

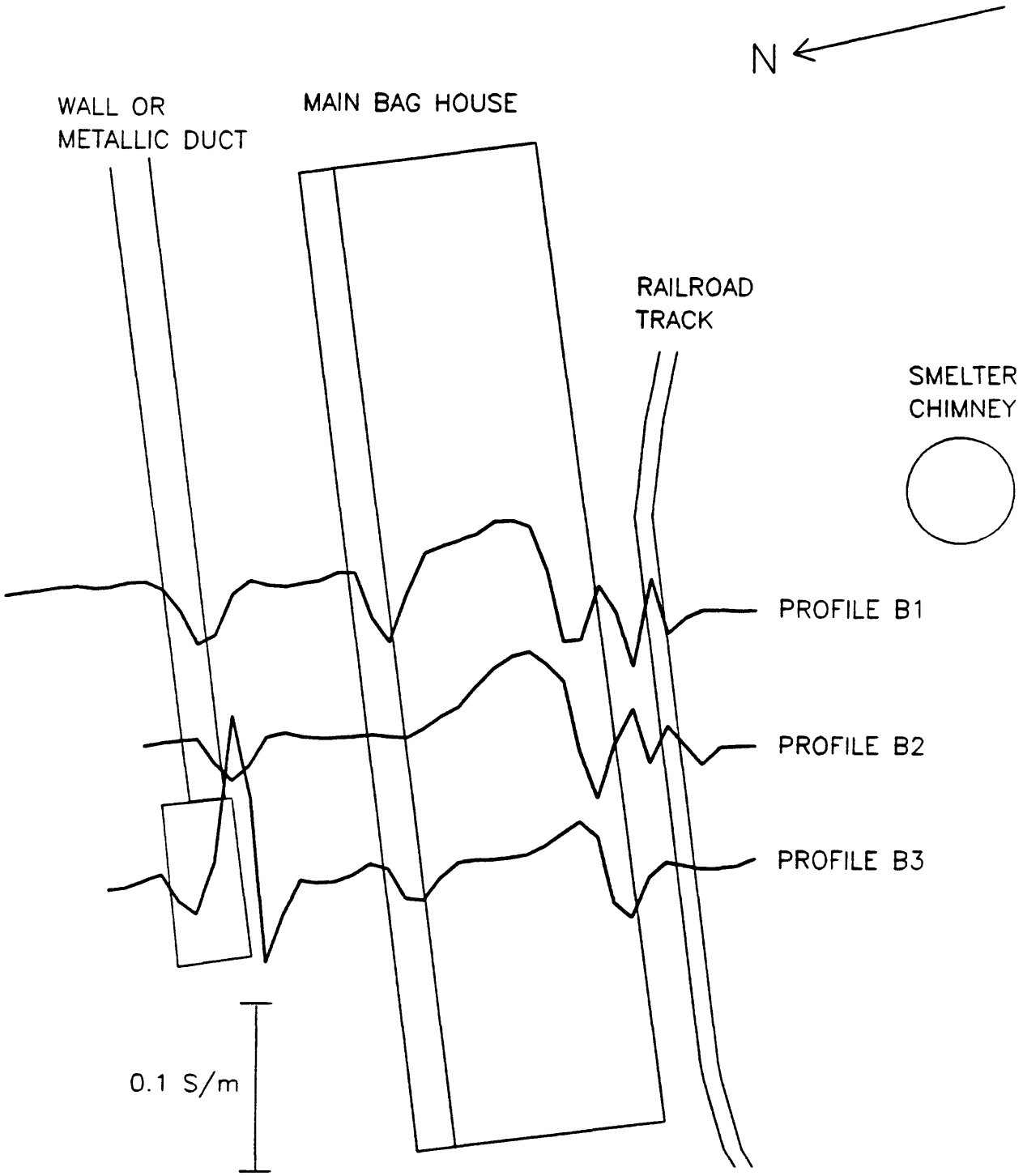

Figure 34. Apparent conductivity measured with the terrain conductivity meter (EM-31) in the inline direction along the three profiles over the bag house.

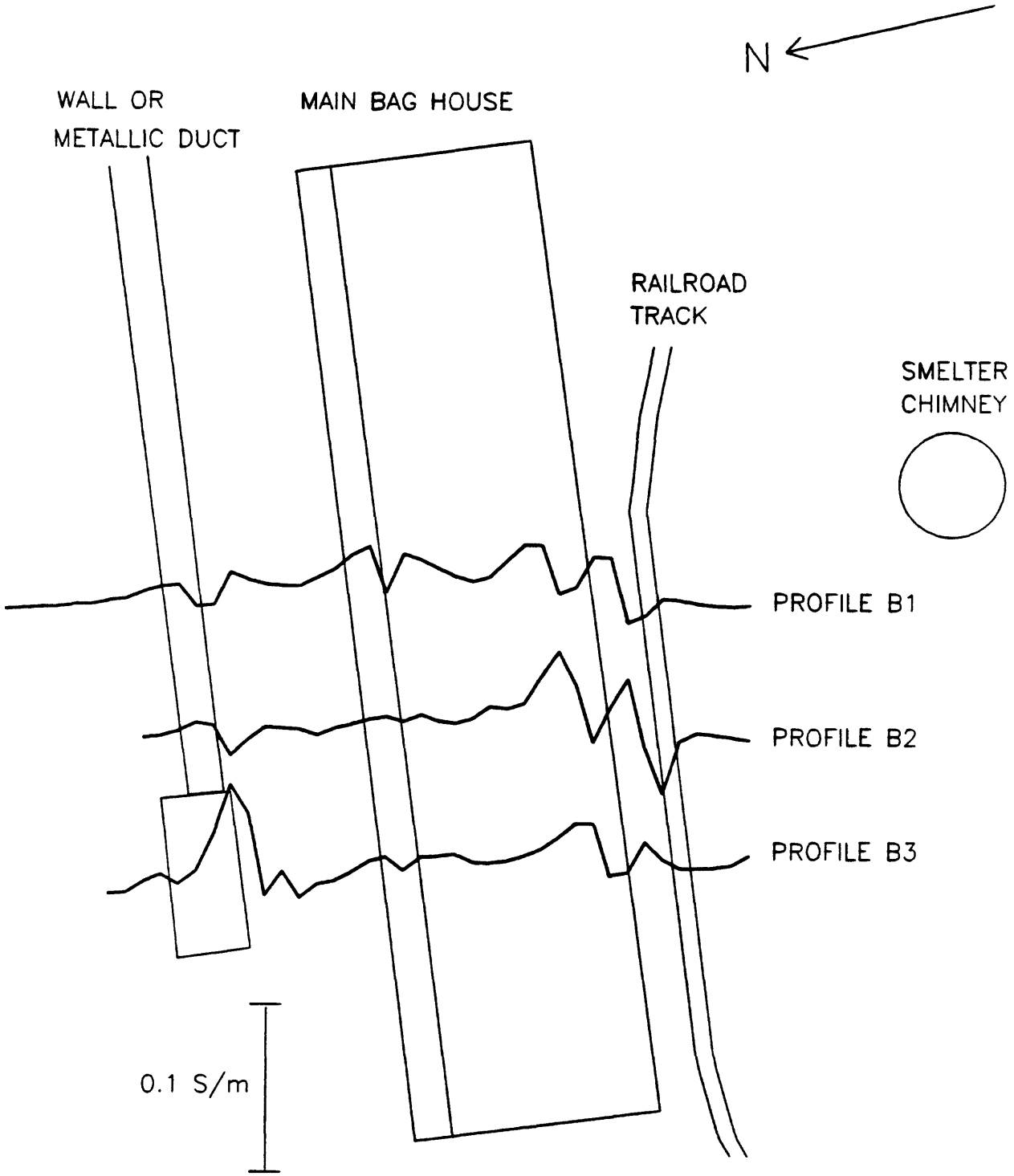

Figure 35. Apparent conductivity measured with the terrain conductivity meter (EM-31) in the crossline direction along the three profiles over the bag house.

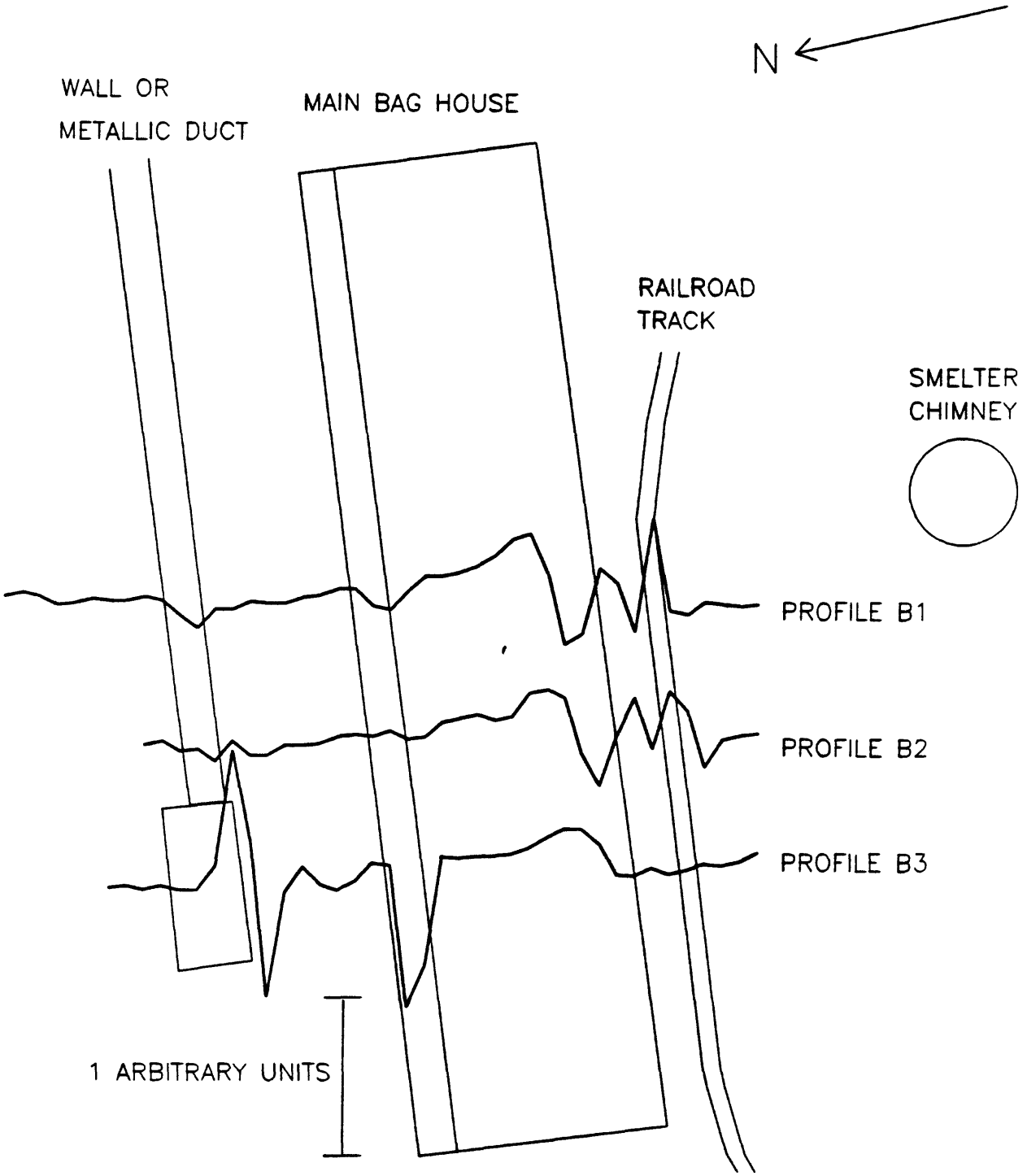

Figure 36. In-phase component measured with the terrain conductivity meter (EM-31) in the inline direction along the three profiles over the bag house.

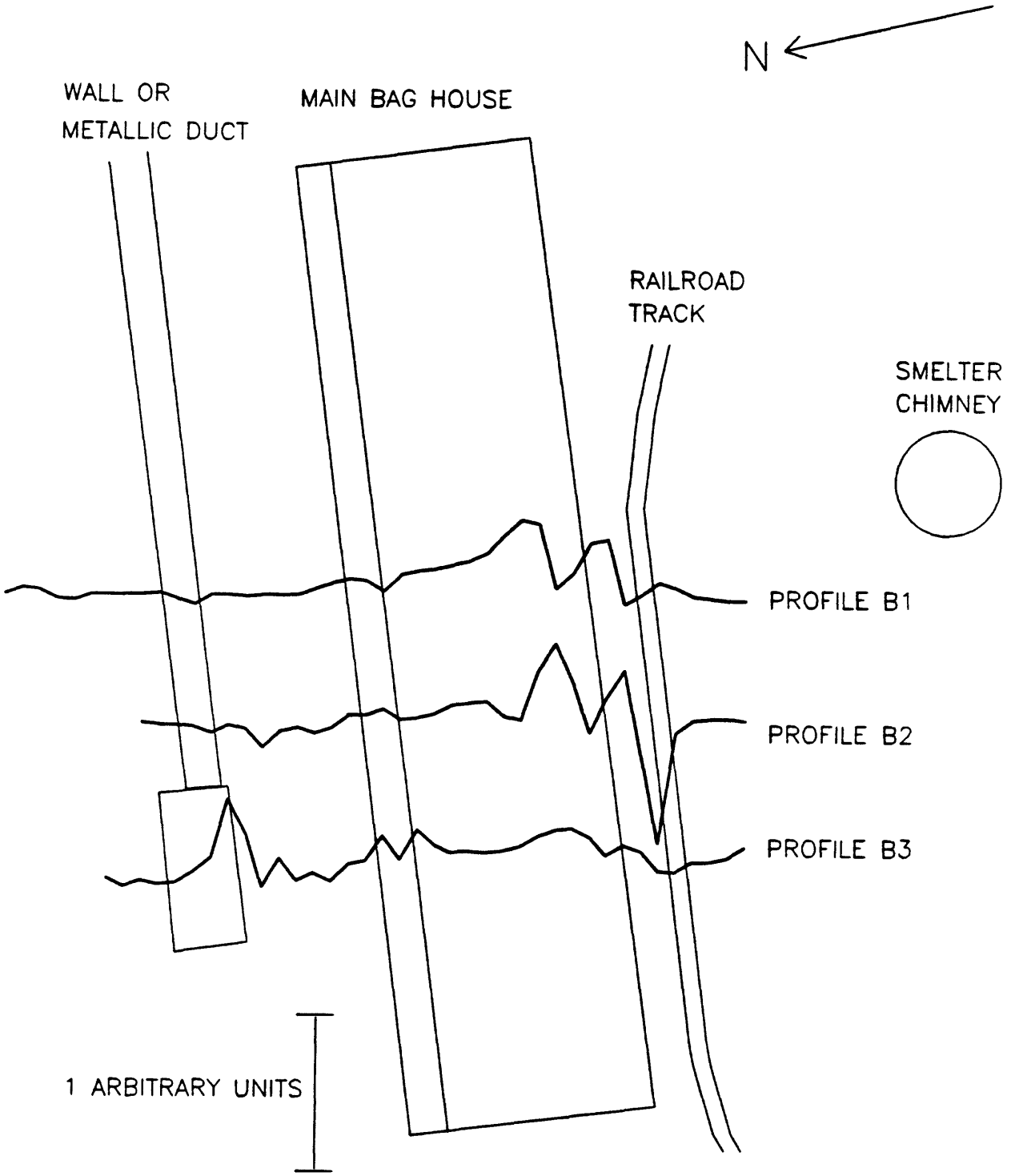

Figure 37. In-phase component measured with the terrain conductivity meter (EM-31) in the crossline direction along the three profiles over the bag house.

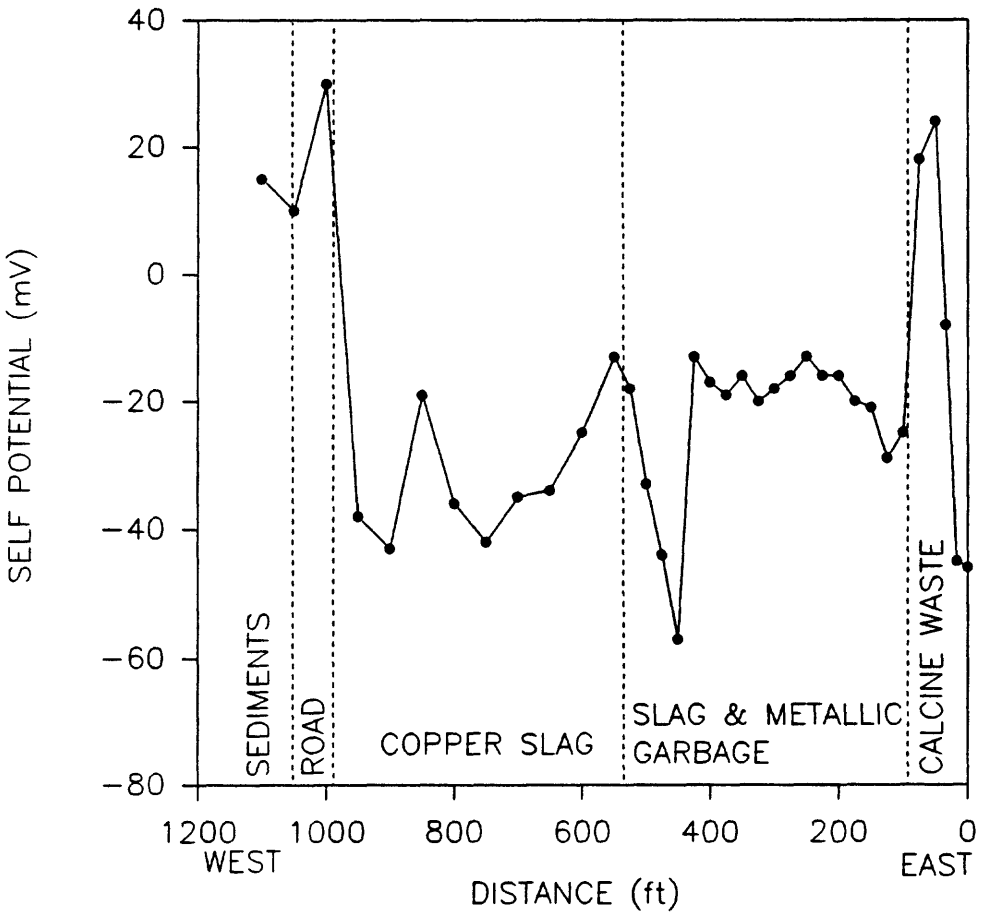

Figure 38. Self potential along profile P1.

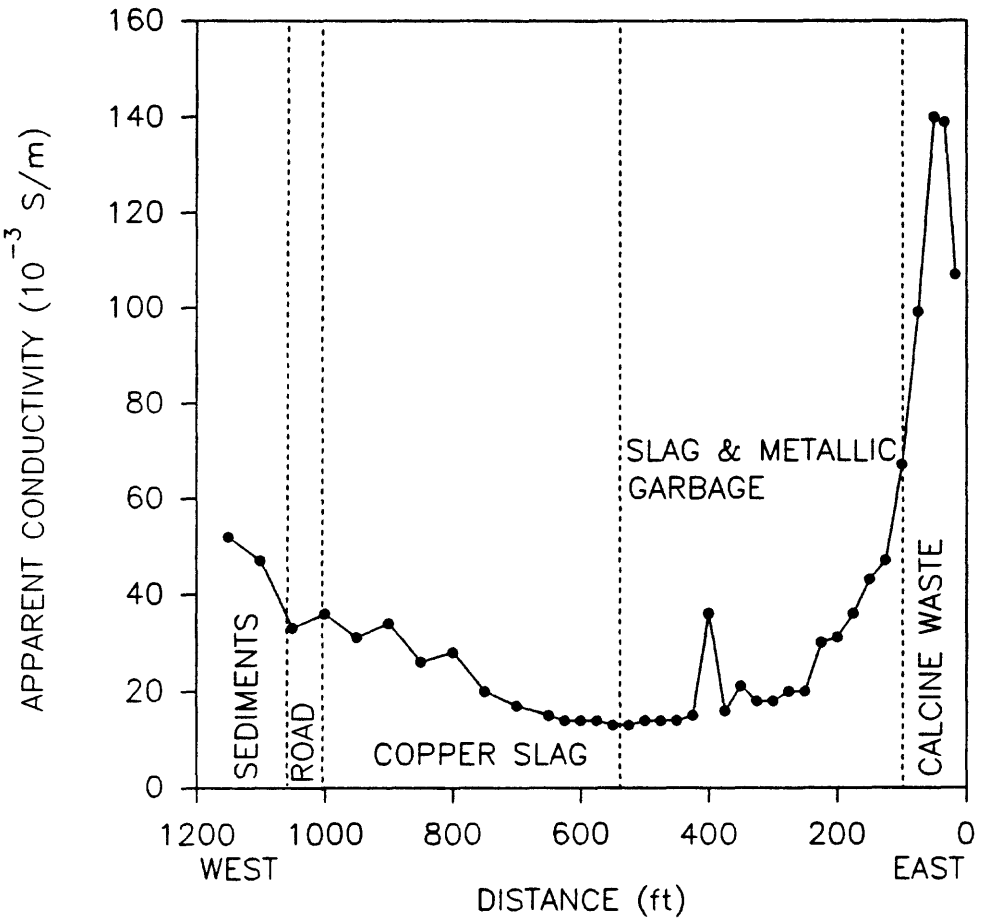

Figure 39. Terrain conductivity data (EM-31) in the HCP configuration for profile P1.

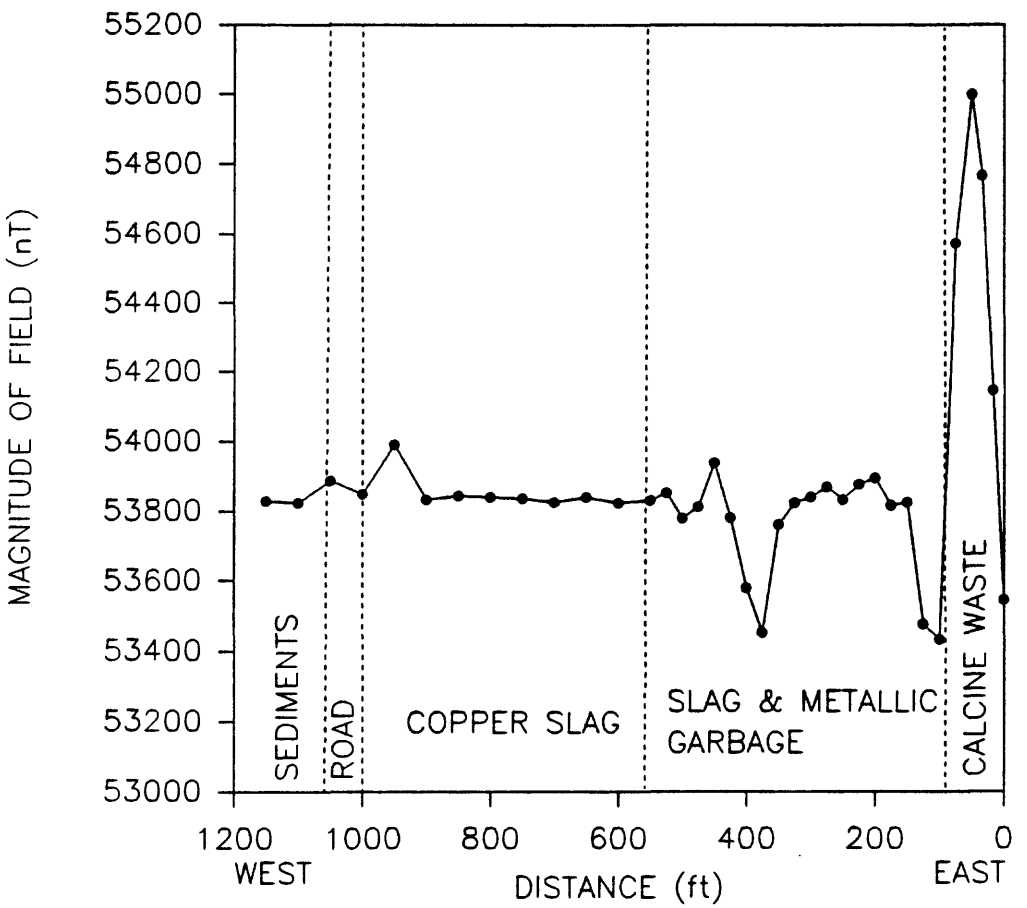

Figure 40. Magnetic field data along profile P1.

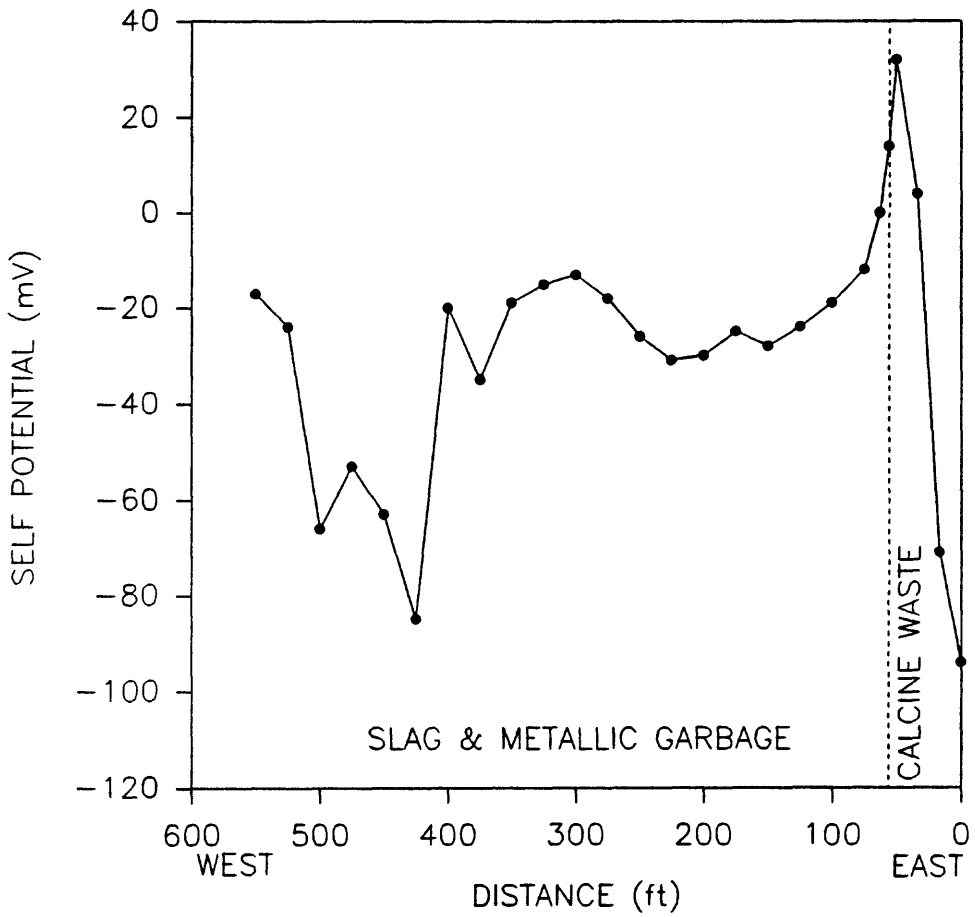

Figure 41. Self potential along profile P2.

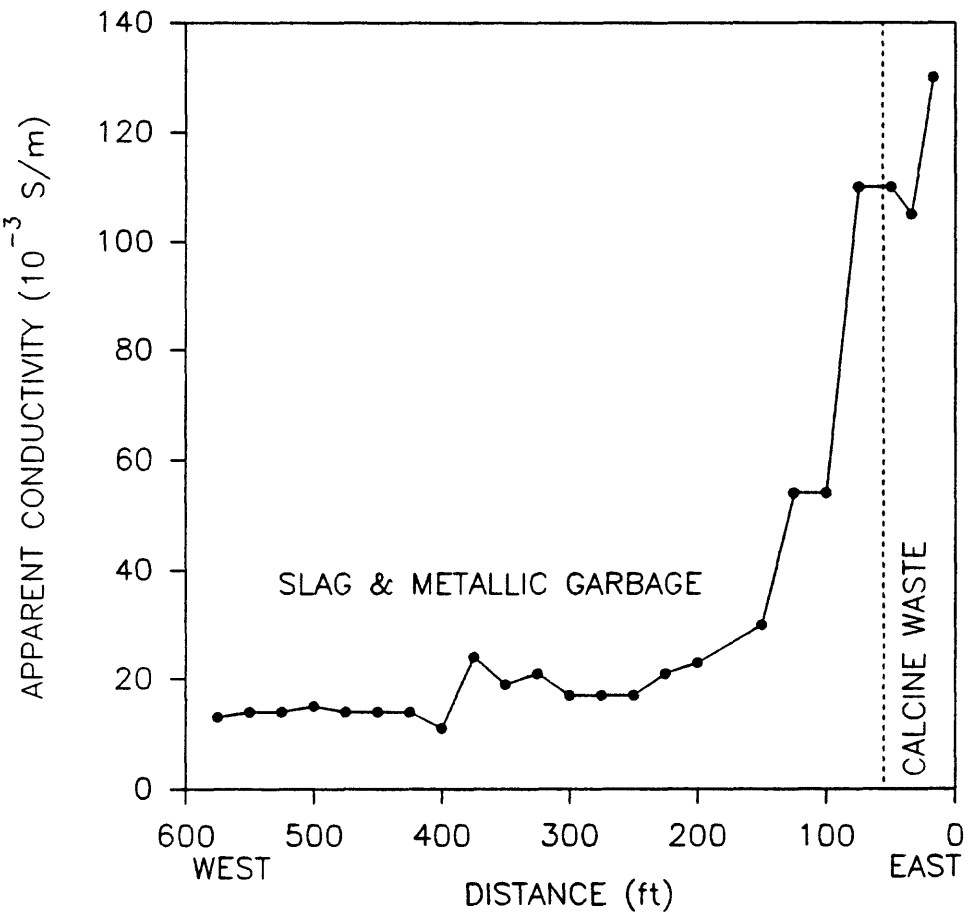

Figure 42. Terrain conductivity data (EM-31) in the HCP configuration for profile P2.

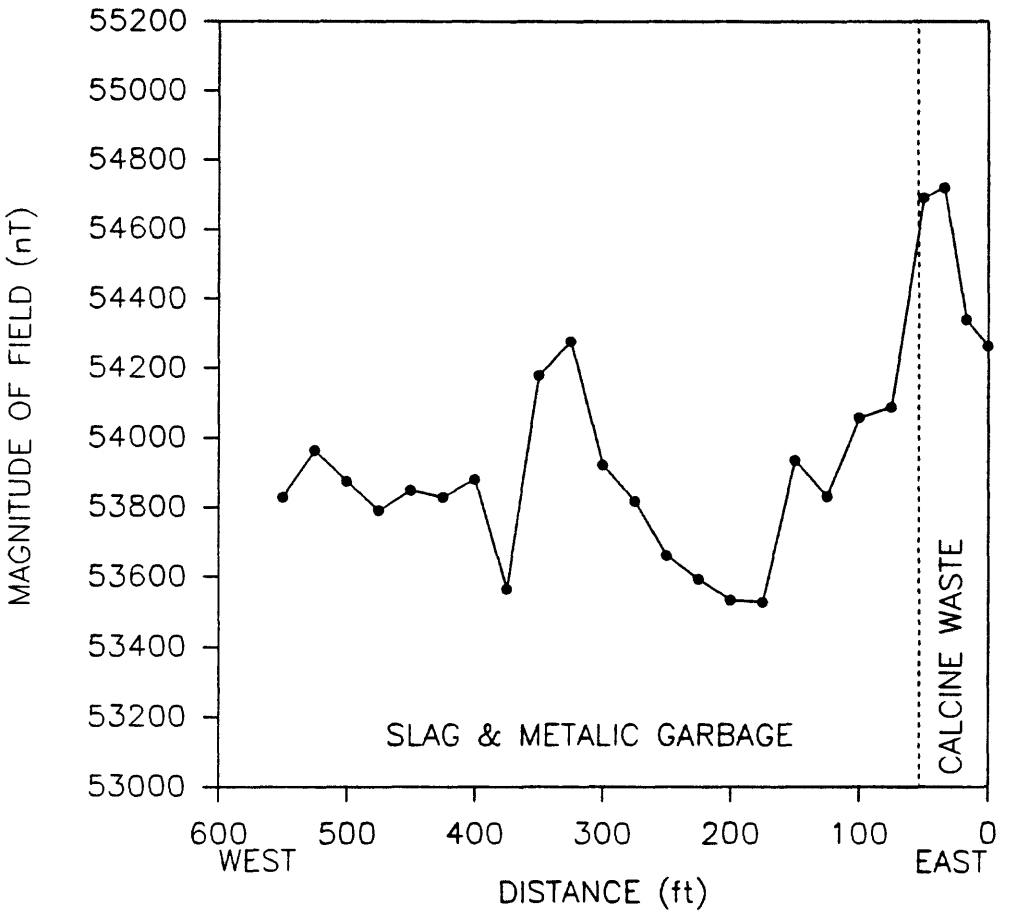

Figure 43. Magnetic field data along profile P2.

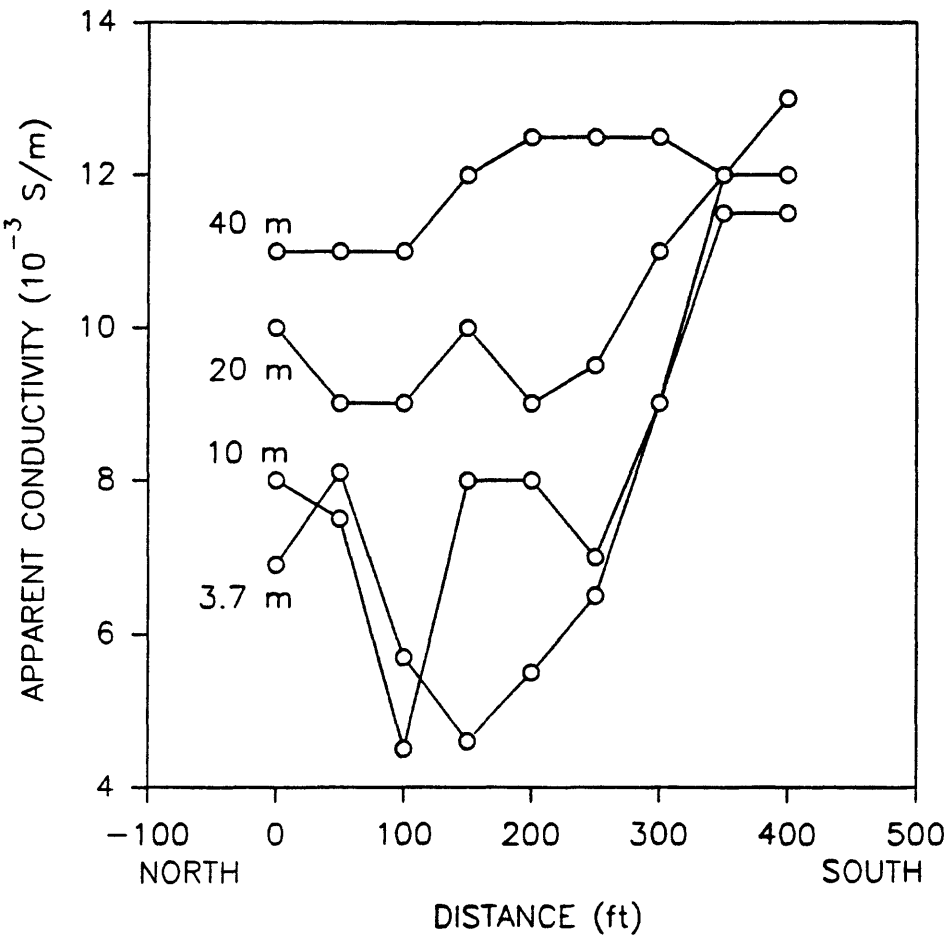

Figure 44. Terrain conductivity data measured in the HCP configuration for profile W1. The four distances refer to the inter-coil spacing.

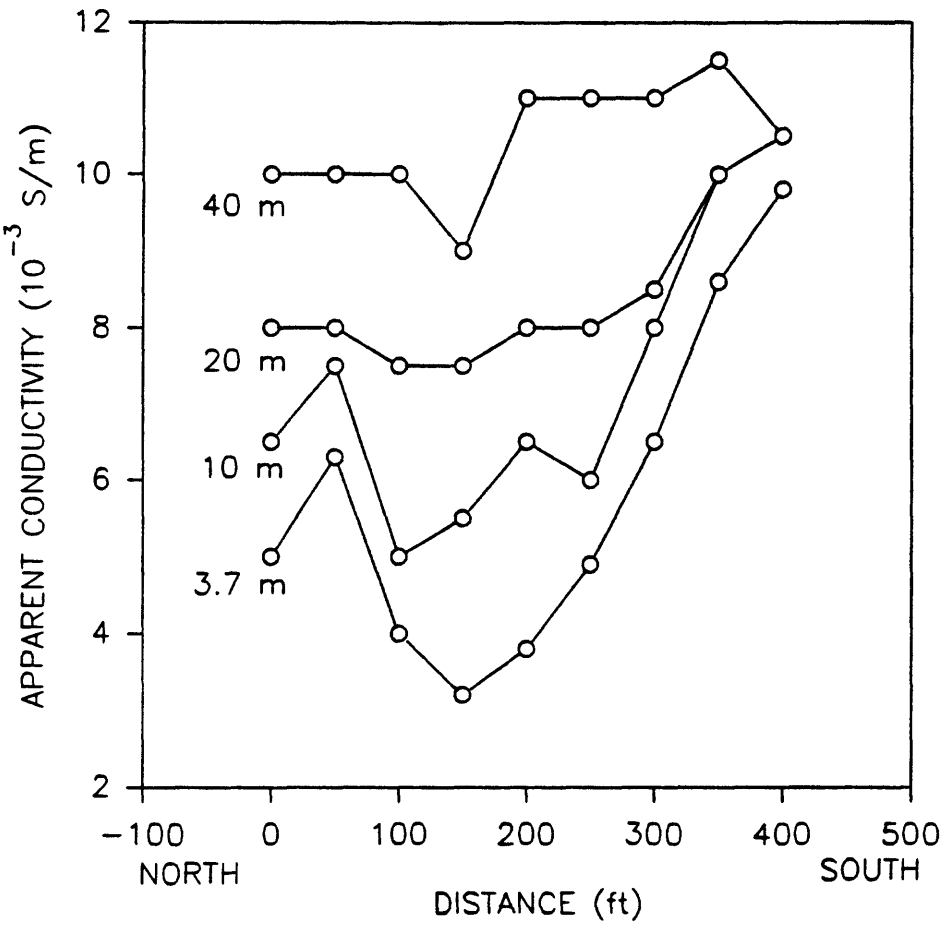

Figure 45. Terrain conductivity data measured in the VCP configuration for profile W1. The four distances refer to the inter-coil spacing.

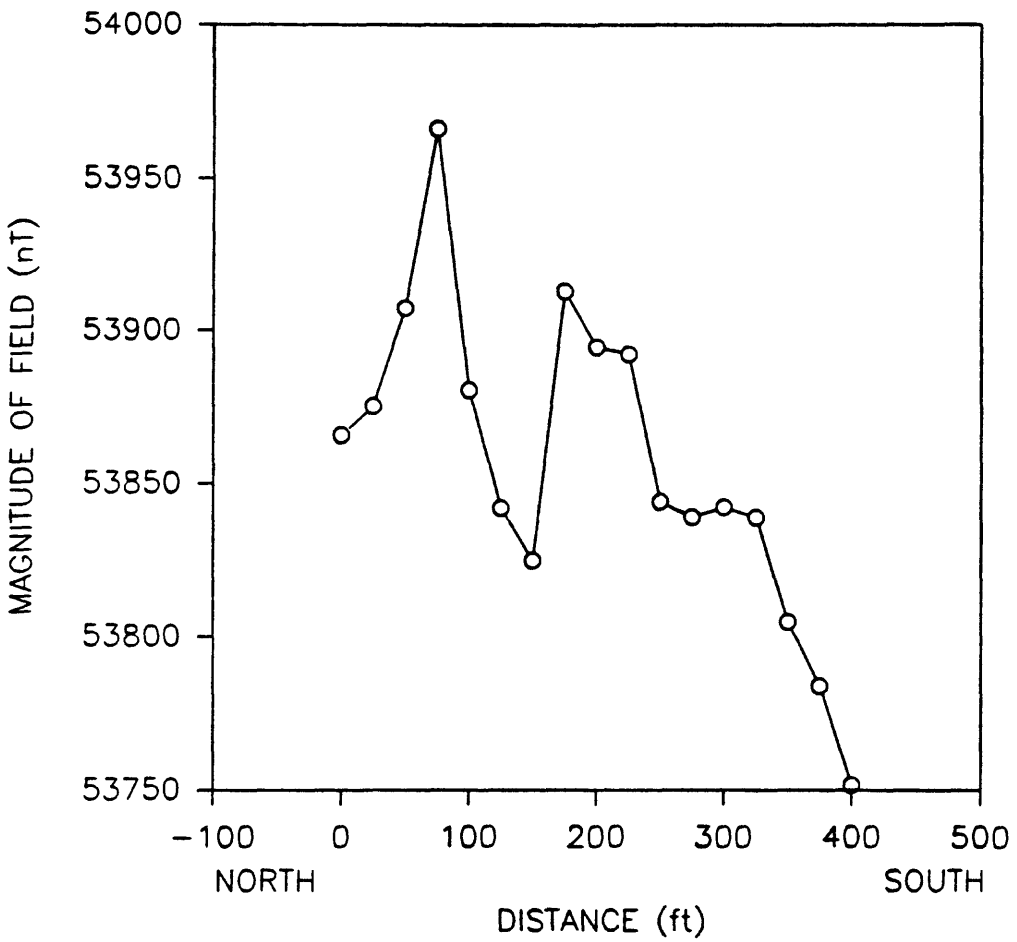

Figure 46. Magnitude of the magnetic induction field along profile W1.

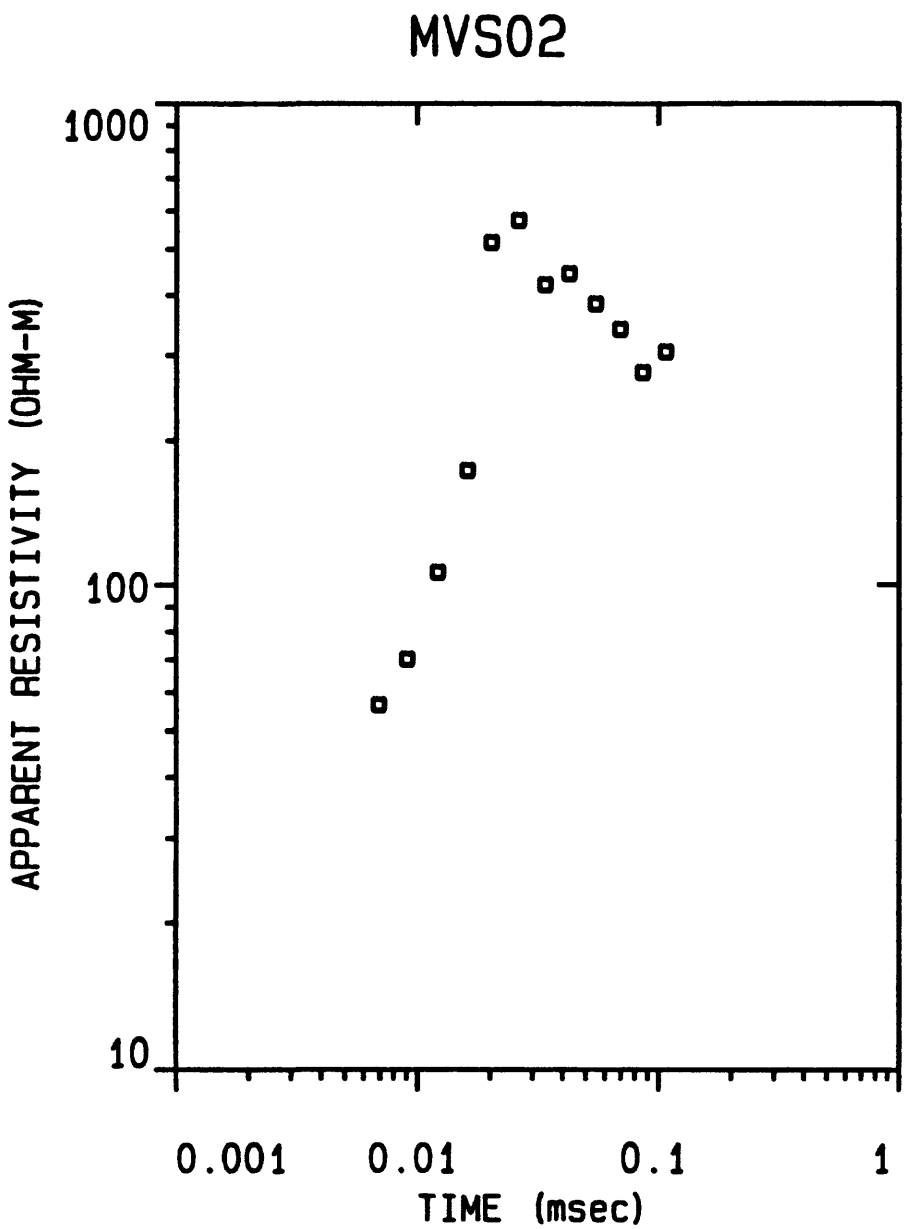

Figure 47. Time-domain electromagnetic data collected at sounding S2, which is near profile W1.

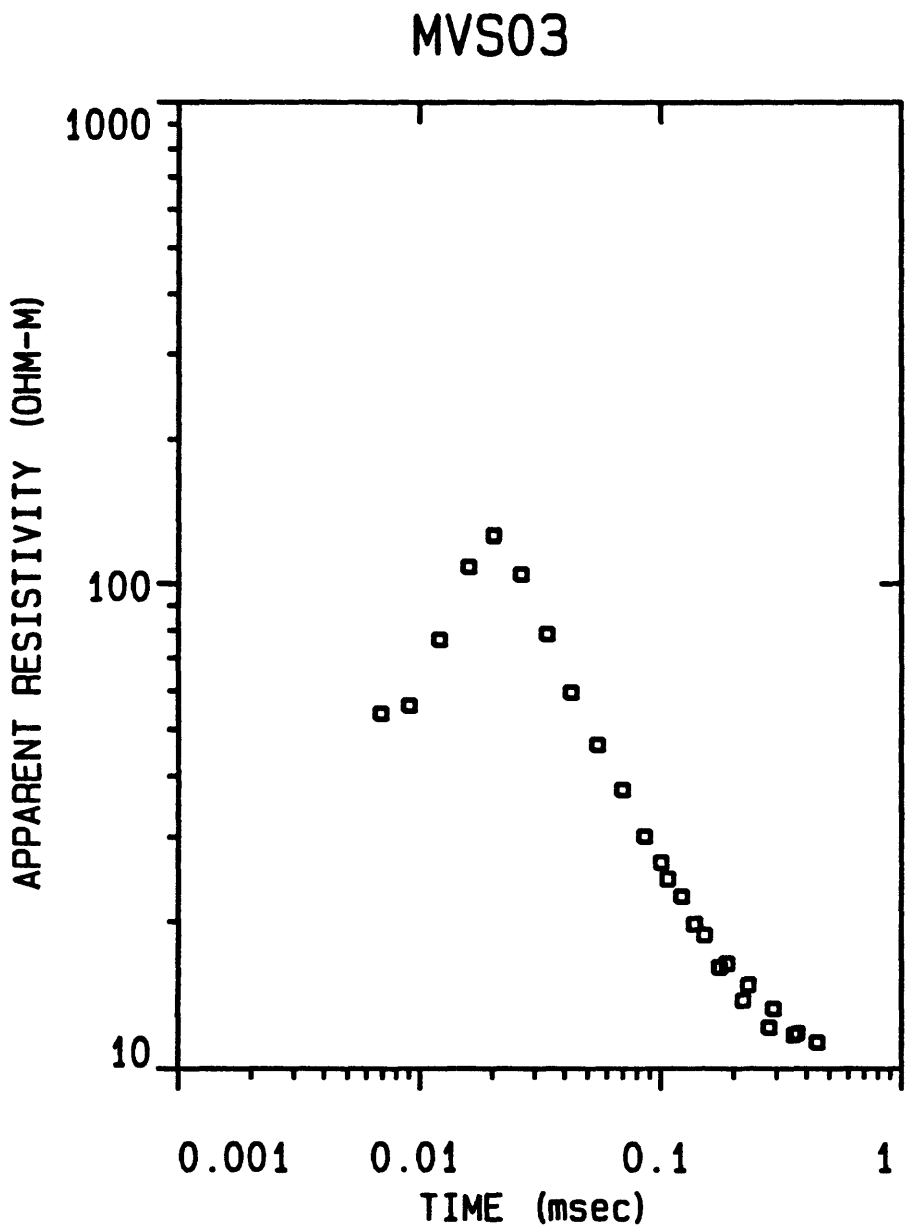

Figure 48. Time-domain electromagnetic data collected at sounding S3, which is near profile W1.

APPENDIX A

GEOPHYSICAL LOGGING

A.1 Background

On October 22 and 23, 1992, R. Hodges and J. Hutchens, who are members of the Water Resources Division of the U. S. Geological Survey, logged the 13 monitoring wells at the Midvale Superfund Site. (The locations and elevations of the wells are listed in Table 1.) Induction logs were collected to determine the electrical resistivity of the slag and natural sediments; gamma and neutron logs to determine the hydrologic properties of the sediments.

The data were collected using standard practices (see e.g., Keys, 1990, p. 66, 79-82, and 93-104), and only a few remarks are necessary. In well MW-3, which is filled with sediment, only a gamma log could be recorded. In well MW-12, a shim was used to help lower the tools into the well because the boom on the logging truck could not reach the well; consequently, logging measurements near the top are absent. The depths on the logs are relative the ground surface at the well. The data are displayed in the figures for this appendix.

A.2 Results of the Induction Logging

The resistivity logs generally correlate with each other and with the stratigraphic logs, which Earthfax, an engineering company, constructed from observation of the drill cuttings, The resistivity in all wells except MW-12 is almost zero near the top. In this zone, the tool is measuring the resistivity of the steel casing. In the next zone, which extends to approximately 15 ft and which is below the waste, all logs indicate the resistivity is moderately high — it usually ranges from 10 to 30 Ωm, although in MW-2 and MW-10 the resistivity for short intervals is as high as 120 and 90 Ωm, respectively. These resistivity measurements correlate with the terrain conductivity measurements of the natural sediments made by Robert Horton. Because all wells (except MW-1, MW-4, MW-5, and MW-13) are only approximately 15 ft deep, the resistivity below this depth could not be measured.

Monitoring wells MW-1, MW-4, MW-5, and MW-13 provide some information about what we believe to be a perched aquifer. In MW-13, the stratigraphic log indicates that the perched aquifer exists in a sandy layer between 4303 and 4301 ft. Between 4306 and 4300 ft, the resistivity is slightly higher than the resistivities immediately above and below this zone. Since a layer with a low clay content (e.g., a sand) can have a higher resistivity than a layer with a high clay content (McNeill, 1990, p. 192), this high resistivity is probably the perched aquifer. The character of the resistivity log for this well is very similar to that in MW-1 which is only 37 m (122 ft) away, and the high resistivity zone in MW-1 between 4306 and 4301 ft is probably the perched aquifer.

A similar analysis applies to MW-5 and MW-4. In MW-5, the stratigraphic log indicates that a perched aquifer exists in a sandy layer between 4311 and 4304 ft. Between 4309 and 4306 ft, the resistivity is high, and this zone may be the perched aquifer. The character of the log for this well is very similar to that for MW-4; and the zone with the slightly high resistivity between 4308 and 4305 ft may be the perched aquifer.

Although the general features on the induction and stratigraphic logs match, the details do not. The likely cause for this discrepancy is the inaccuracy of the stratigraphic logs — the cuttings do not necessarily come from the same depth as the drill bit and they can be mixed with other sediments. At best, these logs delineate the general features of the stratigraphy.

A.3 Results of the Gamma and Neutron Absorption Logging

The gamma and neutron absorption logs correlate neither with the stratigraphic logs nor with each other. Regarding the latter point, the stratigraphy at two wells that are close together, say MW-1 and MW-13, should be similar, but the logs cannot be correlated.

A hypothesis for these poor results is that the tools were not working correctly. Because the gamma radiation was measured with two different tools and the results are similar, these two tools were probably operating properly. During the neutron absorption logging, the measurements from the near and far detectors generally correlate well, and when the tool entered water the number of neutrons measured by the far detector usually dropped by approximately 50 percent. For these reasons, the neuton absorption tool was probably operating properly also.

Another hypothesis for these poor results, which we believe is likely, is that the tools were measuring mostly the properties of the cement grout not those of the formation. The cement grout for the wells is made with bentonite and is between 2 and 4 1/2 in of the center, within the zone contributing the most to the gamma radiation measurement (Keys, 1990, p. 80-81). An important constituent of the cement is water, which is a excellent moderator of neutrons due to the hydrogen it contains (Keys, 1990, p. 95).

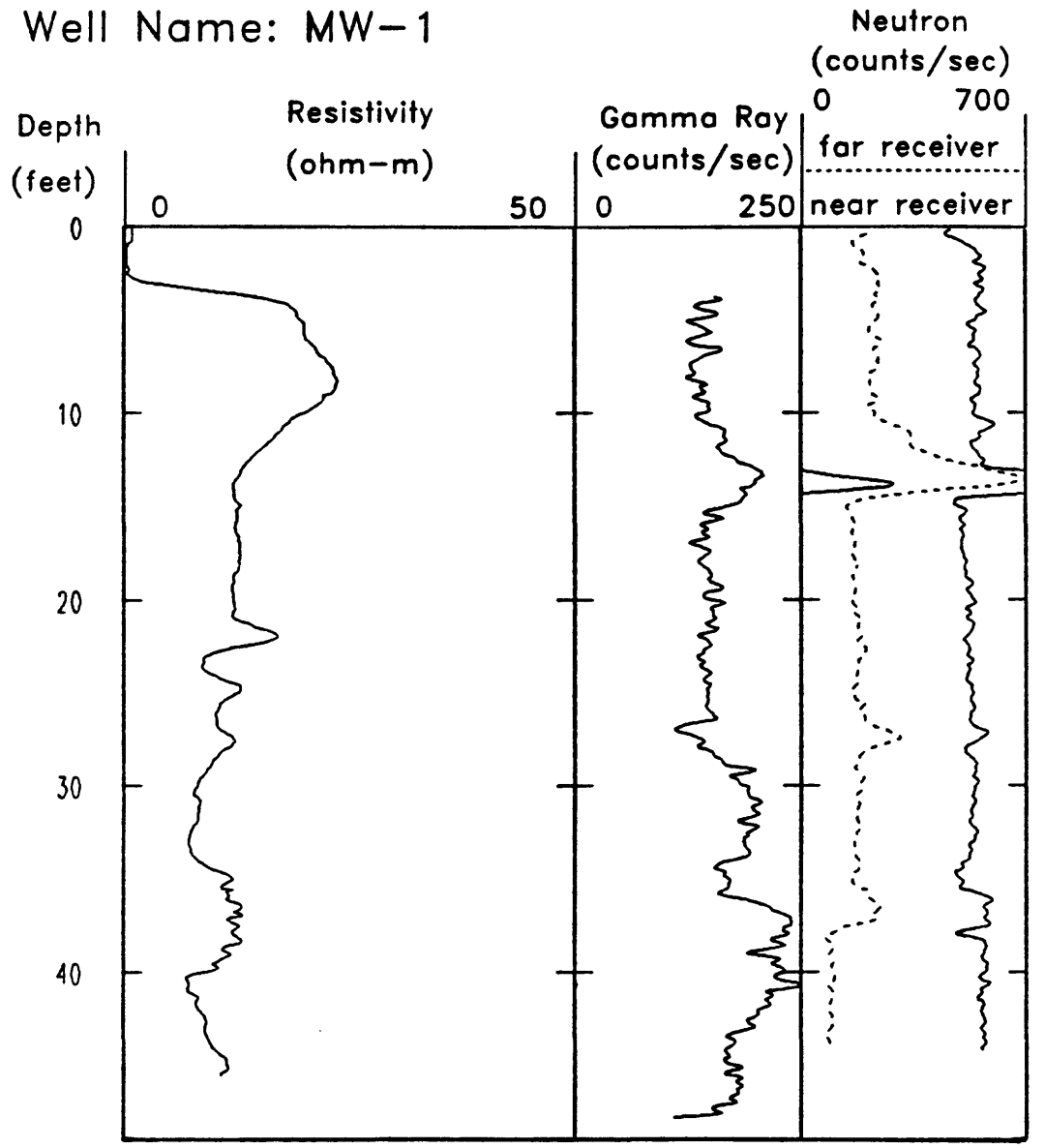

Figure A-1. Geophysical logging data collected in monitoring well MW-1.

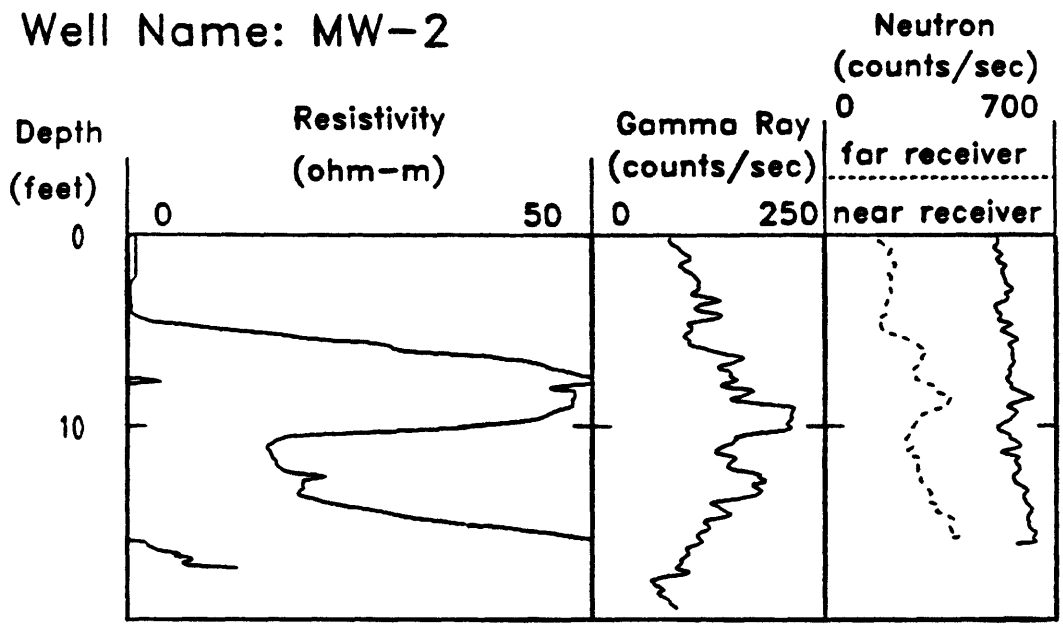

Figure A-2. Geophysical logging data collected in monitoring well MW-2.

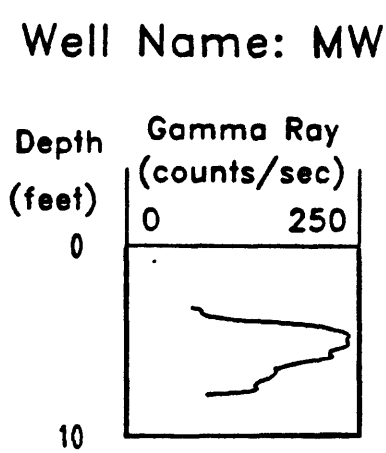

Figure A-3. Geophysical logging data collected in monitoring well MW-3.

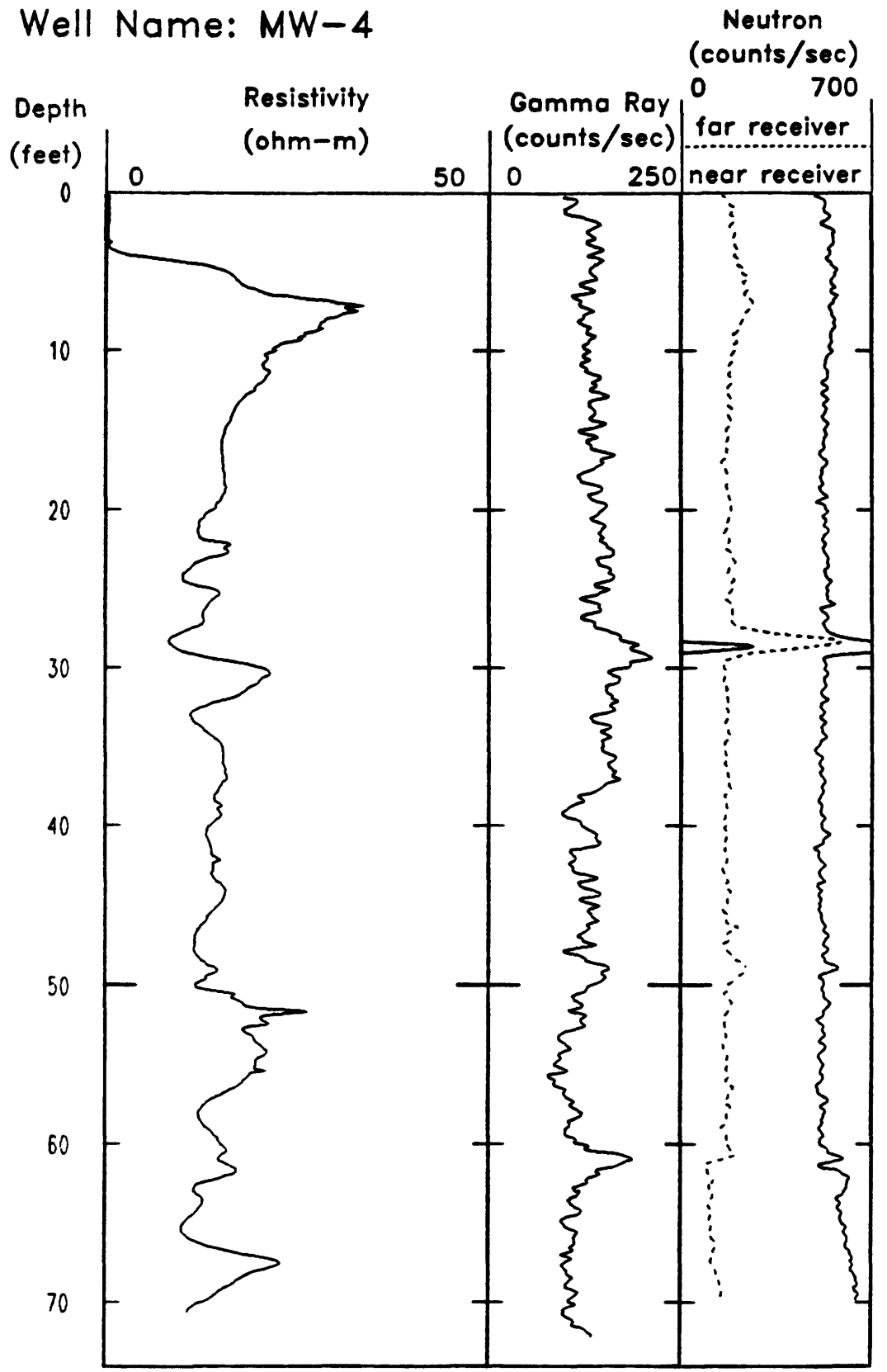

Figure A-4. Geophysical logging data collected in monitoring well MW-4.

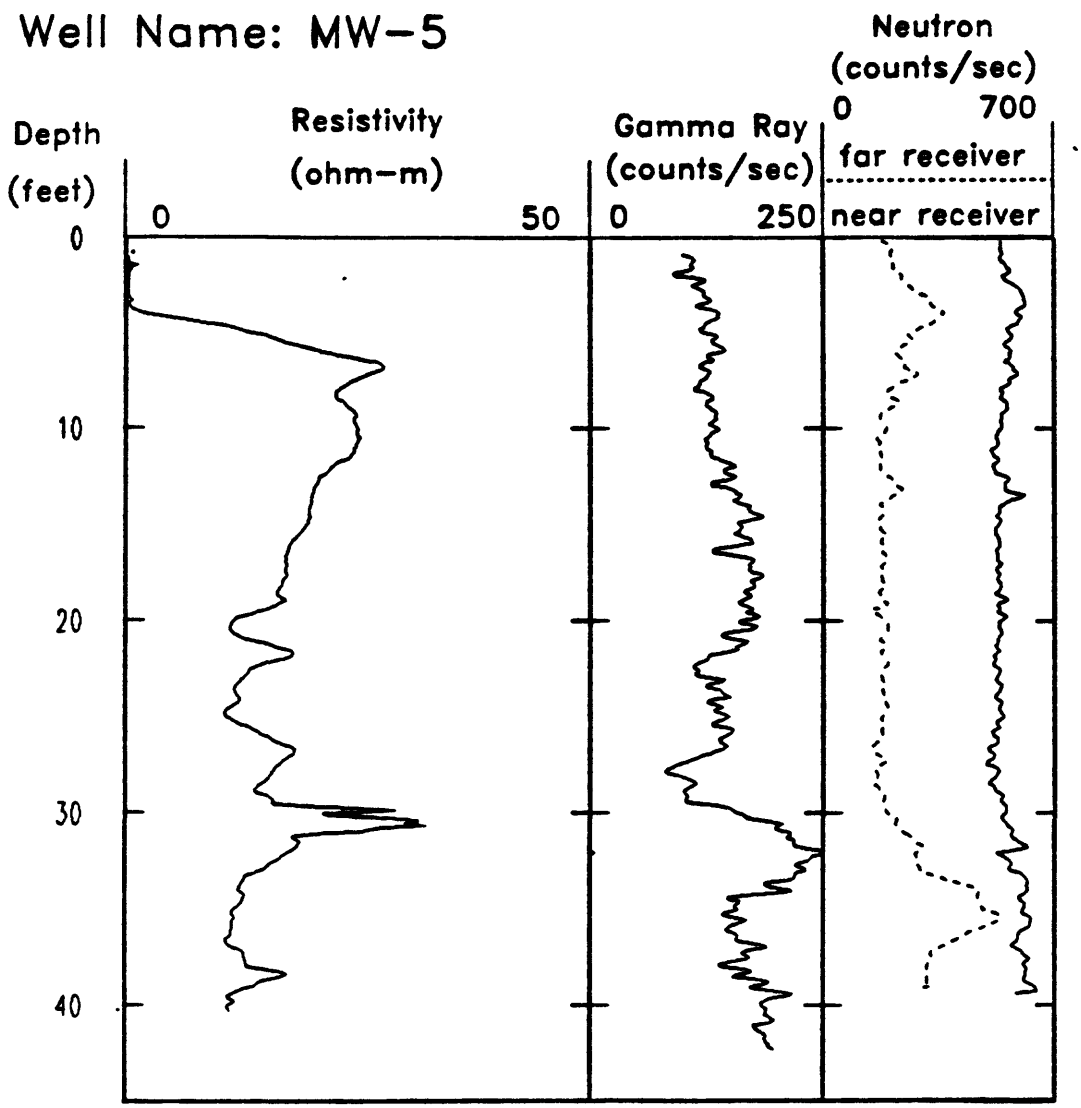

Figure A-5. Geophysical logging data collected in monitoring well MW-5.

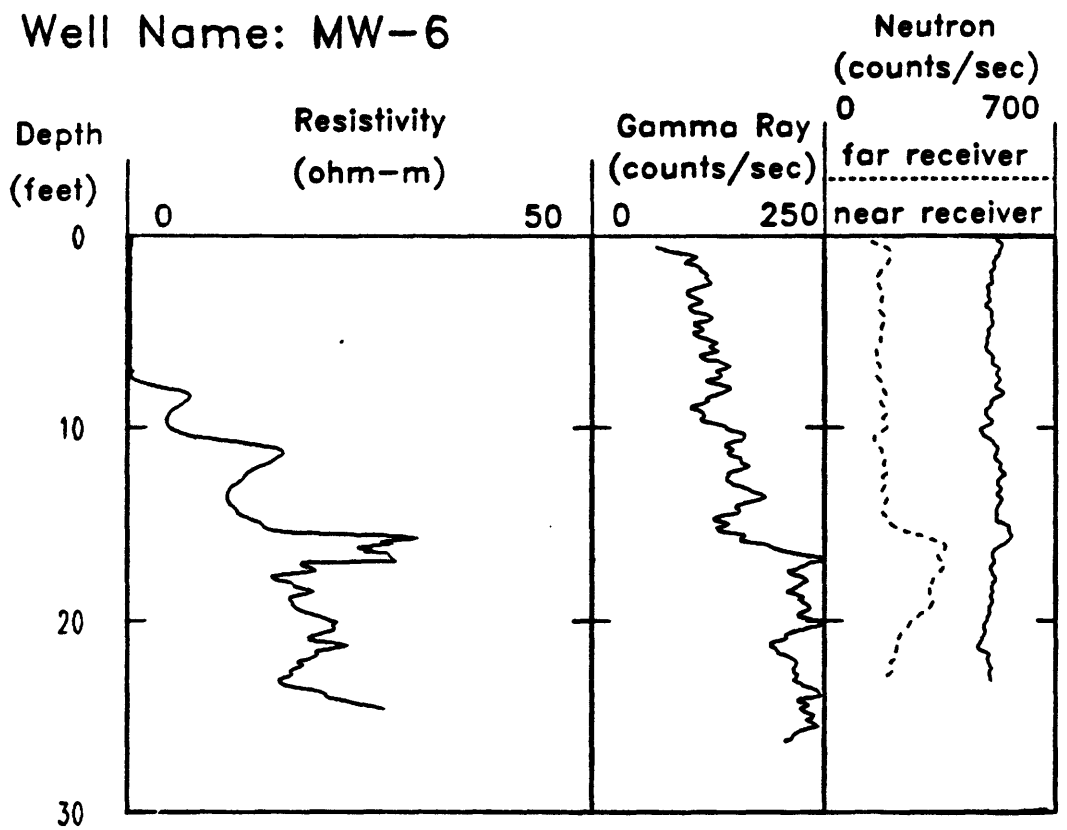

Figure A-6. Geophysical logging data collected in monitoring well MW-6.

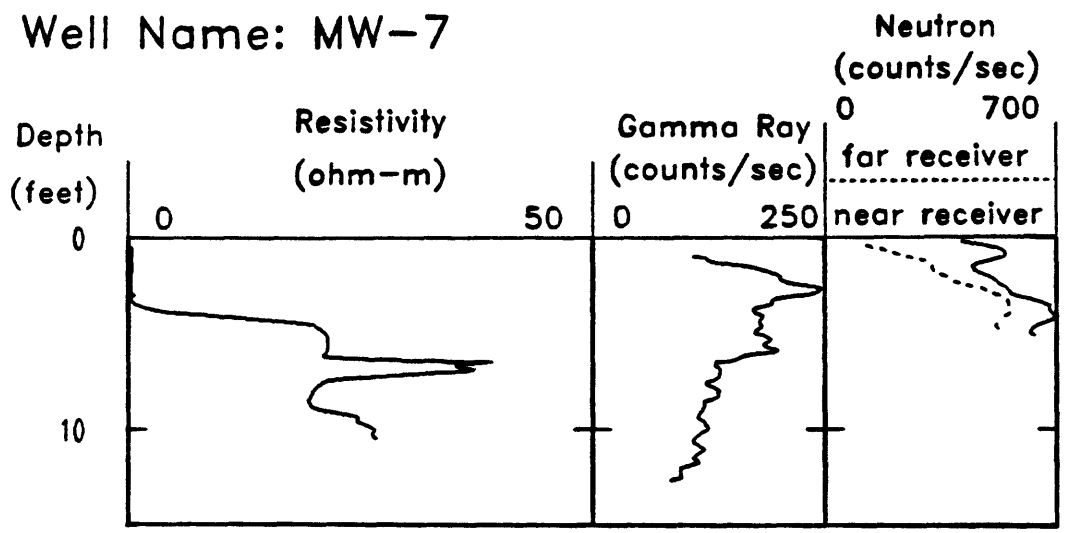

Figure A-7. Geophysical logging data collected in monitoring well MW-7.

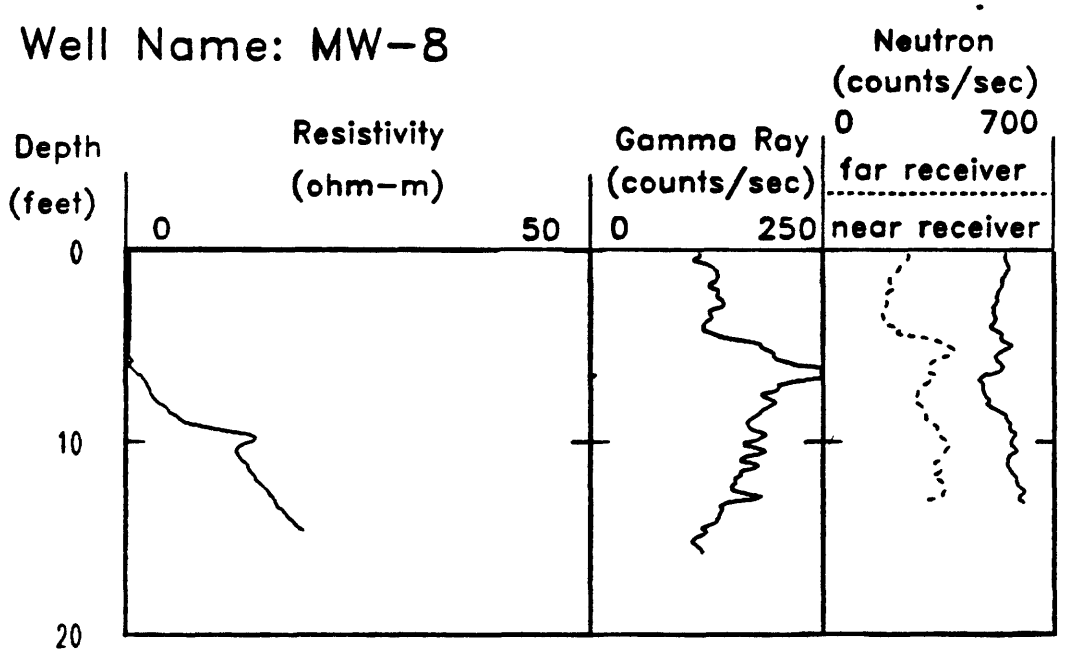

Figure A-8. Geophysical logging data collected in monitoring well MW-8.

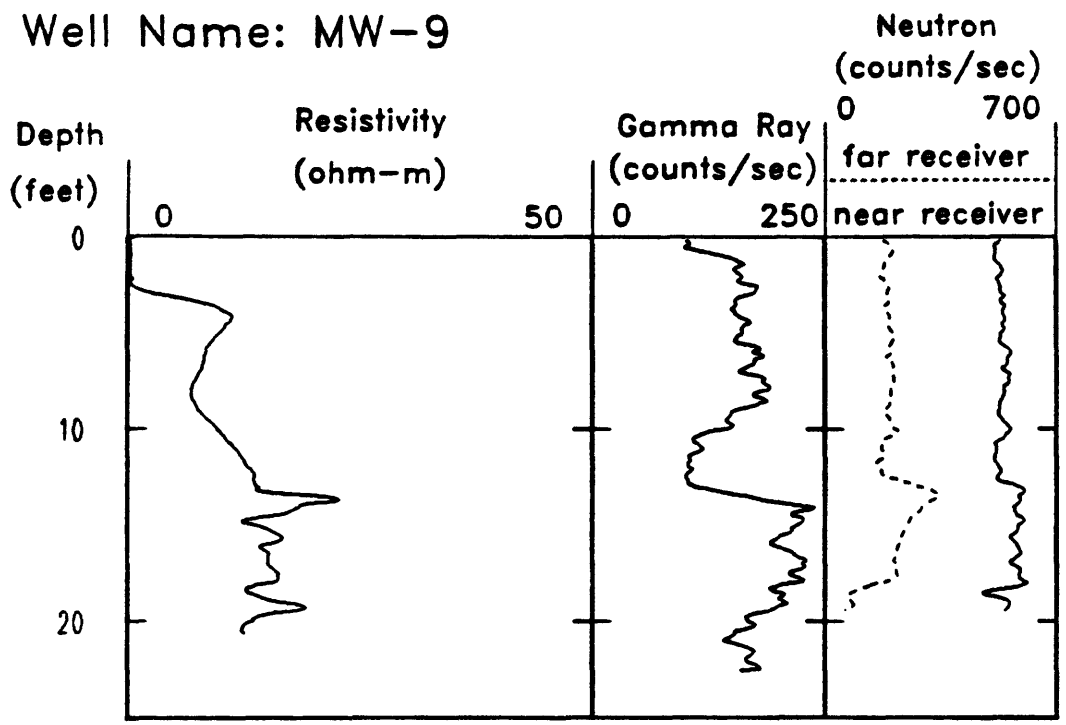

Figure A-9. Geophysical logging data collected in monitoring well MW-9.

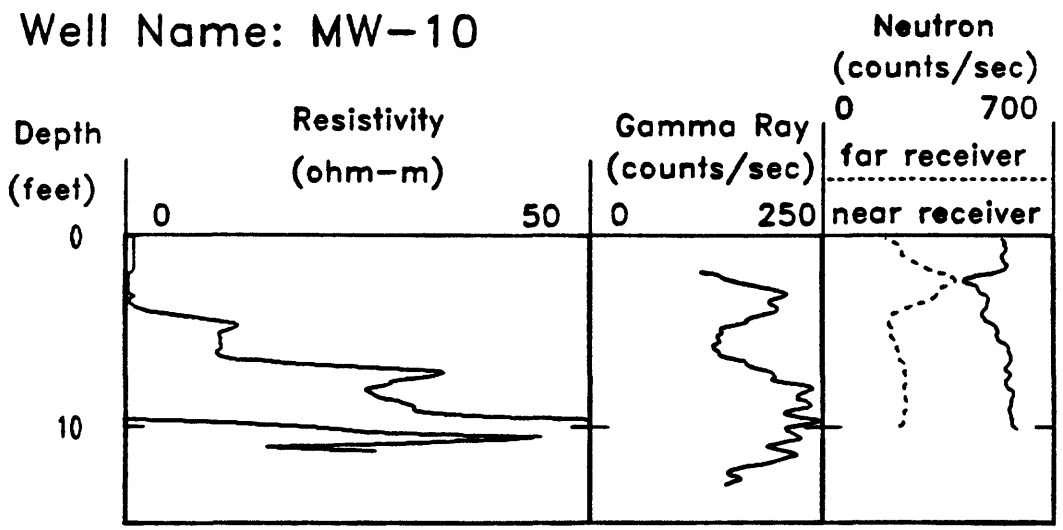

Figure A-10. Geophysical logging data collected in monitoring well MW-10.

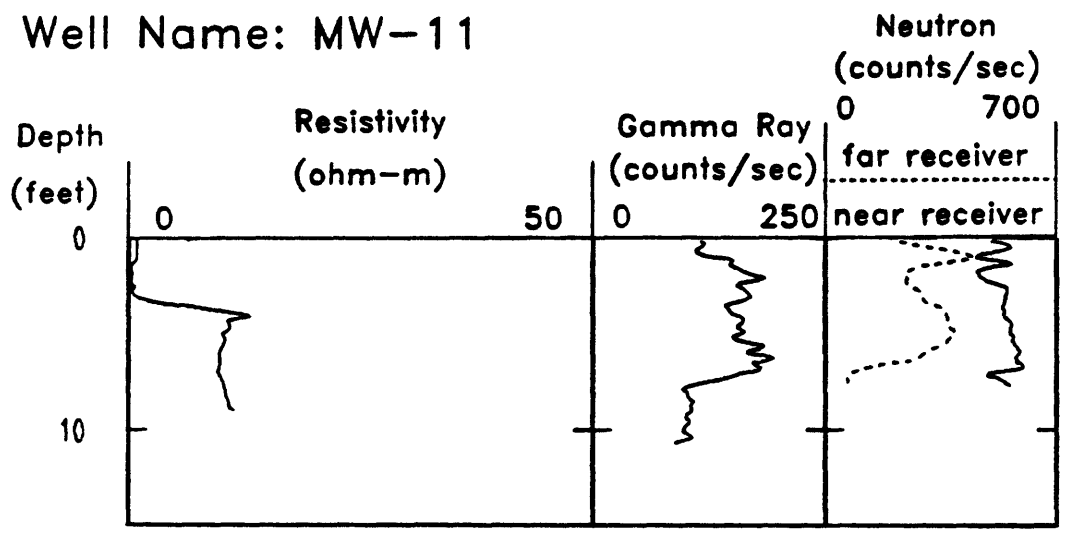

Figure A-11. Geophysical logging data collected in monitoring well MW-11.

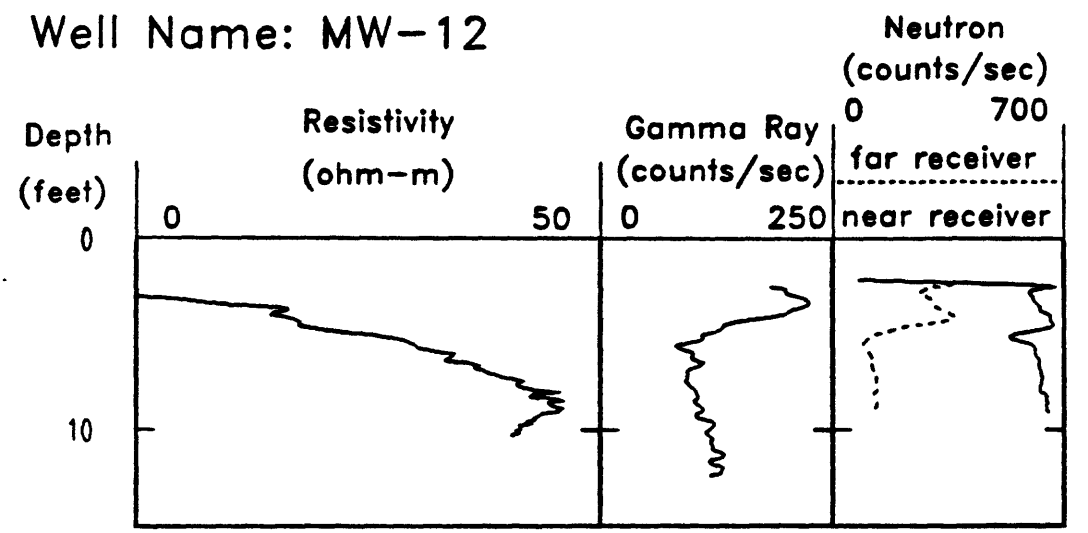

Figure A-12. Geophysical logging data collected in monitoring well MW-12.

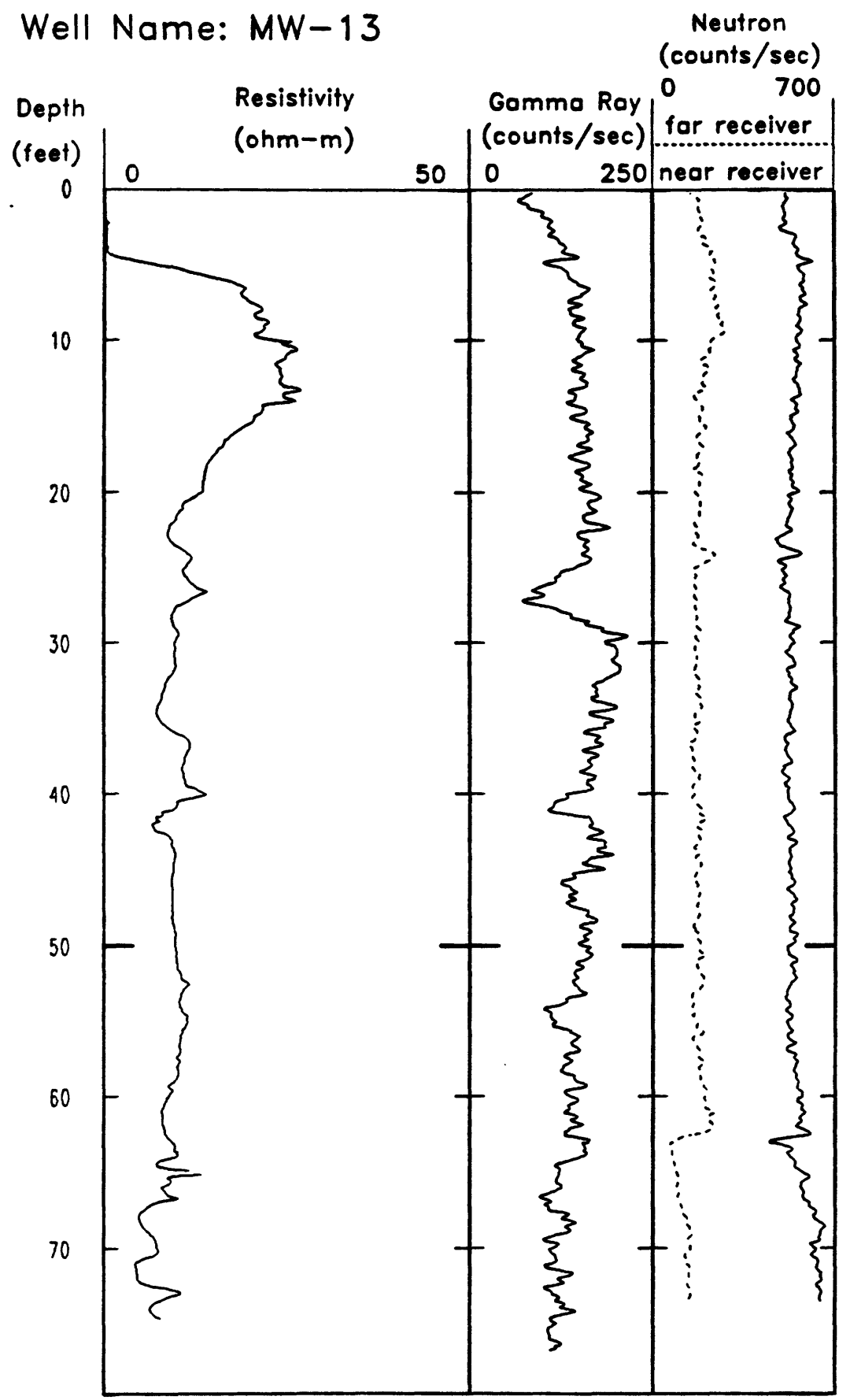

Figure A-13. Geophysical logging data collected in monitoring well MW-13.

Table A-1.Locations of the monitoring wells expressed in state plane coordinates.

Name of Well	Elevation (ft)	Location Northing (ft)	Easting (ft)
MW-1	4340.58	829743.04	1884673.90
MW-2	4297.05	829691.92	1884045.55
MW-3	4286.25	829494.69	1883276.30
MW-4	4337.15	830615.11	1885053.98
MW-5	4338.65	831295.03	1885532.90
MW-6	4305.45	831265.22	1884567.99
MW-7	4282.39	831129.96	1883592.26
MW-8	4289.63	832201.92	1884697.79
MW-9	4309.66	832548.04	1886248.92
MW-10	4286.60	832637.07	1885021.67
MW-11	4281.93	833101.89	1884609.12
MW-12	4275.77	835781.96	1883416.02
MW-13	4341.68	829749.99	1884795.52

APPENDIX B

TERRAIN CONDUCTIVITY DATA (EM-31)

This appendix contains the terrain conductivity data collected along the profiles using the Geonics EM-31. The locations were determined using the method described in the section entitled "Data Collection and Processing", which is in the main body of the report. The in-phase component is uncalibrated and has arbitrary units (V. Labson, 1993, person. commun.). "HCP" and "VCP" refer to the horizontal coplanar and vertical coplanar coil configurations, respectively (Frischknecht et al., 1991, p. 106). "Inline" means that the orientation of an imaginary line connecting the coils is parallel to the direction of the profile; "crossline" means that it is perpendicular. The station is the distance along the profile.

Table B-1. Terrain conductivity data (EM-31) collected along profile A1. All measurements were made with the coils inline.

Station (ft)	Location		Apparent Conductivity (10^{-3} S/m)	
	Northing (ft)	Easting (ft)	HCP	VCP
0	831280	1884630	8.94	5.82
10	831271	1884635	8.88	5.46
20	831263	1884641	8.70	5.34
30	831255	1884646	8.70	5.16
40	831246	1884652	8.46	4.86
50	831238	1884657	8.16	5.04
60	831230	1884663	7.98	4.98
70	831221	1884668	8.10	4.68
80	831213	1884674	8.02	4.92
90	831205	1884679	7.84	4.76
100	831196	1884685	7.28	4.22
110	831188	1884691	6.26	4.02

Table B-2. Terrain conductivity data (EM-31) collected along profile A2. All measurements were made with the coils inline.

Station (ft)	Location		Apparent Conductivity (10^{-3} S/m)	
	Northing (ft)	Easting (ft)	HCP	VCP
0	831530	1884420	12.30	6.30
25	831505	1884413	12.60	6.72
50	831481	1884407	13.14	6.90
75	831457	1884400	13.80	7.62
100	831433	1884394	14.70	7.80
125	831409	1884387	18.24	9.84
150	831385	1884381	18.54	9.24

Table B-3. Terrain conductivity data (EM-31) collected along profile A3. All measurements were made with the coils inline.

Station (ft)	Location		Apparent Conductivity (10^{-3} S/m)	
	Northing (ft)	Easting (ft)	HCP	VCP
0	831410	1884440	10.92	5.82
25	831418	1884416	12.36	7.20
50	831426	1884392	14.88	8.28
75	831435	1884369	17.28	9.24
100	831443	1884345	15.66	8.16
125	831452	1884322	16.20	8.04
150	831460	1884298	10.38	5.52

Table B-4. Terrain conductivity data (EM-31) collected along profile A4. All measurements were made with the coils inline.

Station (ft)	Location		Apparent Conductivity (10^{-3} S/m)	
	Northing (ft)	Easting (ft)	HCP	VCP
0	831990	1884910	20.64	13.26
50	831969	1884864	21.18	12.00
100	831948	1884818	20.34	10.86
150	831928	1884773	19.02	9.66
200	831907	1884727	23.40	11.34
250	831887	1884682	27.06	13.56
300	831866	1884636	34.20	19.20
350	831846	1884591	26.80	14.80
400	831825	1884545	26.82	15.18
450	831804	1884499	30.60	18.80
500	831784	1884454	34.60	22.20
550	831763	1884408	31.40	13.60
600	831743	1884363	40.80	21.80
650	831722	1884317	27.60	13.00
700	831702	1884272	27.60	14.80
750	831681	1884226	36.20	26.80
800	831661	1884180	43.40	35.20
850	831640	1884135	37.00	120.20
900	831619	1884089	28.38	18.24

Table B-5. Terrain conductivity data (EM-31) collected along profile B1. All measurements were made with the horizontal coplanar configuration.

Station (ft)	Location		Apparent Conductivity (10^{-3} S/m)		In-phase Component	
	Northing (ft)	Easting (ft)	Inline	Crossline	Inline	Crossline
0	832170	1885490	48.0	39.0	0.192	0.168
5	832165	1885489	49.8	40.0	0.216	0.204
10	832160	1885488	50.8	40.6	0.192	0.192
15	832155	1885487	52.8	41.0	0.144	0.144
20	832150	1885487	53.6	42.2	0.156	0.132
25	832145	1885486	52.0	42.2	0.180	0.168
30	832140	1885485	53.0	44.4	0.168	0.168
35	832135	1885485	55.6	45.8	0.168	0.168
40	832130	1885484	56.2	49.8	0.192	0.168
45	832125	1885483	51.4	52.4	0.168	0.180
50	832120	1885482	39.6	53.6	0.084	0.144
55	832115	1885482	20.8	41.0	0.012	0.108
60	832110	1885481	26.0	42.0	0.120	0.168
65	832105	1885480	49.4	60.8	0.120	0.168
70	832100	1885480	57.4	56.8	0.168	0.156
75	832095	1885479	54.8	54.0	0.156	0.168
80	832090	1885478	54.0	53.0	0.156	0.168
85	832085	1885478	56.4	53.0	0.192	0.168
90	832080	1885477	57.8	57.8	0.204	0.204
95	832075	1885476	62.2	63.0	0.240	0.240
100	832071	1885475	62.0	71.2	0.240	0.264
105	832066	1885475	36.2	76.2	0.144	0.252
110	832061	1885474	22.8	49.2	0.120	0.192
115	832056	1885473	50.8	71.8	0.228	0.289
120	832051	1885473	74.2	68.2	0.313	0.313
125	832046	1885472	78.4	63.4	0.313	0.325
130	832041	1885471	82.0	58.6	0.337	0.349
135	832036	1885470	85.4	55.6	0.373	0.373
140	832031	1885470	92.8	58.4	0.433	0.421
145	832026	1885469	93.4	68.4	0.529	0.529
150	832021	1885468	89.8	77.6	0.565	0.614
155	832016	1885468	64.8	76.8	0.337	0.590
160	832011	1885467	23.4	48.6	-0.072	0.216
165	832006	1885466	24.6	52.6	-0.012	0.301
170	832001	1885466	55.2	70.2	0.361	0.481
175	831996	1885465	40.4	69.8	0.276	0.505
180	831991	1885464	9.6	31.8	0.000	0.120
185	831986	1885463	59.2	36.0	0.650	0.180
190	831981	1885463	28.2	45.8	0.120	0.252
195	831976	1885462	37.4	44.8	0.096	0.216
200	831972	1885461	41.6	42.6	0.168	0.168
205	831967	1885461	41.8	41.6	0.156	0.156
210	831962	1885460	41.2	41.0	0.144	0.144
215	831957	1885459	41.4	41.8	0.156	0.144

Table B-6. Terrain conductivity data (EM-31) collected along profile B2. All measurements were made with the horizontal coplanar configuration.

Station (ft)	Location		Appararent Conductivity (10^{-3} S/m)		In-phase Component	
	Northing (ft)	Easting (ft)	Inline	Crossline	Inline	Crossline
0	832130	1885440	41.4	42.2	0.156	0.180
5	832125	1885439	43.4	43.0	0.180	0.168
10	832120	1885438	44.8	46.0	0.120	0.168
15	832115	1885438	45.8	50.8	0.132	0.156
20	832110	1885437	31.6	49.0	0.060	0.120
25	832105	1885437	21.8	31.8	0.180	0.168
30	832100	1885436	30.8	41.0	0.096	0.144
35	832095	1885435	47.0	48.0	0.096	0.036
40	832090	1885435	49.6	47.6	0.156	0.132
45	832085	1885434	47.4	46.8	0.156	0.156
50	832080	1885434	46.8	43.4	0.168	0.120
55	832075	1885433	47.2	47.6	0.204	0.156
60	832070	1885433	47.6	49.8	0.216	0.228
65	832065	1885432	49.0	52.8	0.204	0.228
70	832060	1885431	47.8	54.2	0.240	0.264
75	832055	1885431	47.0	51.4	0.192	0.204
80	832050	1885430	52.8	55.4	0.204	0.216
85	832045	1885430	59.6	52.0	0.289	0.240
90	832040	1885429	65.2	50.4	0.313	0.289
95	832035	1885428	76.8	53.2	0.337	0.301
100	832030	1885428	87.2	60.4	0.301	0.313
105	832025	1885427	94.2	59.2	0.325	0.228
110	832020	1885427	97.0	62.2	0.457	0.204
115	832015	1885426	89.8	78.2	0.481	0.493
120	832010	1885426	80.0	92.0	0.433	0.650
125	832005	1885425	39.4	73.0	0.108	0.433
130	832000	1885424	12.6	39.8	-0.072	0.132
135	831995	1885424	44.4	60.0	0.216	0.337
140	831990	1885423	64.0	76.4	0.433	0.493
145	831986	1885423	33.4	35.4	0.144	-0.012
150	831981	1885422	54.6	10.2	0.469	-0.505
155	831976	1885421	43.4	40.4	0.361	0.132
160	831971	1885421	32.4	44.8	0.036	0.204
165	831966	1885420	42.2	43.6	0.192	0.216
170	831961	1885420	42.8	42.4	0.216	0.216
175	831956	1885419	43.2	40.8	0.228	0.204

Table B-7. Terrain conductivity data (EM-31) collected along profile B3. All measurements were made with the horizontal coplanar configuration.

Station (ft)	Location		Apparent Conductivity (10^{-3} S/m)		In-phase Component	
	Northing (ft)	Easting (ft)	Inline	Crossline	Inline	Crossline
0	832144	1885399	34.4	33.6	0.120	0.144
5	832139	1885398	35.6	34.0	0.132	0.096
10	832134	1885398	39.4	40.2	0.108	0.132
15	832129	1885397	43.2	44.4	0.132	0.108
20	832124	1885397	28.4	38.8	0.108	0.120
25	832119	1885396	21.4	46.2	0.108	0.180
30	832114	1885396	49.4	67.4	0.240	0.264
35	832109	1885395	134.	96.0	0.903	0.602
40	832104	1885395	89.4	80.2	0.397	0.409
45	832099	1885394	-6.20	32.6	-0.493	0.096
50	832094	1885394	21.8	46.4	0.096	0.264
55	832089	1885393	41.0	31.4	0.240	0.132
60	832084	1885393	39.0	38.6	0.144	0.180
65	832079	1885392	39.8	40.6	0.108	0.132
70	832074	1885392	43.6	45.6	0.156	0.228
75	832069	1885391	50.2	52.0	0.264	0.252
80	832064	1885391	47.6	54.6	0.252	0.397
85	832059	1885390	31.2	47.0	-0.553	0.264
90	832054	1885390	29.6	54.4	-0.325	0.433
95	832049	1885389	42.0	55.0	0.301	0.349
100	832044	1885388	50.8	56.4	0.289	0.301
105	832039	1885388	52.2	52.0	0.301	0.313
110	832034	1885387	52.6	51.2	0.301	0.301
115	832029	1885387	53.6	52.2	0.313	0.313
120	832024	1885386	55.6	55.2	0.349	0.337
125	832019	1885386	60.6	59.2	0.409	0.397
130	832014	1885385	67.6	66.0	0.457	0.433
135	832009	1885385	74.4	73.6	0.457	0.445
140	832004	1885384	65.8	74.0	0.373	0.397
145	831999	1885384	28.6	43.8	0.204	0.289
150	831994	1885383	20.4	45.8	0.192	0.349
155	831989	1885383	43.2	63.4	0.240	0.313
160	831984	1885382	52.0	53.8	0.204	0.204
165	831979	1885382	50.0	48.6	0.228	0.192
170	831974	1885381	48.4	48.0	0.264	0.252
175	831969	1885381	48.2	48.4	0.252	0.252
180	831965	1885380	49.4	50.0	0.276	0.276
185	831960	1885380	53.6	55.6	0.325	0.337

Table B-8. Terrain conductivity data (EM-31) collected along profile I1. All measurements were made with the coils inline.

Station (ft)	Location		Apparent Conductivity (10^{-3} S/m)	
	Northing (ft)	Easting (ft)	HCP	VCP
0	833116	1885774	9.56	6.72
50	833066	1885768	8.46	6.24
100	833016	1885763	7.64	5.78
150	832967	1885757	7.62	4.88
200	832917	1885751	7.16	5.32
250	832867	1885745	6.76	4.74
300	832818	1885739	6.46	5.04
350	832768	1885733	5.34	4.36
400	832718	1885727	5.62	4.04
450	832669	1885721	5.90	4.20
500	832619	1885715	5.82	3.92
550	832570	1885710	9.42	5.14
600	832520	1885704	6.16	4.56
650	832470	1885698	11.8	7.44

Table B-9. Terrain conductivity data (EM-31) collected along profile I2. All measurements were made with the coils inline.

Station (ft)	Location		Apparent Conductivity (10^{-3} S/m)	
	Northing (ft)	Easting (ft)	HCP	VCP
0	833070	1886020	6.76	4.64
50	833021	1886006	6.08	3.80
100	832973	1885993	6.56	3.82
150	832925	1885980	6.72	4.28
200	832876	1885967	5.68	3.84
250	832828	1885954	5.50	3.64
300	832780	1885941	5.46	3.74
350	832732	1885928	5.88	3.86
400	832683	1885915	5.18	3.74
450	832635	1885902	7.38	4.32
500	832587	1885889	6.36	4.56

Table B-10. Terrain conductivity data (EM-31) collected along profile I3. All measurements were made with the coils inline.

Station (ft)	Location		Apparent Conductivity (10^{-3} S/m)	
	Northing (ft)	Easting (ft)	HCP	VCP
0	833160	1886500	33.8	18.0
50	833165	1886450	29.8	15.4
100	833169	1886400	30.8	17.2
150	833174	1886350	29.4	16.8
200	833179	1886301	30.0	16.8
250	833184	1886251	32.0	19.2
300	833189	1886201	31.0	19.2

Table B-11. Terrain conductivity data (EM-31) collected along profile M1. All measurements were made with the coils inline.

Station (ft)	Location		Apparent Conductivity (10^{-3} S/m)	
	Northing (ft)	Easting (ft)	HCP	VCP
0	830290	1884860	6.2	4.2
50	830302	1884811	6.9	5.4
100	830315	1884763	7.0	4.2
150	830327	1884714	8.0	5.2
200	830340	1884666	13.	6.0
250	830352	1884618	14.5	6.5
300	830365	1884569	11.	6.0
350	830377	1884521	14.	12.
400	830390	1884472	23.	11.
450	830402	1884424	21.	12.
500	830415	1884375	33.	18.
550	830427	1884327	39.	25.
600	830440	1884279	40.	26.

Table B-12. Terrain conductivity data (EM-31) collected along profile M2. All measurements were made with the coils inline.

Station (ft)	Location		Apparent Conductivity (10^{-3} S/m)	
	Northing (ft)	Easting(ft)	HCP	VCP
0	830010	1884740	24.5	14.5
50	830024	1884692	20.5	14.
100	830038	1884644	17.5	11.
150	830052	1884596	22.5	13.5
200	830066	1884548	17.	10.
250	830080	1884500	11.	7.0
300	830095	1884452	11.	7.0
350	830109	1884404	12.	7.0
400	830123	1884356	22.	13.
450	830137	1884308	19.	11.5

Table B-13. Terrain conductivity data (EM-31) collected along profile M3. All measurements were made with the coils inline.

Station (ft)	Location		Apparent Conductivity (10^{-3} S/m)	
	Northing (ft)	Easting (ft)	HCP	VCP
0	830680	1884610	30.	22.
25	830656	1884603	48.	38.
50	830631	1884596	64.	22.
75	830607	1884589	44.	16.
100	830583	1884582	26.5	14.
150	830535	1884568	19.5	11.
200	830487	1884554	19.	15.
250	830439	1884540	15.	12.
300	830391	1884526	14.	11.
350	830343	1884512	13.	8.0
400	830295	1884498	11.5	7.0
450	830247	1884485	12.	7.5
500	830199	1884471	13.	8.5
550	830151	1884457	12.5	9.0
600	830103	1884443	11.	8.0
650	830055	1884429	13.	11.
700	830007	1884415	14.5	11.
750	829959	1884401	15.5	10.
800	829911	1884387	17.5	10.5
850	829863	1884373	27.	16.5

Table B-14. Terrain conductivity data (EM-31) collected along profile M4. All measurements were made with the coils inline.

Station (ft)	Location		Apparent Conductivity (10^{-3} S/m)	
	Northing (ft)	Easting (ft)	HCP	VCP
0	830660	1884860	6.0	3.7
50	830611	1884847	5.3	3.4
100	830563	1884834	5.3	3.4
150	830515	1884821	5.4	3.6
200	830466	1884808	5.4	4.0
250	830418	1884795	5.6	3.7
300	830370	1884782	6.2	4.0
350	830322	1884769	6.0	4.3
400	830273	1884756	7.5	4.6
450	830225	1884743	9.2	5.2
500	830177	1884730	18.	10.
550	830128	1884717	26.	17.
600	830080	1884704	28.	16.
650	830032	1884691	23.	16.
700	829984	1884678	20.	18.
750	829935	1884665	25.	15.
800	829887	1884652	29.	16.

Table B-15. Terrain conductivity data (EM-31) collected along profile M5. All measurements were made with the coils inline.

Station (ft)	Location		Apparent Conductivity (10^{-3} S/m)	
	Northing (ft)	Easting (ft)	HCP	VCP
0	830440	1884280	42.	32.
50	830391	1884266	36.	27.
100	830343	1884253	35.	26.
150	830295	1884240	33.	24.
200	830246	1884227	32.	23.
250	830198	1884214	24.	16.
300	830150	1884201	23.	15.
350	830102	1884188	21.	14.
400	830053	1884175	19.5	14.
450	830005	1884162	22.	18.
500	829957	1884149	28.5	21.

Table B-16. Terrain conductivity data (EM-31) collected along profile P1. All measurements were made with the horizontal coplanar configuration and with the coils inline. A measurement could not be made at station 0 because it was less that 3 feet from a metal fence.

Station (ft)	Location		Apparent Conductivity (10^{-3} S/m)
	Northing (ft)	Easting (ft)	
0	830489	1885462	
17	830487	1885445	107.
34	830485	1885428	139.
50	830483	1885413	140.
75	830480	1885388	99.
100	830477	1885363	67.
125	830475	1885338	47.
150	830472	1885313	43.
175	830469	1885288	36.
200	830466	1885264	31.
225	830463	1885239	30.
250	830461	1885214	20.
275	830458	1885189	20.
300	830455	1885164	18.
325	830452	1885139	18.
350	830449	1885114	21.
375	830447	1885090	16.
400	830444	1885065	36.
425	830441	1885040	15.
450	830438	1885015	14.
475	830435	1884990	14.
500	830433	1884965	14.
525	830430	1884941	13.
550	830427	1884916	13.
575	830424	1884891	14.
600	830421	1884866	14.
625	830419	1884841	14.
650	830416	1884816	15.
700	830410	1884767	17.
750	830404	1884717	20.
800	830399	1884667	28.
850	830393	1884618	26.
900	830388	1884568	34.
950	830382	1884518	31.
1000	830376	1884469	36.
1050	830371	1884419	33.
1100	830365	1884369	47.
1150	830360	1884320	52.

Table B-17. Terrain conductivity data (EM-31) collected along profile P2. All measurements were made with the horizontal coplanar configuration and with the coils inline. A measurement could not be made at station 0 because it was less that 3 feet from a fence.

Station (ft)	Location		Apparent Conductivity (10^{-3} S/m)
	Northing (ft)	Easting (ft)	
0	830361	1885442	
17	830363	1885425	130.
34	830365	1885408	105.
50	830366	1885392	110.
75	830369	1885367	110.
100	830371	1885342	54.
125	830374	1885317	54.
150	830377	1885292	30.
200	830382	1885243	23.
225	830384	1885218	21.
250	830387	1885193	17.
275	830389	1885168	17.
300	830392	1885143	17.
325	830394	1885118	21.
350	830397	1885093	19.
375	830399	1885069	24.
400	830402	1885044	11.
425	830404	1885019	14.
450	830407	1884994	14.
475	830409	1884969	14.
500	830412	1884944	15.
525	830414	1884919	14.
550	830417	1884894	14.
575	830420	1884870	13.

Table B-18. Terrain conductivity data (EM-31) collected along profile W1. All measurements were made with the coils inline.

Station (ft)	Location		Apparent Conductivity (10^{-3} S/m)	
	Northing (ft)	Easting (ft)	HCP	VCP
0	833080	1884570	6.9	5.0
25	833055	1884573	8.1	5.8
50	833030	1884576	8.1	6.3
75	833005	1884579	7.0	5.2
100	832980	1884582	5.7	4.0
125	832955	1884585	4.2	3.1
150	832931	1884588	4.6	3.2
175	832906	1884591	5.5	3.7
200	832881	1884594	5.5	3.8
225	832856	1884597	6.6	5.5
250	832831	1884601	6.5	4.9
275	832807	1884604	6.7	4.2
300	832782	1884607	9.0	6.5
325	832757	1884610	10.5	8.6
350	832732	1884613	11.5	8.6
375	832707	1884616	10.5	8.6
400	832683	1884619	11.5	9.8

Table B-19. Terrain conductivity data (EM-31) collected along profile W2. All measurements were made with the coils inline.

Station (ft)	Location		Apparent Conductivity (10^{-3} S/m)	
	Northing (ft)	Easting (ft)	HCP	VCP
0	832930	1884690	5.40	5.20
25	832927	1884665	5.36	4.12
50	832924	1884640	4.74	3.14
75	832921	1884615	4.84	2.92
100	832918	1884590	5.10	3.08
125	832915	1884565	6.02	3.48
150	832912	1884541	5.80	4.46
175	832909	1884516	5.98	3.72
200	832906	1884491	6.06	4.38
225	832903	1884466	6.86	4.52
250	832900	1884441	5.76	3.76

Table B-20. Terrain conductivity data (EM-31) collected along profile W3. All measurements were made with the coils inline.

Station (ft)	Location		Apparent Conductivity (10^{-3} S/m)	
	Northing (ft)	Easting (ft)	HCP	VCP
0	832780	1885350	27.6	17.8
25	832778	1885325	31.8	19.0
50	832777	1885300	33.2	20.2
75	832776	1885275	31.0	19.8
100	832775	1885250	33.6	25.0
125	832774	1885225	34.4	23.8
150	832773	1885200	34.2	20.4
175	832772	1885175	36.0	24.4
200	832771	1885150	32.6	20.4
225	832770	1885125	25.8	15.8
250	832768	1885100	29.0	17.4
275	832767	1885075	31.2	18.2
300	832766	1885050	31.2	17.6
325	832765	1885025	34.6	19.4
350	832764	1885000	36.4	21.6
375	832763	1884975	36.2	21.6
400	832762	1884950	37.2	23.2
425	832761	1884925	39.2	25.8
450	832760	1884900	38.4	26.2

APPENDIX C

TERRAIN CONDUCTIVITY DATA (EM-34)

This appendix contains the terrain conductivity data collected along the profiles using the Geonics EM-34. The horizontal coplanar and vertical coplanar coil configurations are described in Frischknecht et al. (1991, p. 106). The locations were determined using the method described in the section entitled "Data Collection and Processing", which is in the main body of the report. The spacings refer to the distance between the transmitting and receiving coils. The station is the distance along the profile.

In these tables are a few entries that do not have a measurement. For these cases, the measurement was either negative or the measurement could not be made because a fence blocked the way.

Table C-1. Terrain conductivity data (EM-34) for the HCP configuration collected along profile A1.

Station (ft)	Location		Apparent Conductivity (10^{-3} S/m)		
	Northing (ft)	Easting (ft)	10 m Spacing	20 m Spacing	40 m Spacing
0	831280	1884630	15.	17.	28.
20	831263	1884641	13.5	16.5	18.
40	831246	1884652	15.	19.	17.
50	831238	1884657	14.	17.5	18.
60	831230	1884663	13.	18.	26.5
70	831221	1884668	12.	16.	27.
90	831205	1884679	12.	19.	19.
120	831188	1884691	13.	20.5	20.

Table C-2. Terrain conductivity data (EM-34) for the VCP configuration collected along profile A1.

Station (ft)	Location		Apparent Conductivity (10^{-3} S/m)		
	Northing (ft)	Easting (ft)	10 m Spacing	20 m Spacing	40 m Spacing
0	831280	1884630	11.	14.5	16.
20	831263	1884641	11.5	13.5	14.5
40	831246	1884652	10.5	14.	16.
50	831238	1884657	10.5	13.5	16.
60	831230	1884663	9.5	14.	14.5
70	831221	1884668	9.5	12.5	15.
90	831205	1884679	8.0	12.5	16.
120	831188	1884691	7.0	13.	17.

Table C-3. Terrain conductivity data (EM-34) for the HCP configuration collected along profile A2.

Station (ft)	Location		Apparent Conductivity (10-3 S/m)		
	Northing (ft)	Easting (ft)	10 m Spacing	20 m Spacing	40 m Spacing
0	831530	1884420	21.	18.	14.
25	831505	1884413	21.	21.5	29.
50	831481	1884407	21.	20.	20.
75	831457	1884400	18.5	21.	18.
100	831433	1884394	20.5	16.5	17.
125	831409	1884387	18.5	21.5	17.
150	831385	1884381	28.	20.	12.

Table C-4. Terrain conductivity data (EM-34) for the VCP configuration collected along profile A2.

Station (ft)	Location		Apparent Conductivity (10-3 S/m)		
	Northing (ft)	Easting (ft)	10 m Spacing	20 m Spacing	40 m Spacing
0	831530	1884420	14.5	18.	21.
25	831505	1884413	14.5	18.	19.5
50	831481	1884407	15.	19.	19.5
75	831457	1884400	16.	19.	19.5
100	831433	1884394	18.	20.	19.
125	831409	1884387	19.	19.	19.
150	831385	1884381	19.	21.	20.5

Table C-5. Terrain conductivity data (EM-34) for the HCP configuration collected along profile A3.

Station (ft)	Location		Apparent Conductivity (10^{-3} S/m)		
	Northing (ft)	Easting (ft)	10 m Spacing	20 m Spacing	40 m Spacing
0	831410	1884440	21.5	22.	27.
25	831418	1884416	19.	21.	24.
50	831426	1884392	21.5	17.5	19.
75	831435	1884369	24.	19.	15.
100	831443	1884345	22.	17.	20.
125	831452	1884322	25.	25.5	18.5
150	831460	1884298	24.	19.	13.

Table C-6. Terrain conductivity data (EM-34) for the VCP configuration collected along profile A3.

Station (ft)	Location		Apparent Conductivity (10-3 S/m)		
	Northing (ft)	Easting (ft)	10 m Spacing	20 m Spacing	40 m Spacing
0	831410	1884440	12.	15.	17.
25	831418	1884416	15.	16.	18.
50	831426	1884392	17.	19.	17.
75	831435	1884369	20.	22.	18.
100	831443	1884345	18.5	22.	19.
125	831452	1884322	15.5	19.	19.
150	831460	1884298	14.	20.	21.

Table C-7. Terrain conductivity data (EM-34) for the HCP configuration collected along profile A4.

Station (ft)	Location		Apparent Conductivity (10^{-3} S/m)		
	Northing (ft)	Easting (ft)	10 m Spacing	20 m Spacing	40 m Spacing
0	831990	1884910	32.	27.	24.
100	831948	1884818	33.	26.	23.
200	831907	1884727	23.	14.5	13.
300	831866	1884636	26.	17.	14.
400	831825	1884545	26.	22.	21.
500	831784	1884454	2.5	11.	14.5
600	831743	1884363	24.	6.0	15.
700	831702	1884272	38.	19.	13.
800	831661	1884180	40.	46.	4.0
900	831619	1884089	35.	32.	50.

Table C-8. Terrain conductivity data (EM-34) for the VCP configuration collected along profile A4.

Station (ft)	Location		Apparent Conductivity (10^{-3} S/m)		
	Northing (ft)	Easting (ft)	10 m Spacing	20 m Spacing	40 m Spacing
0	831990	1884910	32.	31.	27.
100	831948	1884818	22.	25.	24.
200	831907	1884727	24.	24.	22.5
300	831866	1884636	44.	30.	22.5
400	831825	1884545	30.	28.	24.
500	831784	1884454	32.	31.	24.5
600	831743	1884363	41.	31.	22.
700	831702	1884272	30.	32.	25.
800	831661	1884180	44.	40.	22.
900	831619	1884089	32.	32.	28.

Table C-9. Terrain conductivity data (EM-34) for the HCP configuration collected along profile I1.

Station (ft)	Location		Apparent Conductivity (10-3 S/m)		
	Northing (ft)	Easting (ft)	10 m Spacing	20 m Spacing	40 m Spacing
0	833116	1885774	16.	16.	16.
50	833066	1885768	16.	17.	17.
100	833016	1885763	14.5	17.5	17.
150	832967	1885757	15.	16.	17.
200	832917	1885751	12.	16.5	16.5
250	832867	1885745	12.5	16.	17.
300	832818	1885739	11.	15.	17.
350	832768	1885733	10.	17.	20.
400	832718	1885727	11.5	15.5	19.
450	832669	1885721	11.5	13.5	19.
500	832619	1885715	10.	14.	19.
550	832570	1885710	10.5	13.	22.
600	832520	1885704	14.	19.5	29.
650	832470	1885698	22.5	21.	24.

Table C-10. Terrain conductivity data (EM-34) for the VCP configuration collected along profile I1.

Station (ft)	Location		Apparent Conductivity (10^{-3} S/m)		
	Northing (ft)	Easting (ft)	10 m Spacing	20 m Spacing	40 m Spacing
0	833116	1885774	11.	14.	18.
50	833066	1885768	10.5	15.5	16.
100	833016	1885763	9.0	13.5	18.
150	832967	1885757	9.0	13.5	16.
200	832917	1885751	8.0	7.5	16.
250	832867	1885745	8.0	12.5	18.
300	832818	1885739	8.0	7.5	20.
350	832768	1885733	7.0	10.5	18.
400	832718	1885727	7.0	10.	19.
450	832669	1885721	8.0	11.	18.
500	832619	1885715	7.0	10.5	18.
550	832570	1885710	9.0	12.	20.
600	832520	1885704	9.5	13.5	22.
650	832470	1885698	15.	17.	28.

Table C-11. Terrain conductivity data (EM-34) for the HCP configuration collected along profile I2.

Station (ft)	Location		Apparent Conductivity (10^{-3} S/m)		
	Northing (ft)	Easting (ft)	10 m Spacing	20 m Spacing	40 m Spacing
0	833070	1886020	6.5	12.	17.
50	833021	1886006	8.5	13.	12.
100	832973	1885993	9.0	12.	18.
150	832925	1885980	9.0	11.	16.
200	832876	1885967	8.5	14.	19.
250	832828	1885954	8.5	14.5	16.
300	832780	1885941	9.0	14.	16.
350	832732	1885928	9.0	14.5	18.
400	832683	1885915	10.	14.	17.
450	832635	1885902	11.	15.	18.
500	832587	1885889	12.	17.5	22.

Table C-12. Terrain conductivity data (EM-34) for the VCP configuration collected along profile I2.

Station (ft)	Location		Apparent Conductivity (10^{-3} S/m)		
	Northing (ft)	Easting (ft)	10 m Spacing	20 m Spacing	40 m Spacing
0	833070	1886020	5.5	9.0	18.
50	833021	1886006	5.5	9.5	14.
100	832973	1885993	5.5	9.0	18.
150	832925	1885980	6.0	9.5	18.
200	832876	1885967	5.0	9.0	17.
250	832828	1885954	5.0	9.0	18.
300	832780	1885941	5.0	9.5	18.
350	832732	1885928	5.5	9.5	20.
400	832683	1885915	6.0	9.5	16.
450	832635	1885902	6.0	10.	18.
500	832587	1885889	7.0	11.	20.

Table C-13. Terrain conductivity data (EM-34) for the HCP configuration collected along profile I3.

Station (ft)	Location		Apparent Conductivity (10^{-3} S/m)		
	Northing (ft)	Easting (ft)	10 m Spacing	20 m Spacing	40 m Spacing
0	833160	1886500	36.		
50	833165	1886450	46.	53.	
100	833169	1886400	38.	36.	38.
150	833174	1886350	35.	37.	30.
200	833179	1886301	33.	31.	32.
250	833184	1886251	30.	18.	20.
300	833189	1886201	24.	22.	19.

Table C-14. Terrain conductivity data (EM-34) for the VCP configuration collected along profile I3.

Station (ft)	Location		Apparent Conductivity (10^{-3} S/m)		
	Northing (ft)	Easting (ft)	10 m Spacing	20 m Spacing	40 m Spacing
0	833160	1886500	50.	59.	42.
50	833165	1886450	33.	38.	40.
100	833169	1886400	36.	36.	30.
150	833174	1886350	34.	34.	32.
200	833179	1886301	32.	34.	32.
250	833184	1886251	35.	33.	31.
300	833189	1886201	32.	31.	27.

Table C-15. Terrain conductivity data (EM-34) for the HCP configuration collected along profile M1.

Station (ft)	Location		Apparent Conductivity (10^{-3} S/m)		
	Northing (ft)	Easting (ft)	10 m Spacing	20 m Spacing	40 m Spacing
0	830290	1884860	14.	17.	13.
50	830302	1884811	13.	23.	21.
100	830315	1884763	16.	21.5	19.
150	830327	1884714	14.5	17.5	20.
200	830340	1884666	31.	20.	
250	830352	1884618	19.		
300	830365	1884569	21.	27.	10.
350	830377	1884521	17.	16.5	18.
400	830390	1884472	24.	10.	13.
450	830402	1884424	30.	26.5	14.
500	830415	1884375	19.	21.	21.
550	830427	1884327	28.	22.	13.
600	830440	1884279	21.	17.	13.

Table C-16. Terrain conductivity data (EM-34) for the VCP configuration collected along profile M1.

Station (ft)	Location		Apparent Conductivity (10^{-3} S/m)		
	Northing (ft)	Easting (ft)	10 m Spacing	20 m Spacing	40 m Spacing
0	830290	1884860	8.0	15.	16.
50	830302	1884811	7.5	14.5	18.
100	830315	1884763	8.5	15.5	18.
150	830327	1884714	9.0	15.5	17.
200	830340	1884666	13.	17.5	14.
250	830352	1884618	11.	14.5	13.
300	830365	1884569	11.	18.5	18.
350	830377	1884521	16.	19.	18.
400	830390	1884472	21.	21.5	18.
450	830402	1884424	20.	24.	20.
500	830415	1884375	27.	27.5	23.
550	830427	1884327	35.	30.	23.
600	830440	1884279	38.	30.	24.

Table C-17. Terrain conductivity data (EM-34) for the HCP configuration collected along profile M2.

Station (ft)	Location		Apparent Conductivity (10^{-3} S/m)		
	Northing (ft)	Easting (ft)	10 m Spacing	20 m Spacing	40 m Spacing
0	830010	1884740	37.	28.	21.
50	830024	1884692	20.	19.	24.
100	830038	1884644	26.	30.	29.
150	830052	1884596	21.	0.7	3.0
200	830066	1884548	29.5	5.0	6.0
250	830080	1884500	20.5	25.	14.
300	830095	1884452	16.	19.5	26.
350	830109	1884404	21.	16.	12.
400	830123	1884356	13.	6.0	12.
450	830137	1884308	19.	20.	16.

Table C-18. Terrain conductivity data (EM-34) for the VCP configuration collected along profile M2.

Station (ft)	Location		Apparent Conductivity (10^{-3} S/m)		
	Northing (ft)	Easting (ft)	10 m Spacing	20 m Spacing	40 m Spacing
0	830010	1884740	23.	31.	30.
50	830024	1884692	22.	26.	26.
100	830038	1884644	20.	27.	24.
150	830052	1884596	19.	20.	17.
200	830066	1884548	18.5	19.5	16.
250	830080	1884500	14.	19.5	19.
300	830095	1884452	10.	17.	17.
350	830109	1884404	12.	17.	16.
400	830123	1884356	18.	18.	17.
450	830137	1884308	15.	20.	19.

Table C-19. Terrain conductivity data (EM-34) for the HCP configuration collected along profile M3.

Station (ft)	Location		Apparent Conductivity (10^{-3} S/m)		
	Northing (ft)	Easting (ft)	10 m Spacing	20 m Spacing	40 m Spacing
0	830680	1884610	27.0	20.0	24.0
50	830631	1884596			6.0
100	830583	1884582	47.0	63.0	6.0
150	830535	1884568	28.0	27.0	22.0
200	830487	1884554	18.0	16.0	15.0
250	830439	1884540	26.0	24.0	17.0
300	830391	1884526	28.0	26.0	15.0
350	830343	1884512	24.0	24.0	18.0
400	830295	1884498	22.0	23.0	18.0
450	830247	1884485	22.0	19.0	16.0
500	830199	1884471	20.0	20.0	14.0
550	830151	1884457	18.0	18.0	17.0
600	830103	1884443	17.0	25.0	20.0
650	830055	1884429	18.0	21.0	16.0
700	830007	1884415	18.0	19.0	20.0
750	829959	1884401	22.0	22.0	19.0
800	829911	1884387	24.0	19.0	25.0
850	829863	1884373	22.0	28.0	

Table C-20. Terrain conductivity data (EM-34) for the VCP configuration collected along profile M3.

Station (ft)	Location		Apparent Conductivity (10^{-3} S/m)		
	Northing (ft)	Easting (ft)	10 m Spacing	20 m Spacing	40 m Spacing
0	830680	1884610	30.	24.	24.
50	830631	1884596	47.	30.	21.
100	830583	1884582	24.	27.	19.
150	830535	1884568	21.	26.	27.
200	830487	1884554	27.	30.	24.
250	830439	1884540	20.	27.	21.
300	830391	1884526	18.	21.5	20.
350	830343	1884512	18.	21.5	19.
400	830295	1884498	12.	21.	18.
450	830247	1884485	15.	19.	18.
500	830199	1884471	18.	22.	19.
550	830151	1884457	18.	20.	19.
600	830103	1884443	14.	19.	21.
650	830055	1884429	20.	23.	21.
700	830007	1884415	20.	24.	22.
750	829959	1884401	19.	23.	26.
800	829911	1884387	20.	25.	27.
850	829863	1884373	27.	31.	

Table C-21. Terrain conductivity data (EM-34) for the HCP configuration collected along profile M4.

Station (ft)	Location		Apparent Conductivity (10^{-3} S/m)		
	Northing (ft)	Easting (ft)	10 m Spacing	20 m Spacing	40 m Spacing
0	830660	1884860	13.	16.	18.
50	830611	1884847	12.	16.	18.
100	830563	1884834	11.5	17.	18.
150	830515	1884821	11.	16.	17.
200	830466	1884808	12.	18.5	20.
250	830418	1884795	12.5	20.5	20.
300	830370	1884782	13.5	21.5	22.
350	830322	1884769	16.	23.	20.
400	830273	1884756	19.	26.5	25.
450	830225	1884743	22.	30.	28.
500	830177	1884730	27.	25.	20.
550	830128	1884717	37.	25.	14.
600	830080	1884704	34.	25.	16.
650	830032	1884691	28.	30.	27.
700	829984	1884678	18.	28.	33.
750	829935	1884665	32.	34.	
800	829887	1884652	32.	55.	

Table C-22. Terrain conductivity data (EM-34) for the VCP configuration collected along profile M4.

Station (ft)	Location		Apparent Conductivity (10^{-3} S/m)		
	Northing (ft)	Easting (ft)	10 m Spacing	20 m Spacing	40 m Spacing
0	830660	1884860	6.5	12.	14.
50	830611	1884847	6.0	11.	14.
100	830563	1884834	6.0	11.	14.
150	830515	1884821	6.5	11.	14.
200	830466	1884808	6.5	11.5	14.
250	830418	1884795	6.0	12.5	14.
300	830370	1884782	7.5	13.5	16.
350	830322	1884769	8.5	15.	16.
400	830273	1884756	9.5	16.5	20.
450	830225	1884743	11.	20.	22.
500	830177	1884730	20.	22.	19.
550	830128	1884717	26.	26.	20.
600	830080	1884704	29.	28.	25.
650	830032	1884691	30.	34.	25.
700	829984	1884678	29.	33.	28.
750	829935	1884665	24.	30.	27.
800	829887	1884652	30.	35.	

Table C-23. Terrain conductivity data (EM-34) for the HCP configuration collected along profile M5.

Station (ft)	Location		Apparent Conductivity (10^{-3} S/m)		
	Northing (ft)	Easting (ft)	10 m Spacing	20 m Spacing	40 m Spacing
0	830440	1884280	18.	18.	15.
50	830391	1884266	24.	22.	14.
100	830343	1884253	21.	16.	16.
150	830295	1884240	27.	17.	13.
200	830246	1884227	21.	17.	14.
250	830198	1884214	21.	18.	13.
300	830150	1884201	22.	17.	15.
350	830102	1884188	18.	17.	18.
400	830053	1884175	20.	18.	19.
450	830005	1884162	20.	18.	15.
500	829957	1884149	19.	13.	13.

Table C-24. Terrain conductivity data (EM-34) for the VCP configuration collected along profile M5.

Station (ft)	Location		Apparent Conductivity (10^{-3} S/m)		
	Northing (ft)	Easting (ft)	10 m Spacing	20 m Spacing	40 m Spacing
0	830440	1884280	34.	29.	24.
50	830391	1884266	32.	27.	25.
100	830343	1884253	29.	25.	23.
150	830295	1884240	28.	25.	21.
200	830246	1884227	27.	24.	21.
250	830198	1884214	22.	22.	22.
300	830150	1884201	20.	20.	22.
350	830102	1884188	19.	20.	20.
400	830053	1884175	17.	19.	21.
450	830005	1884162	18.	20.	21.
500	829957	1884149	23.	22.	21.

Table C-25. Terrain conductivity data (EM-34) for the HCP configuration collected along profile W1.

Station (ft)	Location		Apparent Conductivity (10^{-3} S/m)		
	Northing (ft)	Easting (ft)	10 m Spacing	20 m Spacing	40 m Spacing
0	833080	1884570	8.0	10.	11.
50	833030	1884576	7.5	9.0	11.
100	832980	1884582	4.5	9.0	11.
150	832931	1884588	8.0	10.0	12.
200	832881	1884594	8.0	9.0	12.5
250	832831	1884601	7.0	9.5	12.5
300	832782	1884607	9.0	11.	12.5
350	832732	1884613	12.	12.	12.
400	832683	1884619	13.	13.	12.

Table C-26. Terrain conductivity data (EM-34) for the VCP configuration collected along profile W1.

Station (ft)	Location		Apparent Conductivity (10^{-3} S/m)		
	Northing (ft)	Easting (ft)	10 m Spacing	20 m Spacing	40 m Spacing
0	833080	1884570	6.5	8.0	10.
50	833030	1884576	7.5	8.0	10.
100	832980	1884582	5.0	7.5	10.
150	832931	1884588	5.5	7.5	9.0
200	832881	1884594	6.5	8.0	11.
250	832831	1884601	6.0	8.0	11.
300	832782	1884607	8.0	8.5	11.
350	832732	1884613	10.	10.	11.5
400	832683	1884619	10.5	10.5	10.5

Table C-27. Terrain conductivity data (EM-34) for the HCP configuration collected along profile W2.

Station (ft)	Location		Apparent Conductivity (10^{-3} S/m)		
	Northing (ft)	Easting (ft)	10 m Spacing	20 m Spacing	40 m Spacing
0	832930	1884690	6.0	10.	12.
50	832924	1884640	7.5	10.	12.
100	832918	1884590	7.5	8.0	12.
150	832912	1884541	6.0	8.0	12.5
200	832906	1884491	6.0	8.0	11.5
250	832900	1884441	6.0	9.0	12.

Table C-28. Terrain conductivity data (EM-34) for the VCP configuration collected along profile W2.

Station (ft)	Location		Apparent Conductivity (10^{-3} S/m)		
	Northing (ft)	Easting (ft)	10 m Spacing	20 m Spacing	40 m Spacing
0	832930	1884690	5.5	8.0	10.
50	832924	1884640	5.0	7.0	10.5
100	832918	1884590	5.0	6.5	9.0
150	832912	1884541	6.5	8.0	10.
200	832906	1884491	6.5	7.0	10.
250	832900	1884441	5.5	6.5	9.0

Table C-29. Terrain conductivity data (EM-34) for the HCP configuration collected along profile W3.

Station (ft)	Location		Apparent Conductivity (10^{-3} S/m)		
	Northing (ft)	Easting (ft)	10 m Spacing	20 m Spacing	40 m Spacing
0	832780	1885350	28.	21.	17.
50	832777	1885300	19.	15.	16.
100	832775	1885250	23.	21.	19.
150	832773	1885200	24.	19.5	16.
200	832771	1885150	20.	16.5	19.
250	832768	1885100	18.	23.	21.
300	832766	1885050	26.	19.	12.
350	832764	1885000	28.	14.5	12.
400	832762	1884950	24.	18.	12.
450	832760	1884900	16.	17.	16.

Table C-30. Terrain conductivity data (EM-34) for the VCP configuration collected along profile W3.

Station (ft)	Location		Apparent Conductivity (10^{-3} S/m)		
	Northing (ft)	Easting (ft)	10 m Spacing	20 m Spacing	40 m Spacing
0	832780	1885350	27.	25.5	26.
50	832777	1885300	29.	25.	22.
100	832775	1885250	30.	25.	23.
150	832773	1885200	28.	26.	24.
200	832771	1885150	28.	25.	25.
250	832768	1885100	26.	25.	26.
300	832766	1885050	29.	26.	23.
350	832764	1885000	33.	27.	23.
400	832762	1884950	32.	27.	25.
450	832760	1884900	30.	25.	23.

APPENDIX D

TIME-DOMAIN ELECTROMAGNETIC DATA

This appendix contains the locations of the eight time-domain electromagnetic soundings and the data, which are expressed in terms of apparent resistivity. The receiver was a Geonics EM-37, and the transmitter a Geonics EM-47. The side of the transmitter coil is 38.1 m (125 ft) long, and its turn-off time is 2.44×10^{-6} s. High frequency refers to a transmitter repetition rate of 30 Hz; very high frequency 315 Hz. We deleted those date that are noisy (i.e., their standard deviations, which are expressed as a percentage of the means, are greater than approximately 10 percent).

Table D-1. Locations of the center of the transmitter coil for the time-domain electromagnetic soundings. The locations are expressed in state plane coordinates, which we rounded to the nearest 10 ft interval.

Name of Sounding	Location	
	Northing (ft)	Easting (ft)
S1	830390	1884220
S2	832870	1884610
S3	833000	1884600
S4	832740	1885850
S5	832810	1885960
S6	832720	1884960
S7	830400	1884750
S8	831870	1884540

Table D-2. Time-domain electromagnetic data from sounding S1 (very high frequency). The current in the transmitter loop was 0.5 A, and 256 measurements were stacked.

Time (10^{-3} s)	Apparent Resistivity (Ω-m)
0.00690	30.93
0.00900	28.87
0.0121	29.34
0.0160	30.54
0.0202	31.44
0.0263	32.78
0.0338	34.77
0.0425	36.55
0.0547	39.38
0.0693	43.30
0.0860	42.88
0.107	43.66
0.138	46.05
0.175	45.36
0.219	44.36
0.280	44.33
0.354	40.33
0.441	46.93
0.561	51.38
0.707	37.24

Table D-3. Time-domain electromagnetic data from sounding S1 (high frequency). The current in the transmitter loop was 2.0 A, and 256 measurements were stacked.

Time (10^{-3} s)	Apparent Resistivity (Ω-m)
0.101	40.31
0.122	41.31
0.152	42.54
0.188	43.56
0.230	44.52
0.291	44.31
0.367	44.05
0.455	44.75
0.575	44.86
0.720	41.32

Table D-4. Time-domain electromagnetic data from sounding S2 (very high frequency). The current in the transmitter loop was 1.0 A, and 256 measurements were stacked. (Because we did not observe any signal at the high frequency, we did not record any data.)

Time (10^{-3} s)	Apparent Resistivity (Ω-m)
0.00690	56.47
0.00900	70.06
0.0121	106.2
0.0160	173.2
0.0202	515.6
0.0263	573.2
0.0338	419.6
0.0425	443.1
0.0547	383.6
0.0693	339.4
0.0860	276.0
0.107	304.5

Table D-5. Time-domain electromagnetic data from sounding S3 (very high frequency). The current in the transmitter loop was 1.0 A, and 256 measurements were stacked.

Time (10^{-3} s)	Apparent Resistivity (Ω-m)
0.00690	53.90
0.00900	55.99
0.0121	76.62
0.0160	108.7
0.0202	126.4
0.0263	104.8
0.0338	78.63
0.0425	59.52
0.0547	46.57
0.0693	37.62
0.0860	30.13
0.107	24.60
0.138	19.84
0.175	16.16
0.219	13.82
0.280	12.18
0.354	11.75
0.441	11.36

Table D-6. Time-domain electromagnetic data from sounding S3 (high frequency). The current in the transmitter loop was 1.0 A, and 256 measurements were stacked.

Time (10^{-3} s)	Apparent Resistivity (Ω-m)
0.101	26.57
0.122	22.61
0.152	18.82
0.188	16.46
0.230	14.88
0.291	13.31
0.367	11.83

Table D-7. Time-domain electromagnetic data from sounding S4 (very high frequency). The current in the transmitter loop was 1.0 A, and 256 measurements were stacked.

Time (10^{-3} s)	Apparent Resistivity (Ω-m)
0.00690	54.36
0.00900	50.49
0.0121	50.35
0.0160	49.44
0.0202	48.61
0.0263	48.62
0.0338	49.49
0.0425	49.63
0.0547	50.19
0.0693	51.33
0.0860	49.66
0.107	50.15
0.138	49.64
0.175	46.91
0.219	44.78

Table D-8. Time-domain electromagnetic data from sounding S4 (high frequency). The current in the transmitter loop was 2.0 A, and 1024 measurements were stacked.

Time (10^{-3} s)	Apparent Resistivity (Ω-m)
0.101	52.53
0.122	54.11
0.152	51.77

Table D-9. Time-domain electromagnetic data from sounding S5 (very high frequency). The current in the transmitter loop was 1.0 A, and 256 measurements were stacked.

Time (10^{-3} s)	Apparent Resistivity (Ω-m)
0.00690	59.00
0.00900	48.52
0.0121	50.99
0.0160	48.45
0.0202	46.82
0.0263	46.04
0.0338	46.40
0.0425	46.43
0.0547	48.12
0.0693	50.83
0.0860	50.25
0.107	51.80
0.138	54.02
0.175	56.40

Table D-10. Time-domain electromagnetic data from sounding S5 (high frequency). The current in the transmitter loop was 2.0 A, and 256 measurements were stacked.

Time (10^{-3} s)	Apparent Resistivity (Ω-m)
0.101	49.46
0.122	51.12
0.152	54.07
0.188	57.46

Table D-11. Time-domain electromagnetic data from sounding S6 (very high frequency). The current in the transmitter loop was 0.5 A, and 256 measurements were stacked.

Time (10^{-3} s)	Apparent Resistivity (Ω-m)
0.00690	33.58
0.00900	32.28
0.0121	35.42
0.0160	37.79
0.0202	38.82
0.0263	39.40
0.0338	40.25
0.0425	40.73
0.0547	42.64
0.0693	45.63
0.0860	46.87
0.107	49.69
0.138	55.78
0.175	55.56
0.219	59.80
0.280	63.03

Table D-12. Time-domain electromagnetic data from sounding S6 (high frequency). The current in the transmitter loop was 2.0 A, and 1024 measurements were stacked.

Time (10^{-3} s)	Apparent Resistivity (Ω-m)
0.101	45.91
0.122	48.78
0.152	52.74
0.188	57.87
0.230	62.24
0.291	67.38
0.367	74.94
0.455	82.48
0.575	88.32
0.720	90.29

Table D-13. Time-domain electromagnetic data from sounding S7 (very high frequency). The current in the transmitter loop was 0.8 A, and 256 measurements were stacked.

Time (10^{-3} s)	Apparent Resistivity (Ω-m)
0.00690	46.45
0.00900	40.14
0.0121	38.41
0.0160	36.81
0.0202	35.47
0.0263	34.77
0.0338	34.68
0.0425	34.54
0.0547	35.44
0.0693	37.57
0.0860	38.23
0.107	40.01
0.138	42.63
0.175	44.93
0.219	43.66
0.280	46.54
0.354	45.40

Table D-14. Time-domain electromagnetic data from sounding S7 (high frequency). The current in the transmitter loop was 2.0 A, and 1024 measurements were stacked.

Time (10^{-3} s)	Apparent Resistivity (Ω-m)
0.101	37.48
0.122	39.93
0.152	42.59
0.188	44.02
0.230	47.08
0.291	44.84
0.367	46.22
0.455	43.29
0.575	41.37
0.720	35.65
0.880	37.66

Table D-15. Time-domain electromagnetic data from sounding S8 (very high frequency). The current in the transmitter loop was 0.5 A, and 256 measurements were stacked.

Time (10^{-3} s)	Apparent Resistivity (Ω-m)
0.00690	37.38
0.00900	32.96
0.0121	33.35
0.0160	33.85
0.0202	34.23
0.0263	35.82
0.0338	38.60
0.0425	41.52
0.0547	46.47
0.0693	53.89
0.0860	57.57
0.107	65.59
0.138	72.21
0.175	82.21
0.219	97.79
0.280	127.4

Table D-16. Time-domain electromagnetic data from sounding S8 (high frequency). The current in the transmitter loop was 2.0 A, and 1024 measurements were stacked.

Time (10^{-3} s)	Apparent Resistivity (Ω-m)
0.101	53.62
0.122	58.65
0.152	65.61
0.188	73.30
0.230	81.34
0.291	91.18
0.367	110.4
0.455	125.0

APPENDIX E

MAGNETIC DATA

This appendix contains the magnetic data collected along the profiles. The locations were determined using the method described in the section entitled "Data Collection and Processing", which is in the main body of the report. The station is the distance along the profile.

Table E-1. Magnetic data collected along profile A1.

Station (ft)	Location		Magnitude of Magnetic Field (nT)
	Northing (ft)	Easting (ft)	
0	831280	1884630	56461.6
10	831271	1884635	56710.9
20	831263	1884641	57020.2
30	831255	1884646	57457.
40	831246	1884652	57748.1
50	831238	1884657	57938.2
60	831230	1884663	57989.7
70	831221	1884668	57975.7
80	831213	1884674	57981.7
90	831205	1884679	58077.6
100	831196	1884685	58264.9
110	831188	1884691	58495.8

Table E-2. Magnetic data collected along profile A2.

Station (ft)	Location		Magnitude of Magnetic Field (nT)
	Northing (ft)	Easting(ft)	
0	831530	1884420	56182.8
12.5	831517	1884416	56287.6
25	831505	1884413	56276.4
37.5	831493	1884410	55844.3
50	831481	1884407	55264.3
62.5	831469	1884403	54759.1
75	831457	1884400	54388.9
87.5	831445	1884397	54095.2
100	831433	1884394	53872.9
112.5	831421	1884391	53716.7
125	831409	1884387	53622.7
137.5	831397	1884384	53594.
150	831385	1884381	53604.8

Table E-3. Magnetic data collected along profile A3.

Station (ft)	Location		Magnitude of Magnetic Field (nT)
	Northing (ft)	Easting (ft)	
0	831410	1884440	53599.1
12.5	831414	1884428	53687.5
25	831418	1884416	53774.6
37.5	831422	1884404	53822.1
50	831426	1884392	53877.6
62.5	831431	1884381	53847.2
75	831435	1884369	53785.8
87.5	831439	1884357	53720.9
100	831443	1884345	53726.3
112.5	831447	1884334	53726.6
125	831452	1884322	53695.7
137.5	831456	1884310	53784.4
150	831460	1884298	53919.9

Table E-4. Magnetic data collected along profile A4.

Station (ft)	Location		Magnitude of Magnetic Field (nT)
	Northing (ft)	Easting (ft)	
0	831990	1884910	55767.4
50	831969	1884864	55045.6
100	831948	1884818	56479.3
150	831928	1884773	54468.2
200	831907	1884727	54581
250	831887	1884682	55742.2
300	831866	1884636	54607.7
350	831846	1884591	56567.8
400	831825	1884545	52401.1
450	831804	1884499	52068.2
500	831784	1884454	53848.6
550	831763	1884408	52538.8
600	831743	1884363	54226.7
650	831722	1884317	55708.2
700	831702	1884272	53627.1
750	831681	1884226	53481.3
800	831661	1884180	53548.8
850	831640	1884135	53631.6
900	831619	1884089	53735.1

Table E-5. Magnetic data collected along profile B1.

Station (ft)	Location		Magnitude of Magnetic Field (nT)
	Northing (ft)	Easting (ft)	
0	832170	1885490	53589.4
5	832165	1885489	53605.8
10	832160	1885488	53596.2
15	832155	1885487	53616.6
20	832150	1885487	53643.
25	832145	1885486	53649.4
30	832140	1885485	53621.3
35	832135	1885485	53590.2
40	832130	1885484	53599.3
45	832125	1885483	53671.
50	832120	1885482	53763.4
55	832115	1885482	53816.4
60	832110	1885481	53790.1
65	832105	1885480	53678.4
70	832100	1885480	53584.9
75	832095	1885479	53538.2
80	832090	1885478	53589.2
85	832085	1885478	53704.9
90	832080	1885477	53744.6
95	832075	1885476	53728.2
100	832071	1885475	53696.2
105	832066	1885475	53605.8
110	832061	1885474	53475.1
115	832056	1885473	53397.3
120	832051	1885473	53376.1
125	832046	1885472	53359.
130	832041	1885471	53317.8
135	832036	1885470	53285.7
140	832031	1885470	53256.1
145	832026	1885469	53223.3
150	832021	1885468	53249.4
155	832016	1885468	53311.5
160	832011	1885467	53353.
165	832006	1885466	53252.9
170	832001	1885466	52690.2
175	831996	1885465	51889.6
180	831991	1885464	51742.2
185	831986	1885463	52667.8
190	831981	1885463	53967.2
195	831976	1885462	54667.3
200	831972	1885461	54771.7
205	831967	1885461	54391.
210	831962	1885460	53992.6
215	831957	1885459	53786.9

Table E-6. Magnetic data collected along profile B2.

Station (ft)	Location		Magnitude of Magnetic Field (nT)
	Northing (ft)	Easting (ft)	
0	832130	1885440	53513.1
5	832125	1885439	53417.7
10	832120	1885438	53396.4
15	832115	1885438	53383.7
20	832110	1885437	53433.8
25	832105	1885437	53626.
30	832100	1885436	53841.7
35	832095	1885435	53755.4
40	832090	1885435	53648.9
45	832085	1885434	53666.6
50	832080	1885434	53873.9
55	832075	1885433	53896.5
60	832070	1885433	53727.4
65	832065	1885432	53640.4
70	832060	1885431	53624.5
75	832055	1885431	53570.5
80	832050	1885430	53423.2
85	832045	1885430	53321.1
90	832040	1885429	53315.4
95	832035	1885428	53361.2
100	832030	1885428	53391.2
105	832025	1885427	53396.7
110	832020	1885427	53392.4
115	832015	1885426	53407.3
120	832010	1885426	53439.5
125	832005	1885425	53509.1
130	832000	1885424	53569.2
135	831995	1885424	53557.3
140	831990	1885423	53407.6
145	831986	1885423	53603.1
150	831981	1885422	53940.7
155	831976	1885421	54120.
160	831971	1885421	54103.3
165	831966	1885420	53940.
170	831961	1885420	53739.4
175	831956	1885419	53683.9

Table E-7. Magnetic data collected along profile B3.

Station (ft)	Location		Magnitude of Magnetic Field (nT)
	Northing (ft)	Easting (ft)	
0	832144	1885399	53309.7
5	832139	1885398	53162.1
10	832134	1885398	52975.9
15	832129	1885397	52911.4
20	832124	1885397	52916.4
25	832119	1885396	52980.4
30	832114	1885396	53336.1
35	832109	1885395	54288.7
40	832104	1885395	55096.5
45	832099	1885394	54807.3
50	832094	1885394	54075.5
55	832089	1885393	54032.9
60	832084	1885393	54462.6
65	832079	1885392	54833.3
70	832074	1885392	54619.
75	832069	1885391	54199.1
80	832064	1885391	53734.8
85	832059	1885390	53654.
90	832054	1885390	53850.2
95	832049	1885389	53993.1
100	832044	1885388	53981.
105	832039	1885388	53847.
110	832034	1885387	53733.4
115	832029	1885387	53677.4
120	832024	1885386	53630.1
125	832019	1885386	53612.
130	832014	1885385	53595.
135	832009	1885385	53583.1
140	832004	1885384	53593.6
145	831999	1885384	53620.6
150	831994	1885383	53647.1
155	831989	1885383	53702.2
160	831984	1885382	53764.2
165	831979	1885382	53757.1
170	831974	1885381	53669.3
175	831969	1885381	53601.8
180	831965	1885380	53556.1
185	831960	1885380	53493.4

Table E-8. Magnetic data collected along profile I1.

Station (ft)	Location		Magnitude of Magnetic Field (nT)
	Northing (ft)	Easting (ft)	
-50	833165	1885780	53491.2
-25	833141	1885777	53584.3
0	833116	1885774	53525.4
25	833091	1885771	52974.6
50	833066	1885768	51653.7
75	833041	1885766	49863.8
100	833016	1885763	48815.3
125	832992	1885760	48560.2
150	832967	1885757	54266.1
175	832942	1885754	52178.2
200	832917	1885751	55000.4
250	832867	1885745	52500.
300	832818	1885739	57882.7
350	832768	1885733	52313.
375	832743	1885730	56066.9
400	832718	1885727	53862.1
425	832694	1885724	55841.5
450	832669	1885721	57408.9
475	832644	1885718	57855.9
500	832619	1885715	55565.7
525	832594	1885713	53979.3
550	832570	1885710	52294.7
600	832520	1885704	58515.5
650	832470	1885698	58747.3

Table E-9. Magnetic data collected along profile I2.

Station (ft)	Location		Magnitude of Magnetic Field (nT)
	Northing (ft)	Easting (ft)	
0	833070	1886020	52311.8
25	833045	1886013	55212.7
50	833021	1886006	56557.9
75	832997	1886000	58964.
100	832973	1885993	58830.8
125	832949	1885987	57355.3
150	832925	1885980	52686.4
175	832901	1885974	52462.4
200	832876	1885967	52446.1
225	832852	1885961	56248.8
250	832828	1885954	55048.2
275	832804	1885948	56265.2
300	832780	1885941	53934.9
325	832756	1885935	52130.
350	832732	1885928	54687.8
375	832708	1885922	53492.2
400	832683	1885915	50540.2
425	832659	1885908	52192.9
450	832635	1885902	52256.7
475	832611	1885895	52412.2
500	832587	1885889	52369.1

Table E-10. Magnetic data collected along profile M1.

Station (ft)	Location		Magnitude of Magnetic Field (nT)
	Northing (ft)	Easting (ft)	
0	830290	1884860	53851.8
50	830302	1884811	53592.8
100	830315	1884763	53902.1
150	830327	1884714	53890.2
200	830340	1884666	53879.3
250	830352	1884618	53883.3
300	830365	1884569	53881.8
350	830377	1884521	54147.
400	830390	1884472	53857.6
450	830402	1884424	53843.4
500	830415	1884375	53879.1
550	830427	1884327	53883.7
600	830440	1884279	53892.7

Table E-11. Magnetic data collected along profile M2.

Station (ft)	Location		Magnitude of Magnetic Field (nT)
	Northing (ft)	Easting (ft)	
0	830010	1884740	53869.6
50	830024	1884692	53889.8
100	830038	1884644	53878.7
150	830052	1884596	53867.5
200	830066	1884548	53872.5
250	830080	1884500	53867.8
300	830095	1884452	53868.5
350	830109	1884404	53895.3
400	830123	1884356	53872.2
450	830137	1884308	53883.4

Table E-12. Magnetic data collected along profile M3.

Station (ft)	Location		Magnitude of Magnetic Field (nT)
	Northing (ft)	Easting (ft)	
0	830680	1884610	52846.4
50	830631	1884596	53647.8
100	830583	1884582	53977.3
150	830535	1884568	53758.7
200	830487	1884554	53713.7
250	830439	1884540	54038.3
300	830391	1884526	54114.2
350	830343	1884512	53905.4
400	830295	1884498	53881.1
450	830247	1884485	53870.
500	830199	1884471	53856.4
550	830151	1884457	53898.9
600	830103	1884443	53866.6
650	830055	1884429	53863.1
700	830007	1884415	53888.8
750	829959	1884401	53871.5
800	829911	1884387	53866.4
850	829863	1884373	53809.4

Table E-13. Magnetic data collected along profile M4.

Station (ft)	Location		Magnitude of Magnetic Field (nT)
	Northing (ft)	Easting (ft)	
0	830660	1884860	53827.3
50	830611	1884847	53834.8
100	830563	1884834	53852.8
150	830515	1884821	53862.1
200	830466	1884808	53882.6
250	830418	1884795	53882.6
300	830370	1884782	53828.4
350	830322	1884769	53906.4
400	830273	1884756	53993.3
450	830225	1884743	53868.3
500	830177	1884730	53872.4
550	830128	1884717	53892.9
600	830080	1884704	53887.4
650	830032	1884691	53890.6
700	829984	1884678	53877.
750	829935	1884665	53847.6
800	829887	1884652	53773.3

Table E-14. Magnetic data collected along profile P1.

Station (ft)	Location		Magnitude of Magnetic Field (nT)
	Northing (ft)	Easting (ft)	
0	830489	1885462	53543.7
17	830487	1885445	54145.5
34	830485	1885428	54766.
50	830483	1885413	54999.
75	830480	1885388	54570.7
100	830477	1885363	53432.
125	830475	1885338	53476.6
150	830472	1885313	53825.3
175	830469	1885288	53816.7
200	830466	1885264	53893.9
225	830463	1885239	53875.6
250	830461	1885214	53832.5
275	830458	1885189	53868.2
300	830455	1885164	53840.0
325	830452	1885139	53823.1
350	830449	1885114	53759.8
375	830447	1885090	53451.8
400	830444	1885065	53578.4
425	830441	1885040	53780.1
450	830438	1885015	53939.3
475	830435	1884990	53812.1
500	830433	1884965	53779.1
525	830430	1884941	53853.4
550	830427	1884916	53830.9
600	830421	1884866	53823.4
650	830416	1884816	53838.8
700	830410	1884767	53825.0
750	830404	1884717	53835.6
800	830399	1884667	53838.7
850	830393	1884618	53843.7
900	830388	1884568	53831.6
950	830382	1884518	53990.6
1000	830376	1884469	53849.0
1050	830371	1884419	53887.1
1100	830365	1884369	53822.1
1150	830360	1884320	53828.5

Table E-15. Magnetic data collected along profile P2.

Station (ft)	Location		Magnitude of Magnetic Field (nT)
	Northing (ft)	Easting (ft)	
0	830361	1885442	54264.
17	830363	1885425	54339.7
34	830365	1885408	54718.7
50	830366	1885392	54688.2
75	830369	1885367	54086.9
100	830371	1885342	54056.6
125	830374	1885317	53830.7
150	830377	1885292	53935.8
175	830379	1885268	53528.
200	830382	1885243	53532.3
225	830384	1885218	53593.6
250	830387	1885193	53661.2
275	830389	1885168	53817.4
300	830392	1885143	53922.8
325	830394	1885118	54277.1
350	830397	1885093	54178.
375	830399	1885069	53563.4
400	830402	1885044	53879.4
425	830404	1885019	53828.4
450	830407	1884994	53848.1
475	830409	1884969	53790.9
500	830412	1884944	53874.8
525	830414	1884919	53965.0
550	830417	1884894	53827.8

Table E-16. Magnetic data collected along profile W1.

Station (ft)	Location		Magnitude of Magnetic Field (nT)
	Northing (ft)	Easting (ft)	
0	833080	1884570	53865.9
25	833055	1884573	53875.3
50	833030	1884576	53907.3
75	833005	1884579	53966.1
100	832980	1884582	53880.5
125	832955	1884585	53842.1
150	832931	1884588	53824.9
175	832906	1884591	53912.8
200	832881	1884594	53894.3
225	832856	1884597	53892.
250	832831	1884601	53844.1
275	832807	1884604	53839.1
300	832782	1884607	53842.3
325	832757	1884610	53839.
350	832732	1884613	53804.7
375	832707	1884616	53783.7
400	832683	1884619	53751.7

Table E-17. Magnetic data collected along profile W2.

Station (ft)	Location		Magnitude of Magnetic Field (nT)
	Northing (ft)	Easting (ft)	
0	832930	1884690	53878.
25	832927	1884665	53866.1
50	832924	1884640	53860.3
75	832921	1884615	53848.7
100	832918	1884590	53825.5
125	832915	1884565	53878.2
150	832912	1884541	53937.2
175	832909	1884516	53871.3
200	832906	1884491	53846.
225	832903	1884466	53850.5
250	832900	1884441	53846.7

Table E-18. Magnetic data collected along profile W3.

Station (ft)	Location		Magnitude of Magnetic Field (nT)
	Northing (ft)	Easting (ft)	
0	832780	1885350	53816.1
25	832778	1885325	53806.7
50	832777	1885300	53799.8
75	832776	1885275	53794.2
100	832775	1885250	53783.6
125	832774	1885225	53770.7
150	832773	1885200	53782.6
175	832772	1885175	53774.6
200	832771	1885150	53722.9
225	832770	1885125	53722.4
250	832768	1885100	53700.4
275	832767	1885075	53686.9
300	832766	1885050	53695.2
325	832765	1885025	53674.5
350	832764	1885000	53634.
375	832763	1884975	53626.4
400	832762	1884950	53630.6
425	832761	1884925	53505.4
450	832760	1884900	53506.8

APPENDIX F

SELF POTENTIAL DATA

This appendix contains the self potential and contact resistance data collected along profiles P1 and P2. The station is the distance along the profile.

Table F-1. Self potential and contact resistance data collected along profile P1. These measurements could not be made at station 1150 because the base electrode was here.

Station (ft)	Location		Potential (10^{-3} V)	Contact Resistance (10^3 Ω)
	Northing (ft)	Easting (ft)		
0	830489	1885462	-46	15
17	830487	1885445	-45	10
34	830485	1885428	-8	11
50	830483	1885413	24	19
75	830480	1885388	18	175
100	830477	1885363	-25	69
125	830475	1885338	-29	55
150	830472	1885313	-21	49
175	830469	1885288	-20	70
200	830466	1885264	-16	15
225	830463	1885239	-16	18
250	830461	1885214	-13	15
275	830458	1885189	-16	13
300	830455	1885164	-18	15
325	830452	1885139	-20	20
350	830449	1885114	-16	13
375	830447	1885090	-19	22
400	830444	1885065	-17	20
425	830441	1885040	-13	42
450	830438	1885015	-57	73
475	830435	1884990	-44	33
500	830433	1884965	-33	44
525	830430	1884941	-18	25
550	830427	1884916	-13	14
600	830421	1884866	-25	31
650	830416	1884816	-34	54
700	830410	1884767	-35	30
750	830404	1884717	-42	40
800	830399	1884667	-36	56
850	830393	1884618	-19	24
900	830388	1884568	-43	36
950	830382	1884518	-38	36
1000	830376	1884469	30	23
1050	830371	1884419	10	12
1100	830365	1884369	15	33
1150	830360	1884320		

Table F-2. Self potential and contact resistance data collected along profile P2.

Station (ft)	Location		Potential (10^{-3} V)	Contact Resistance (10^3 Ω)
	Northing (ft)	Easting(ft)		
0	830361	1885442	-94	3
17	830363	1885425	-71	7
34	830365	1885408	4	13
50	830366	1885392	32	16
62.5	830367	1885386	14	12
75	830368	1885379	0	10
87.5	830369	1885367	-12	23
100	830371	1885342	-19	15
125	830374	1885317	-24	8
150	830377	1885292	-28	18
175	830379	1885268	-25	13
200	830382	1885243	-30	12
225	830384	1885218	-31	12
250	830387	1885193	-26	13
275	830389	1885168	-18	12
300	830392	1885143	-13	14
325	830394	1885118	-15	17
350	830397	1885093	-19	18
375	830399	1885069	-35	17
400	830402	1885044	-20	25
425	830404	1885019	-85	5
450	830407	1884994	-63	38
475	830409	1884969	-53	13
500	830412	1884944	-66	19
525	830414	1884919	-24	25
550	830417	1884894	-17	38

APPENDIX G

MAGNETIC SUSCEPTIBILITY DATA

This appendix contains the magnetic susceptibilty data collected along the profiles. The station is the distance along the profile.

Table G-1. Magnetic susceptibility data collected along profile A1.

Station (ft)	Location		Magnetic Susceptibility (SI units)
	Northing (ft)	Easting (ft)	
0	831280	1884630	0.029
10	831271	1884635	0.020
20	831263	1884641	0.024
30	831255	1884646	0.019
40	831246	1884652	0.026
50	831238	1884657	0.017
60	831230	1884663	0.016
70	831221	1884668	0.020
80	831213	1884674	0.015
90	831205	1884679	0.022
100	831196	1884685	0.023
110	831188	1884691	0.017

Table G-2. Magnetic susceptibility data collected along profile A2.

Station (ft)	Location		Magnetic Susceptibility (SI units)
	Northing (ft)	Easting (ft)	
0	831530	1884420	0.022
25	831505	1884413	0.023
50	831481	1884407	0.016
75	831457	1884400	0.019
100	831433	1884394	0.020
125	831409	1884387	0.020
150	831385	1884381	0.017

Table G-3. Magnetic susceptibility data collected along profile A3.

Station (ft)	Location		Magnetic Susceptibility (SI units)
	Northing (ft)	Easting (ft)	
0	831410	1884440	0.015
25	831418	1884416	0.027
50	831426	1884392	0.026
75	831435	1884369	0.025
100	831443	1884345	0.034
125	831452	1884322	0.024
150	831460	1884298	0.029

Table G-4. Magnetic susceptibility data collected along profile I1.

Station (ft)	Location		Magnetic Susceptibility (SI units)
	Northing (ft)	Easting (ft)	
0	833116	1885774	0.012
50	833066	1885768	0.009
100	833016	1885763	0.011
150	832967	1885757	0.012
200	832917	1885751	0.012
250	832867	1885745	0.007
300	832818	1885739	0.011
350	832768	1885733	0.011
400	832718	1885727	0.014
450	832669	1885721	0.009
500	832619	1885715	0.013
550	832570	1885710	0.007
600	832520	1885704	0.013
650	832470	1885698	0.005

Table G-5. Magnetic susceptibility data collected along profile I2. The data from stations 350 and 400 were lost because rain dissolved the ink in the field notebook.

Station (ft)	Location		Magnetic Susceptibility (SI units)
	Northing (ft)	Easting (ft)	
0	833070	1886020	0.016
50	833021	1886006	0.014
100	832973	1885993	0.014
150	832925	1885980	0.016
200	832876	1885967	0.009
250	832828	1885954	0.008
300	832780	1885941	0.012
350	832732	1885928	
400	832683	1885915	
450	832635	1885902	0.014
500	832587	1885889	0.010

APPENDIX H

RESISTIVITY SOUNDINGS

This appendix contains a description of the resistivity data that William Frangos, who is a registered geophysicist (#81) in the State of California, collected and interpreted. All text, except this introductory paragraph, was written by him.

Two Schlumberger resistivity soundings at the Midvale (Utah) Sharon Steel slag site demonstrate clearly that large electrical properties contrasts exist within the slag material. Between my meager knowlege of the slag geometry and the small sampling, I prefer not to generalize about the overall characterisitics of the slag heap. Herewith are the reduced data, some preliminary interpretations, and a few observations concerning the possible future usefulness of further electrical work in the area.

Instrumentation for this work was a DC resistivity meter manufactured in Slovakia called a GOFA, a Slovak acronym for "Geophysical resistivity equipment." It injects a sinusoidal current at 90 Hz and performs a synchronous detection of the observed voltage, reporting the V/I ratio on a three-and-a-half digit display. Metal stakes provided adequate contact for both transmitting and receiving electrodes; wetting them did not significantly alter the ratio data. Spot samples of the transmitter output showed voltages between 4 and 40v and currents between 8 and 15 mA. Locations of the electrodes were determined by using a surveyor's chain laid out along the line.

The first vertical electrical sounding (VES1) is situated near a stake marked "D10 N830399.9 E1884899.7 Elev 4331.2" and runs in a northeast-southwest direction. The surface consists of hard, black, small-grained cinders, and I had some apprehension about the ability to make adequate electrical contact prior to beginning the work. The reduced data are as follows:

Obs #	AB/2 (m)	MN (m)	RhoA (ohm-m)
1	0.609600	0.304800	3978.6
2	0.914400	0.304800	4393.7
3	1.219200	0.304800	4464.1
4	1.524000	0.304800	4218.5
5	2.133600	0.304800	3734.4
6	3.048000	0.304800	3052.7
7	3.048000	0.609600	2878.0
8	4.572000	0.609600	1956.1
9	6.096000	0.609600	1279.1
10	6.096000	0.609600	1227.9
11	6.096000	0.914400	1218.7
12	7.620000	0.914400	596.3
13	7.620000	1.219200	690.9
14	9.144000	1.219200	536.2
15	12.192000	1.219200	96.2
16	15.240000	1.219200	78.8
17	15.240000	2.438400	80.8
18	21.336000	2.438400	12.8
19	30.480000	2.438400	109.9

Please note that observations 18 and 19 are clearly noisy and not reliable. These data fall off too steeply with separation to be due to a true layered geometry. Nonetheless, as a first approximation, a layered inversion using a routine from UURI/ESL gives a fairly good and stable fit to a 4-layer earth with the following parameters:

Layer	Resistivity (Ω-m)	Thickness (m)
1	4328.19	1.78
2	2077.00	1.51
3	5.96	1.28
4	125.26	

The last two data were weighted very lightly (W=0.1) for this inversion, and each repeat point was weighted at one half the regular value. The squared error was 0.134 for this case.

The second sounding, VES2, was located on a bench approximately 100 feet east of VES1 and runs roughly parallel to it. The surface appears to be typical of the dross material; it is a very fine silt, almost a clay, and has a serious sulfurous stench.

Obs #	AB/2 (m)	MN (m)	RhoA (ohm-m)
1	0.609600	0.304800	127.8
2	0.914400	0.304800	106.9
3	1.219200	0.304800	87.4
4	1.524000	0.304800	75.8
5	2.133600	0.304800	55.8
6	3.048000	0.304800	45.0
7	3.048000	0.609600	44.5
8	4.572000	0.609600	42.8
9	4.572000	1.219200	44.4
10	6.096000	1.219200	47.7
11	7.620000	1.219200	49.9
12	9.144000	1.219200	48.9
13	9.144000	1.828800	51.1
14	12.192000	1.828800	48.7
15	15.240000	1.828800	47.7
16	15.240000	2.438400	48.7
17	18.288000	2.438400	46.3
18	18.288000	3.048000	46.5
19	21.336000	3.048000	46.6
20	30.480000	3.048000	53.4
21	30.480000	6.096000	51.1

These data are much better behaved than those of the first set, due mostly to improved experimental technique. The following two-layer fit to the data gives a squared error of 0.0346:

Layer	Resistivity (Ω-m)	Thickness (m)
1	154.62	.48
2	45.93	

A four-layer fit, yielding a similarly acceptable squared error of 0.143, seems a bit more intuitively satisfying with the following parameter estimates:

Layer	Resistivity (W-m)	Thickness (m)
1	125.00	.67
2	35.33	6.63
3	40.03	.84
4	54.37	

Discussion

On the basis of this limited sample, it is clear that we may use electrical conductivity to distinguish between the coarse cinder slag material and the dross. The data confirm the slag to be quite resistive, on the order of a few thousand ohm-meters, as would be expected. The dross, on the other hand, is considerably more conductive; my guess is that the second layer interpreted at VES2 is most likely to represent the dross resistivity overall at some 30 to 40 ohm-meters. (The upper layer at 125 ohm-m may be a dried or weathered feature, since it's so thin. The 6 ohm-m of layer 3 at VES1 may be an artifact of the non-layered structure or of some piece of buried junk.) Identifying the bottom of the slag heap is uncertain in these data. While we are certainly sensitive to the material below the slag heap, it is not clear that a distinctive resistivity may be assigned to the soil, sand, gravel, and clay which are there. Perhaps further work would allow some resolution of this issue. Another possible useful approach would be to measure the IP response of the materials involved. I believe that there is a good chance of finding an IP effect associated with the dross, in that it may be sulfide bearing and/or cation exchanging. Now that it is clear that DC electrical measurements can be made with accuracy at the Sharon Steel site, I suggest that some IP measurements should be considered.